Copyright Warning & Restrictions

The copyright law of the United States (Title 17, United States Code) governs the making of photocopies or other reproductions of copyrighted material.

Under certain conditions specified in the law, libraries and archives are authorized to furnish a photocopy or other reproduction. One of these specified conditions is that the photocopy or reproduction is not to be "used for any purpose other than private study, scholarship, or research." If a, user makes a request for, or later uses, a photocopy or reproduction for purposes in excess of "fair use" that user may be liable for copyright infringement,

This institution reserves the right to refuse to accept a copying order if, in its judgment, fulfillment of the order would involve violation of copyright law.

Please Note: The author retains the copyright while the New Jersey Institute of Technology reserves the right to distribute this thesis or dissertation

Printing note: If you do not wish to print this page, then select "Pages from: first page # to: last page #" on the print dialog screen

ABSTRACT

TIME DOMAIN MEASUREMENT OF THE NONLINEAR REFRACTIVE INDEX IN OPTICAL FIBERS AND SEMICONDUCTOR FILMS

by
Hernando Garcia

A new technique to measure the nonlinear refractive index n_2 in optical fibers and semiconductor films has been developed. It is based on the time delay two-beam coupling of very intense picosecond laser pulses that have been self-phase modulated in the nonlinear optical medium. The two beams are coupled in a slow responding medium that is sensitive to time dependent phase distortions. We determine that the amount of phase distortion experienced by the pulse is proportional to the nonlinear refractive index of the medium. This time domain approach can also be applied to optical fiber amplifiers in the presence of gain and to semiconductor films. Because the technique is base on pure refraction the measurement of n_2 is insensitive to nonlinear absorption, thermal effects, and surface roughness. With this technique we have measured n_2 in 20-m length of Silica-glass, Ytterbium-doped, and Erbium-doped optical fibers at 1.064-μm. Also we have measured the change of n_2 at 1.064-μm in the presence of a 980-nm pump laser in Yb^{3+}-doped and Er^{3+}-doped fibers. Finally we have extended the technique to measure n_2 in 2-mm thick samples of GaAs, CdTe and ZnTe semiconductors. In the language of ultrafast spectroscopist, if the best tool to characterize an ultrashort optical pulse is the pulse itself, then the best tool to characterize an optical nonlinear medium is a pulse that has been modified by the medium.

TIME DOMAIN MEASUREMENT OF THE NONLINEAR REFRACTIVE INDEX IN OPTICAL FIBERS AND SEMICONDUCTOR FILMS

by
Hernando Garcia

A Dissertation
Submitted to the Faculty of
New Jersey Institute of Technology and
Rutgers, The State University of New Jersey
In Partial Fulfillment of the Requirements for the Degree of
Doctor of Philosophy in Applied Physics

Federated Physics Department

May 2000

APPROVAL PAGE

TIME DOMAIN MEASUREMENT OF THE NONLINEAR REFRACTIVE INDEX IN OPTICAL FIBERS AND SEMICONDUCTOR FILMS

Hernando Garcia

Dr. Anthony M. Johnson, Dissertation Advisor
Chairperson, and Distinguished Professor of Physics,
Physics Department, NJIT

Dr. Earl Shaw, Committee Member
Professor of Physics, Physics Department
Rutgers, the State University of New Jersey

Dr. John Federici, Committee Member
Professor of Physics, Physics Department, NJIT

Dr. Wayne H. Knox, Committee Member
Head Advance Photonics Research Department
Bell Laboratories, Lucent Technologies

Dr. David J. DiGiovanni, Committee Member
Head Optical Fiber Research
Bell Laboratories, Lucent Technologies

BIOGRAPHICAL SKETCH

Author: Hernando Garcia

Degree: Doctor of Philosophy in Applied Physics

Date: May, 2000

Undergraduate and Graduate Education:

- Ph.D in Applied Physics,
  New Jersey Institute of Technology, May 2000

- Master of Science in Physics,
  Rutgers, The State University of New Jersey, New Brunswick, NJ, 1996

- Bachelor of Science in Engineering Science,
  New Jersey Institute of Technology, Newark, NJ, 1989

Major: Applied Physics

Presentation and Publications:

- *Nonlinear optical properties of silicon nanoclusters made by laser ablation,* Paper QW A7 (p. 88) CLEO/IQEC 1998, San Francisco, CA.

- *Ultrafast Spectroscopy and Ultrafast Optical Phenomena,* Third National School of Condense Matter Physics, Proceedings, Armenia, Quindio, Colombia S.A, 144, 1998.

- *Photorefractive Beam Coupling - A new Approach to the measurement of the nonlinear Refractive Index of Short (<25 m) Lengths of Silica and Erbium-doped Fibers,* Paper Ctu V7 (p. 209) CLEO/QELS 1999, Baltimore, MD.

- *Photorefractive Autocorrelation Measurement of the Nonlinear Refractive index in Silica Fibers,* Ibero-American Conference on Optics, Lasers, and Applications 1998, Cartagena, Colombia, South America.

- *Photorefractive Beam Coupling measurement of the Nonlinear Refractive index of semiconductor Films,* Paper WLL 104 (p. 124) 1999 OSA Annual Meeting, Santa Clara, Ca.

- *Nonlinear Refractive Index of Semiconductor Films,* paper M03-4 (p. 39) 15th Latin American Symposium on Solid State Physics 1999, Cartagena, Colombia, South American.

- *Measurement of the Nonlinear Refractive Index in Semiconductor Films using IGA,* to be submitted to Optics Letters.

- *Dynamical Nonlinearities in Er^{3+} and Yb^{3+} doped fibers,* to be submitted to Optics Letters.

- *Photorefractive Autocorrelation Measurement of the Nonlinear Refractive Index in Silica Fiber,* to be submitted to Optics Letters.

- *An Infrared Amplitude Modulator Based on Electrical Creation of Intersubband Transitions,* NATO-ARW on Intersubband Transitions in Quantum Wells, 1991, France.

- *Photorefractive beam coupling measurement of the nonlinear refractive index of semiconductor films*, to appear in Phys. Statu. Solidi (b), vol. 220, July 1, 2000.

- Numerous AT&T Bell Laboratories Technical Memos.

This Dissertation is dedicated to
Martha, Natalia, Sebastian, my mother, and to my father's memory

ACKNOWLEDGMENT

I would like to thank Professor Anthony Johnson for his ongoing support throughout the years. He contributed many valuable ideas, shared his knowledge, and allowed me the freedom and independence to pursue the final goal of the thesis. This paved the way to increase my knowledge in other areas of optics and solid state physics, which is paramount to my future as a physicist.

I will always be grateful to Dr. Shirley A. Jackson for "rescuing" me at Rutgers University. She put me in contact with Professor Johnson, helped me through theoretical physics and worked with me in the Kondo effect in lower dimensional systems. The latter helped me understand some of the complex processes that take place in condensed matter physics, and how these processes may be view from an optical point of view.

I would like to thank the members of my committee for their assistance. Dr. Wayne H. Knox provided some of the equipment that was necessary to complete much of the thesis, it is an honor to have him on my committee. Dr. David J. DiGiovanni, for many helpful discussions and for providing some of the fibers used in the experiments. I'm indebted to Dr. DiGiovanni for his kindness in serving on the committee. Dr. Earl Shaw for his willingness to serve in the committee and finally Dr. Federici for many suggestions during the thesis proposal stage.

I would like to express my gratitude to AT&T for the continuous support through the Tuition Assistant Plan Program (TAP). I was able to pay most of school expenses with the program. This types of programs help minorities advance in their professional education, it is important to keep this program alive in corporation like AT&T and Lucent. In AT&T there are two people that have provided me with their support, Joe

Scholl, my former supervisor, and Joseph Vassallo my present supervisor, they both give me the flexibility in my job to complete this degree, I'm indebted with them.

Finally, I would like to express my love and gratitude to my wife Martha, my daughter Natalia, and my son Sebastian who played a fundamental role with their tolerance and understanding during my completion of this project. Without their support and sacrifice, this project would not have been completed. To my mother and to the memory of my father whose tenacity and stubbornness I inherited, this thesis is in their honor.

TABLE OF CONTENTS

TABLE OF CONTENT
(Continued)

LIST OF TABLES

LIST OF FIGURES

LIST OF FIGURES
(Continued)

LIST OF FIGURES
(Continued)

Figure **Page**

LIST OF FIGURES
(Continued)

CHAPTER 1

INTRODUCTION

1.1 Background

The field of nonlinear optics has experienced a very rapid increase in the past 20 years due to its potential applicability in areas such as: optical communications, information processing, medicine, biology, sensors, passive optical components, lasers, etc. Most of today's fentosecond laser systems used in ultrafast optical research are possible because of the use of nonlinear crystals. In optical communications for example, selfphase modulation is used in conjunction with group-velocity dispersion to produce temporal solitons in optical fibers. The quest to find condensed matter system that shows large, fast nonlinearities and low absorption is still one that should be pursues. If it is found this system should be ideal for information processing and switching. This assumes that available integration technology can be developed.

Today's new exotic materials, in terms of doping composition and/or geometrical structures, are paving the way to the synthesis of new nonlinear optical materials. These new structures, fabricated by ion implantation, ion exchange followed by ion implantation, sol-gel synthesis, sputtering, pulse laser ablations, or pulsed-laser deposition, are very common. These chemicals trend in the compositions of matrix glasses with nanoparticles of metals or semiconductors, combined with quantum confinement effects are giving unprecedented results in terms of ultrafast responses and strong nonlinearities. Nanocomposites, such as metal quantum dot composites of Cu embedded in a fused silica matrix [1] are routinely produced in research labs with third

order nonlinear response of the order of 10^{-10} cm^2/W and relaxation times of the order of a few picoseconds.

Another approach to generated huge nonlinear optical response is based on electromagnetically induced transparency [2]. In this case, the nonlinearity comes from the coupling of a metastable state and a lifetime-broadened state. Devices base on this effect have already been proposed [3]. This type of effect can be called *Optical Resonance Engineering*, because it is base on the understanding of the specific resonance of atomic transitions.

Exotic fibers, especially those with novel geometrical structures, are very good candidates for testing nonlinear optical effects that have not been realized before. Microstructure optical fibers [4], or holey-fibers, show anomalous waveguide dispersion in the 800-nm range, and show rigorously single mode behavior, which is impossible in conventional fibers. In this range, powerful fentoseconds lasers can be found. This allows confining TW of peak power in very small areas amplifying nonlinear optical effects such as shock waves, and supercontinuum generation [5]. Holey fibers are particularly attractive for photonic devices because their optical properties can be engineered during fabrications.

Nonlinear optics also plays a key role in optical communications [6,7,8] limiting the amount of power that can be transmitted per pulse before nonlinear optical effects take place. The optical nonlinearities can lead to interference, distortion, and excess attenuation. In general, stimulated Raman scattering, stimulated Brillouin scattering, and four photon mixing will deplete some optical waves, and generate others by means of frequency conversion. This will cause interference for other channels affecting direct

detention and heterodyne detention systems. In the case of angle or phase modulated system effects, such as cross phase modulation and self-phase modulation, will have comparable effects as frequency conversion nonlinear phenomena.

Nonlinear effects in optical fibers can also be cumulative. This is the case of linear, as well as nonlinear index change due to resonance transitions in rare-earth doped fibers like Er^{3+}, and Yb^{3+}. For long-haul communications systems like 10,000 Km, where fiber amplifier spacing is of the order of 100 Km, these effects may be important for system design. These effects arise because of the resonance transitions in each of the amplifier stage; we call these *dynamic linear and nonlinear susceptibilities*, because they come from the presence of a pump laser in the amplifier.

Experimental techniques to quantify the above-mentioned nonlinearities are also a very dynamic and expanding. The crucial need for strong and fast nonlinear optical material demands a reliable method for the measurement of the magnitude and sign of the nonlinear index of refraction. This characterization is important for material design and development.

Previous measurements of nonlinear refraction have used complicated techniques that may be applied to semiconductors or fibers independently. For example, in semiconductors, techniques such as beam distortion [9,10], nonlinear interferometry [11], degenerated four-wave mixing [12], nearly degenerated three-wave mixing [13], and ellipse rotation [14] have been used. The beam distortion is a very simple technique known as Z-scan. This technique is based on the analysis of transmittance in a nonlinear medium through a fine aperture *in the far field* as a function of the sample position. The

other three techniques based on interferometric and wave mixing required more complex experimental setups.

In the case of fibers, Stolen [15] has developed a technique in the frequency domain that allows n_2 to be measured very precisely, but requires very long fibers between 200-300 meters. In the technique described here, only a few meters of fiber are needed.

Induce Grating Autocorrelation (IGA), originally developed for pulse characterization [16] can be implemented for medium characterization. This technique that we call Two-Beam Coupling (TBC) is totally based on a nonlinear effect called Self-Phase Modulation (SPM). When a high intensity optical pulse propagates in a nonlinear medium, it will experience a time dependent phase modulation. It is this phase modulation that is used in a TBC experiment to characterize the nonlinear medium. TBC can be applied to waveguide as well as semiconductor films. In the case of optical fibers, Group Velocity Dispersion (GVD) can be neglected because of the small lengths of fiber needed to generated SPM. In semiconductor films, thermal effects and absorption can be neglected because SPM is based on pure refraction. Another important application of TBC is the measure of dynamic susceptibilities in systems with gain. In this case, the nonlinear third-order susceptibility can be measured at λ_o when there is another λ_1 present. This is important for Erbium Doped Amplifiers.

1.2 Overview of the Dissertation

Our present research is focused in the use of TBC experimental techniques to measure the third-order nonlinear susceptibility in semiconductors and waveguide structures like optical fibers. Emphasis has been given to rare earth doped fiber like Er^{3+} and Yb^{3+}.

These materials are commonly used in optical amplifiers. The third order susceptibility for these fibers have been measured with and without a pump laser. The TBC technique has been extended to semiconductor films where the magnitude and the sign of the third order nonlinear susceptibility has been measured.

The dissertation consists of six chapters including this introduction. In chapter 2, we present the constitutive relation of the induced polarization and the electric field, and examine the relation between the nonlinear susceptibility and the Stark effect. Also, a more complicated approach base on Kramers-Kronig nonlinear dispersion relation will be outline. A density matrix, approach is followed for a quasi-three-level model with gain. This model will be applied to the case of the rare earth-doped fibers. In chapter 3, the theory of self-phase modulation will be described, the zero GVD regime will be analyzed where the TBC technique can be applied. Chapter 4 will describe the photorefractive effect, and the consequences of the TBC experiment in a slow responding medium. It will be shown that the results of photorefractive beam coupling of Yao *et al* [17], and the two beam coupling experiment in a slow responding medium of Trebino *et al* [18] are identical except from a normalization constant. Also, We analyzed TBC experiments in a photorefractive crystal when self-phase modulated pulses are used. Here we will demonstrate how to extract the third-order susceptibility from an electric field autocorrelation function. Chapter 5 describes the experimental technique and a brief description of the laser system and electronics used,, also the main results for silica-glass fibers, Erbium-doped fibers, and Ytterbium-doped fibers are presented. Chapter 6 presents the main results for the semiconductor, conclusions and possible research directions.

CHAPTER 2

NONLINEAR OPTICAL SUSCEPTIBILTY

2.1 Macroscopic Description of the Nonlinear Susceptibility

When very intense light interacts with matter, some of the optical properties of the material system are modified. The study of this interaction is called nonlinear optics. The beginning of nonlinear optics starts with the observation of the second harmonic generation in single-crystal quartz by Franken *et al.* in 1961 [19], after the demonstration of the first working laser by Maiman in 1960 [20]. Generally nonlinear optics refers to the study of the interaction of intense electromagnetic fields with materials, to produce modified fields that are different from the input fields in phase, frequency, and amplitude [21].

The strength and form of the interaction depends on the underlying symmetrical properties of the system. In general, the quantities that control the strength of the interaction are called nonlinear optical susceptibilities. Even order susceptibilities are responsible for harmonic effects such as sum and difference frequency generation, while odd order susceptibilities are responsible for self-interaction effects such as self-phase modulation, self-focusing, etc.

The derivation of the nonlinear susceptibility can be accomplished in different ways. In this section, we will follow closely Boyd's [22] derivation of the nonlinear susceptibility based on the argument used by Jha *et al* [23].

Using the electric dipole approximation, one can define the total polarization of a system interacting with an electromagnetic field as

$$P = \chi^{(1)}\mathcal{E} + \chi^{(2)}\mathcal{E}^2 + \chi^{(3)}\mathcal{E}^3 + ... \qquad (2.0)$$

the total energy density can be defined in terms of the total energy expansion in power of the electric field, which is given by

$$W = -P \cdot \mathcal{E} = -\frac{1}{2}\chi_{ij}\mathcal{E}_i\mathcal{E}_j - \frac{1}{3}\chi^{(2)}_{ijk}\mathcal{E}_i\mathcal{E}_i\mathcal{E}_k - \frac{1}{4}\chi^{(3)}_{ijkl}\mathcal{E}_i\mathcal{E}_j\mathcal{E}_k\mathcal{E}_l + .. \qquad (2.1)$$

So the knowledge of the total energy expansion as a function of the electric field allows one to find the static limit of the total susceptibility of order n from the equation

$$\chi^{(n)}(0) = -\frac{1}{n!}\frac{\partial^{n+1}W}{\partial\mathcal{E}^{n+1}}\bigg|_{\mathcal{E}\to 0} \qquad (2.2)$$

From the above equation; it is easy to see that the nonlinear susceptibility is directly related to the Stark effect in the static limit. We can take the above analysis further by using standard quantum perturbation theory to calculate the energy of the system, assuming that the total Hamiltonian of the system is given by

$$\boldsymbol{H} = \boldsymbol{H_o} + e\mathbf{x}\cdot\boldsymbol{\mathcal{E}} \qquad (2.3)$$

If there are N independent unit cells in the system, then the total energy is

$$W = NE_o \qquad (2.4)$$

$$\begin{aligned}
E_o &= E_o^{(0)} + E_o^{(1)} + E_o^{(2)} + E_o^{(3)} + \ldots\ldots, \\
E_o^{(1)} &= e\mathcal{E}_i\langle 0|x|0\rangle \equiv e\mathcal{E}_i\bar{x}_i \\
E_o^{(2)} &= -e^2\mathcal{E}_i\mathcal{E}_j\sum_s{}'\left[\frac{\langle 0|x_i|s\rangle\langle s|x_j|0\rangle}{E_s^{(0)} - E_o^{(0)}}\right] \\
E_o^{(3)} &= e^3\mathcal{E}_i\mathcal{E}_j\mathcal{E}_k\sum_s{}'\sum_t{}'\left[\frac{\langle 0|x_i|s\rangle\langle s|x_j|t\rangle\langle t|x_k|0\rangle}{(E_s^{(0)} - E_o^{(0)})(E_t^{(0)} - E_o^{(0)})}\right]
\end{aligned} \qquad (2.5)$$

$$E_o^{(4)} = -e^4\mathcal{E}_i\mathcal{E}_j\mathcal{E}_k\mathcal{E}_l\sum_s{}'\sum_t{}'\sum_u{}'\left[\frac{\langle 0|x_i|s\rangle\langle s|x_j|t\rangle\langle t|x_k|u\rangle\langle u|x_l|0\rangle}{(E_s^{(0)} - E_o^{(0)})(E_t^{(0)} - E_o^{(0)})(E_u^{(0)} - E_o^{(0)})}\right] - e^2E_0^{(2)}\mathcal{E}_k\mathcal{E}_l\sum_u{}'\left[\frac{\langle 0|x_k|u\rangle\langle u|x_l|0\rangle}{(E_u^{(0)} - E_o^{(0)}}\right]$$

In the above expressions, the ' denotes the fact that the ground state must be taken out of the summation symbol. If we replace all of the above denominators by some average energy denominator $\hbar\omega_o$, including the ground state won't dramatically change the final result. Using Equation (2.2) to calculate the susceptibilities up to order three, we find that

$$\begin{aligned}\chi^{(1)}(0) &= \left(\frac{2e^2N}{\hbar\omega_o}\right)\langle x^2\rangle \\ \chi^{(2)}(0) &= -\left(\frac{3e^3N}{\hbar^2\omega_o^2}\right)\langle x^3\rangle \\ \chi^{(3)}(0) &= \left(\frac{4e^4N}{\hbar^3\omega_o^3}\right)\left[\langle x^4\rangle - 2\langle x^2\rangle^2\right]\end{aligned} \tag{2.6}$$

We see immediately that the nonlinear susceptibilities are related to the electron distribution function and as such, measure the deviation of the potential from the purely harmonic form.

Approximated quantum results can be extended in terms of the linear index of refraction using the results of [24]. In this case, the total field applied to the solid can be replaced by an individual field acting on each atom that composes the solid with a field correction factor given

$$f = \frac{n^2+2}{3} \tag{2.7}$$

in the above equation, n is the refractive index of the solid. The expressions for the linear and third order nonlinear susceptibilities are given by

$$\begin{aligned}\chi^{(1)} &= \frac{n^2(\omega)-1}{4\pi} = f\sum N^i\alpha^i(\omega) \\ \chi^{(3)} &= \frac{f^4}{24}\sum N^i\gamma^i(\omega)\end{aligned} \tag{2.8}$$

In Eq. (2.8) N^i are the densities of the ith constituent, α represents the linear electronic polarizability, and γ represents the mean second electronic polarizability. These are the Clausius-Mossotti equations for the linear and the nonlinear case. The above equations are approximated using the low frequency limit so that the resonant frequency is the dominant frequency ω_o, and the optical field frequency is much lower than the resonance frequency or $\omega << \omega_o$. In this case the second electronic polarizability can be expressed as

$$\gamma = Q\alpha^2 = Q\left(\frac{\mu e^2}{m\omega_o^2}\right)^2 \tag{2.9}$$

where Q is given by quantum mechanics calculation and expressed as the moments of the ground state electron density

$$Q = \frac{6g}{\hbar\omega_o} = \frac{12}{\hbar\omega_o}\left[\frac{\langle x^4\rangle}{2\langle x^2\rangle^2} - 1\right] \tag{2.10}$$

Where μ is the oscillator strength defined as $\mu = 2m\omega_o\langle x^2\rangle/\hbar$. Substituting the results of Eq. (2.9) and (2.10) in Eq. (2.8), we get for the linear and nonlinear susceptibilities

$$n_2 = \frac{12\pi}{n}\chi^{(3)} = \frac{(g\mu)(n^2+2)^2(n^2-1)^2}{48\pi n\hbar\omega_o(N\mu)} \tag{2.11}$$

$$\frac{n^2-1}{n^2+1} = \frac{4\pi}{3}\frac{(N\mu)(e^2/m)}{\omega_o^2-\omega^2} \tag{2.11a}$$

In Eq. (2.11), the nonlinear refractive index is expressed in terms of the product of the atom density and the dipole strength of the system. The value for $N\mu$ and ω_o can be calculated by measuring the refractive index of two different frequencies. The parameter

$g\mu$ has been found experimentally using Eq. (2.11) and has a value of $g\mu$=3 for most optical solids.

2.1.1 Dispersion Relations for the Nonlinear Susceptibility

The above analysis was used to emphasize the physical origin of the nonlinear susceptibility based on the moments of the charge distribution that were also correlated with the Stark Effect. One of the limitations was the fact that the analysis can only be applied to the low frequency limit -much lower than any resonance frequency of the system- and that all the relevant frequencies were substituted with a mean absorption frequency ω_o. There is a universal dispersion curve for the nonlinear susceptibility that can be calculated from causality principles using similar Kramers-Krönig relationships as the ones used in linear optics [25]. The expression can be considered phenomenological in the sense that it can only be applied to a two-band model for the semiconductor. The expression describes some of the individual processes that contribute to the nonlinear susceptibility.

It is well known that most optical solids show dispersion in the nonlinear index which is positive for values below or near the two-photon absorption edge (2PA), or $\hbar\omega \cong E_g/2$, however, for wavelengths substantially above the 2PA, the nonlinear index of refraction n_2 becomes negative. Eq. (2.11) and Eq. (2.11a) predict the low frequency magnitude of n_2, but not the dispersion. The only process considered in deriving the above equations are the calculations of the different moments of the charge, distribution which are directly related to the DC-Stark effect.

In [25] they include in the calculation of the n_2 contributions such as 2PA, electronic Raman effect, and the optical Stark effect. The analysis is based on extending

the linear Kramers-Krönig (KK) to the case of nonlinear interactions. In this way causality is incorporated naturally in the formalism as it occurs in the linear case. KK formalism states that the change in the refractive index (Δn) at ω is associated with the change in the absorption coefficient ($\Delta\alpha$) through the spectrum (ω'), and vice versa. The nonlinear change can be calculated as

$$\Delta n(\omega;\xi) = \frac{c}{\pi}\int_0^\infty \frac{\Delta\alpha(\omega';\xi)}{\omega'^2-\omega^2}d\omega' \tag{2.13}$$

In the above equation, ξ is a parameter related to the cause of the change. It is important to make clear here that the cause of the change does not necessarily need to be optical in origin. The change of the nonlinear refractive index can be due to thermal or electrical changes. Typical examples are the refractive index change resulting from electron-hole plasma [26], or a thermal shift of the band edge [27].

The scheme to calculate the nonlinear refraction from Eq. (2.13) is to calculate the different contributions to the nonlinear absorption. The absorption is easier to measure than the refractive index itself. In [25], the contribution to the nonlinear absorption comes from degenerate two-photon processes, nondegenerate two-photon absorption, and linear and quadratic Stark effects. After the absorption coefficient is calculated for the different contributions, the nonlinear refraction can be found using Eq. (2.13). A general scaled form for n_2 is given by

$$n_2(esu) = K'\frac{\sqrt{E_p}}{n_0 E_g}G_2\left(\hbar\omega/E_g\right) \tag{2.14}$$

Where K' is a constant found by fitting the experimental data for a wide class of semiconductors. Its value can be approximated by $1.50\text{x}10^{-8}$. E_g is the value of the energy gap of the semiconductor in eV, and E_p is independent of the material and possess a value

of $\cong$ 21 eV. In Fig. 2.1, we show the universal function G_2 as a function of normalized frequency with respect to the energy gap. It is easy to see that at the middle of the band edge there is a change in the slope of the dispersion relation from a positive value for the nonlinear coefficient below the TPA edge. It decreases and eventually reaches negative values for the nonlinear refraction above the TPA edge. Experimentally, direct gap semiconductors and some insulator materials follow this universal curve:

Also, in Fig. 2.1, it can be seen that the most significant contribution to the nonlinear refraction comes from the TPA term, except in the band edge, where the quadratic Stark effect is the dominant contribution. The most important result of this analysis is that below the TPA, the value for the refractive index shows a positive value, when there are only virtual carriers participating in the process. Above the TPA edge, the nonlinear index starts to decrease and eventually becomes negative. This is accompanied by the production of real carriers that increase the absorption. It is interesting to note that TPA is the most significant contribution to the nonlinear refraction, and also one of the most critical parameters that limit the performance of an optical switching device [28].

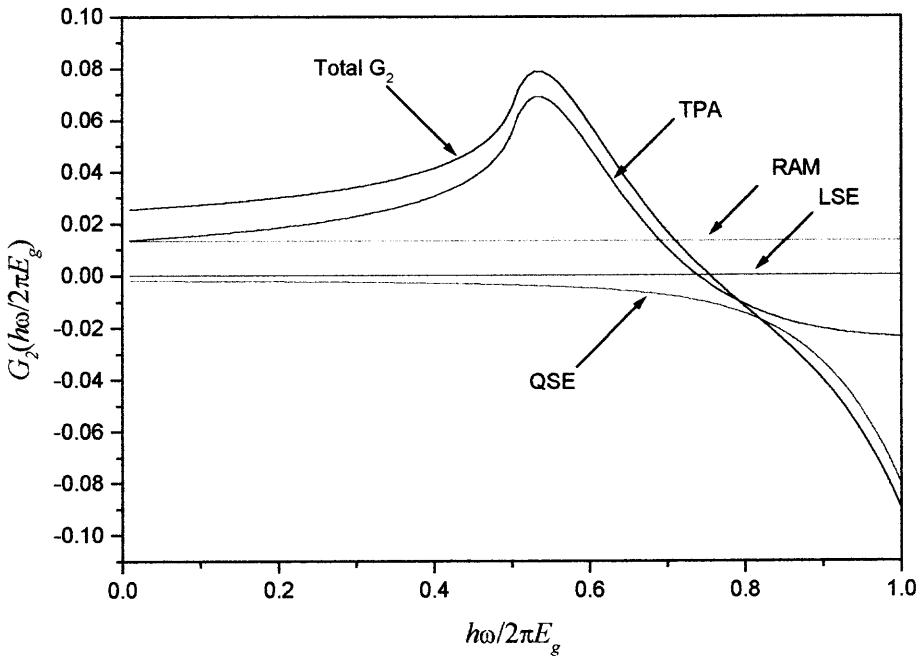

Figure 2.1 Dispersion of the nonlinear refractive index n_2 as a function of the energy normalized to the band gap. Each contribution correspond to Two Photon Absorption (TPA), Raman Transition (RAM), Linear Stark Effect (LES), and Quadratic Stark Effect (QES).

2.2 Density Matrix Calculation of $\chi^{(3)}$

There is an alternative approach for calculating nonlinear susceptibilities where there is no need to specify the basis for the wave function. In fact, the density matrix is totally independent of the wave function representation [29]. The approach used here is called semiclassical description, in which the atomic system is quantized and the electrical field interacting with matter is classical.

We will apply the density matrix for the case of a three-level system where the terminal level is the ground state of the system [30]. The problem addressed here refers to the case of a nondegenerate three-level system, where the total susceptibility of the system is given by the individual contributions of each of the atomic laser transitions.

This approach will be applied to the case of doped optical fibers to prove that in the presence of a pump laser, a gain medium shows a decrease of the nonlinear optical susceptibility.

Before we calculate the susceptibility of a quasi-three level system, let's derive some of the properties of the density matrix approach. Consider a quantum system that is characterized by the state

$$\psi(r,t) = \sum c_n(t) u_n(r) \tag{2.15}$$

where

$$c_n(t) = (u_n(r), \psi(r,t)) \tag{2.16}$$

in the above equation, the $u_n(r)$ are arbitrary complete set of basis functions. From standard quantum mechanics, let A be some operator corresponding to some observable of the system. Its expectation value is given by

$$\langle A \rangle = [\psi(r,t), A\psi(r,t)] = \sum_{m,n} c_m^*(t) [u_m(r), A u_n(r)] c_n(t) \tag{2.17}$$

The term in the square brakes on the right-hand side corresponds to the *mn* element of the product of two matrices, Thus Eq. (2.17) can be expressed as

$$\langle A \rangle = \sum_{m,n} c_m^* A_{mn} c_n \tag{2.18}$$

Assuming that we have enough information to calculate the assembled average for the wave function coefficients of Eq. (2.15), then the expectation value of the operator A is

$$\overline{\langle A \rangle} = \sum_{m,n} \overline{c_m^* c_n} A_{mn} \tag{2.19}$$

Identifying the product under the bar on the right-hand side of the above equation with the density operator ρ_{mn}, and using the rule of matrix multiplication, we finally get for the expectation value of the operator A

$$\overline{\langle A \rangle} = \sum_n (\rho A)_{mn} = tr(\rho A) \tag{2.19}$$

In Eq. (2.19) the symbol "*tr*" is the trace operator, which is the sum of all of the diagonal elements of the above matrix. As can be seen, the expectation value of the operator is independent of the choice of the basis function. Two important properties of the density matrix are that first, it must be Hermitian in order that its eigenvalues are real this can be express as $\rho_{mn} = \rho^*_{nm}$. Second, because the wave function of the system must be normalizable, therefore from Eq. (2.15), we have that $tr\rho = \sum_m c^*_m c_m = 1$.

Because the wave function in Eq. (2.15) satisfies the Schrödinger's equation, we have

$$H\psi(r,t) = i\hbar \frac{\partial \psi(r,t)}{\partial t} \tag{2.20}$$

Substituting Eq. (2.15) into Eq. (2.20), we obtain

$$\sum_n c_n(t) H u_n(r) = i\hbar \sum_n \frac{\partial c_n(t)}{\partial t} u_n(r) \tag{2.21}$$

Operating Eq. (2.21) from the left with $u_m(r)$, using their orthonormality gives us

$$\sum_n c_n(t) H_{mn} = i\hbar \frac{\partial c_m}{\partial t}, \qquad \sum_n H^*_{nm} c^*_n = -i\hbar \frac{\partial c^*_n}{\partial t} \tag{2.22}$$

Using the definition of the density matrix, taking its time derivative, and using the Hermitian properties of the Hamiltonian operator, we finally obtain for the equation of motion of the density matrix

$$i\hbar\frac{\partial\rho_{mn}}{\partial t}=\sum_{k}\left(H_{mk}\rho_{kn}-\rho_{mk}H_{kn}\right) \tag{2.23}$$

This can be written in operator form as

$$\dot{\rho}_{mn}=\frac{-i}{\hbar}\left[\hat{H},\hat{\rho}\right]_{mn} \tag{2.24}$$

Eq. (2.24) describes how the density matrix evolves in time as the result of the interactions that are included in the Hamiltonian. There are certain interactions that cannot be included in the Hamiltonian such as collision of atoms. Such interactions can lead to a change in the state of the systems. These effects must be include phenomenologically, and appear as damping terms to the equation of motion.

2.3 Semiclassical Theory for $\chi^{(3)}$ in a Quasi-Three Level System

The most general system is shown in Fig. 5.2. We will assume that there is no connection between level $|4\rangle$ and $|2\rangle$, and the total electric field in the system is a linear combination of the pump, probe, and signal field (p, pr, s).

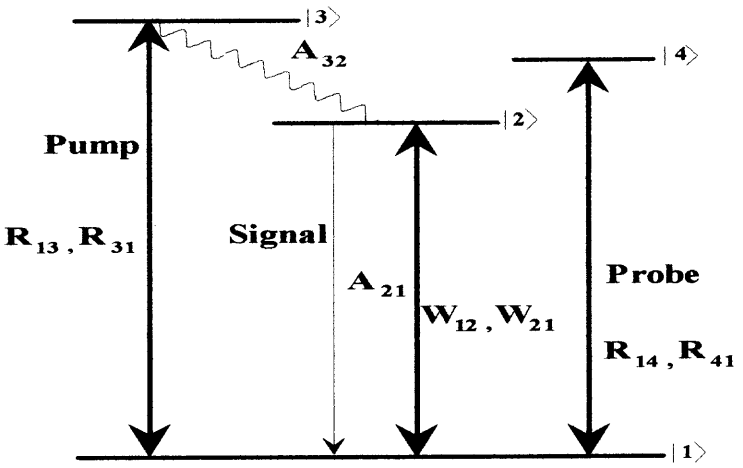

Figure 2.2 Energy State in the quasi-three level system for the study of the nonlinear susceptibility $\chi^{(3)}$ when there is a pump laser present in the system.

Let the transverse electric field in the system be

$$E(z,t) = \left[\hat{e}_p E_p \exp(-i\omega_p t + ik_p z) + \hat{e}_{pr} E_{pr} \exp(-i\omega_{pr} t + ik_{pr} z) + \hat{e}_s E_s \exp(-i\omega_s t + ik_s z) + cc\right] \quad (2.25)$$

In Eq. (2.25), E_j, ω_j, and k_j (j=p, pr, s) are the electric field, angular frequency, and wave vector for the pump, probe, and signal light respectively. The total Hamiltonian of the system is given by

$$H = \sum_{n=1}^{4} \hbar\omega_n |n\rangle\langle n| - \mu_p \cdot E_p (|3\rangle\langle 1| + |1\rangle\langle 3|) - \mu_{pr} \cdot E_{pr} (|4\rangle\langle 1| + |1\rangle\langle 4|) - \mu_s \cdot E_s (|2\rangle\langle 1| + |1\rangle\langle 2|) \quad (2.26)$$

where ε_n=$\hbar\omega_n$ is the eigenenergy of state $|n\rangle$ (n=1,2,3,4). In the absence of a driving field, the density matrix tends to evolved in time as $\exp(-i\omega_{nm}t)$. Thus, the term of the electric field that oscillated with this frequency is a more effective driving term. Therefore, we can drop the positive frequency driving field (this is called the rotating wave approximation [25]). Using Eq. (2.24) to calculate the equation of motion of the density operators we find after some algebra, that

$$\begin{aligned}
\frac{\partial \rho_{11}}{\partial t} &= A_{21}\rho_{22} - R_{13}(\rho_{11} - \rho_{33}) - R_{14}(\rho_{11} - \rho_{44}) - i\Omega_s(\rho_{12} - \rho_{21}) \\
&\quad - i\Omega_p(\rho_{13} - \rho_{31}) - i\Omega_{pr}(\rho_{14} - \rho_{41}) \\
\frac{\partial \rho_{22}}{\partial t} &= A_{32}\rho_{33} - A_{21}\rho_{22} + i\Omega_s(\rho_{21} - \rho_{12}) \\
\frac{\partial \rho_{33}}{\partial t} &= R_{13}(\rho_{11} - \rho_{33}) - A_{32}\rho_{33} + i\Omega_p(\rho_{13} - \rho_{31}) \\
\frac{\partial \rho_{44}}{\partial t} &= R_{14}(\rho_{11} - \rho_{44}) + i\Omega_{pr}(\rho_{14} - \rho_{41})
\end{aligned} \quad (2.27)$$

$$\frac{\partial \rho_{12}}{\partial t} = -(\gamma_{12} + i\Delta_{12})\rho_{12} - i\Omega_s(\rho_{22} - \rho_{11})$$
$$\frac{\partial \rho_{13}}{\partial t} = -(\gamma_{13} + i\Delta_{13})\rho_{13} - i\Omega_p(\rho_{33} - \rho_{11})$$
$$\frac{\partial \rho_{14}}{\partial t} = -(\gamma_{14} + i\Delta_{14})\rho_{14} - i\Omega_{pr}(\rho_{44} - \rho_{11})$$

In Eq. (2.27) γ_{nm} represent the dipole diphase relaxation time, Ω_n are the Rabi frequencies for each of the fields and are equal to $\mu_n E_n/\hbar$, and the $\Delta_{nm}=\omega_j - \omega_{nm}$ are the detuning factor from the resonance transition frequencies. In addition, the R_{nm} are the pumping rates for the pump and the probe fields. We have to assume that the probe fields can promote considerable amount of carriers to state $|4\rangle$. The A's are the corresponding relaxation rate for each transition.

In order to solve Eq. (2.27), we need to know their corresponding rate equation for the system. These equations are expressed in terms of population densities and at the end, correlated with the density matrix, they are

$$\begin{aligned}
\frac{dN_1}{dt} &= R_{13}N_1 + R_{31}N_3 - W_{12}N_1 + W_{21}N_2 + A_{21}N_2 - R_{14}N_1 + R_{41}N_4 \\
\frac{dN_2}{dt} &= W_{12}N_1 - W_{21}N_2 + A_{32}N_3 - A_{21}N_2 \\
\frac{dN_3}{dt} &= R_{13}N_1 - R_{31}N_3 - A_{32}N_3 \\
\frac{dN_4}{dt} &= R_{14}N_1 - R_{41}N_4 \\
N &= N_1 + N_2 + N_3 + N_4
\end{aligned} \tag{2.28}$$

Solving the above set of equations for the steady state case. Assuming that the relaxation rate is $A_{32}>>A_{21}$, the non-radioactive decay rate A_{32} is dominant over the pumping rate $R=R_{13}=R_{31}$, and that $R'=R_{14}=R_{41}$, we can obtain for susceptibilities, using the equations below

$$P = \chi E = N\,Tr(\rho\mu) \tag{2.29}$$

$$\begin{aligned}
\chi_s &= \frac{N\mu_{12}^2}{\hbar}\frac{(\rho_{22}-\rho_{11})}{(\Delta_{12}-i\gamma_{12})} \\
\chi_p &= \frac{N\mu_{13}^2}{\hbar}\frac{(\rho_{33}-\rho_{11})}{(\Delta_{13}-i\gamma_{13})} \\
\chi_{pr} &= \frac{N\mu_{14}^2}{\hbar}\frac{(\rho_{44}-\rho_{11})}{(\Delta_{14}-i\gamma_{14})}
\end{aligned} \tag{2.30}$$

Where N is the density of the rare earth atoms in the system. Using the rate equations to calculated the population difference, we get for the total susceptibility at the signal field

$$\chi_s(\omega_s) = \frac{nNc\sigma_s^{peak}}{\omega_s}\frac{(\delta_s+i)}{1+\delta_s^{\,2}}\frac{\left(\frac{I_p}{I_p^{th}}-1\right)}{\left(\frac{I_s}{I_s^{sat}}+1\right)\left(\frac{I_p}{I_p^{th}}+\frac{I_{pr}}{I_{pr}^{th}}+1\right)} \tag{2.31}$$

In the Eq. (2.31) n is the index of refraction, $\sigma_s^{peak} = {2\mu^2\omega_s}/{nc\varepsilon_o\hbar\Delta\omega_{12}}$, and we have defined the dipole relaxation time to be equal to twice the FWHM of the homogeneously broadened transition, or $\gamma_{12}=\Delta\omega_{12}/2$. The detuning normalized factor is defined as

$$\delta_j = \frac{2\cdot(\omega_j-\omega_{mn})}{\Delta\omega_{mn}} \tag{2.32}$$

If the intensity of the probe beam in Eq. (2.31) is neglected, we recover the same result of Desurvire [30]. In that case, there is a resonance enhancement of the refractive index due to the presence of the pump field. On the other hand, if there is no pump field and no probe field, then the susceptibility is the same as the case of a two level system, which is described in [31]. Eq. (2.31) is the total signal susceptibility. To get the nonlinear susceptibility, we expand Eq. (2.31) in powers of I_s and retain the linear terms in I_s, that gives us

$$\chi_s(\omega_s) = \frac{nNc\sigma_s^{peak}}{\omega_s}\frac{(\delta_s + i)}{(\delta_s^2 + 1)}\frac{\left(\frac{I_p}{I_p^{th}} - 1\right)}{\left(\frac{I_p}{I_p^{th}} + \frac{I_{pr}}{I_{pr}^{th}} + 1\right)}\left(1 - \frac{I_s}{I_s^{sat}} + ...\right) \tag{2.33}$$

Using the expression $\chi = \chi^{(1)} + 3\chi^{(3)}\left|\mathcal{E}^2\right| + ...$, we get for the real part of the third order nonlinear susceptibility

$$\chi_s^{(3)}(\omega_s) = \frac{n^2\varepsilon_o Nc^2\sigma_s^{peak}}{\omega_s \bar{I}_s^{sat}}\frac{\delta_s}{(\delta_s^2 + 1)}\frac{\left(1 - \frac{I_p}{I_p^{th}}\right)}{\left(\frac{I_p}{I_p^{th}} + 1\right)^2} \tag{2.34}$$

The linear susceptibility at the probe field is given by

$$\chi_{pr}(\omega_{pr}) = \frac{nNc\sigma_{pr}^{peak}}{\omega_s}\frac{(\delta_{pr} + i)}{1 + \delta_{pr}^2}\frac{\left(\frac{I_p}{I_p^{th}} - 1\right)}{\left(\frac{I_p}{I_p^{th}} + \frac{I_{pr}}{I_{pr}^{th}} + 1\right)} \tag{2.35}$$

Expanding Eq. (2.35) in term of powers of I_{pr}, and retaining only the linear terms in I_{pr}, we obtain for the nonlinear susceptibility at the probe field frequency as a function of pump power I_p

$$\chi_{pr}^{(3)} = \frac{n^2\varepsilon_o Nc^2\sigma_{pr}^{peak}}{\omega_s \bar{I}_{pr}^{sat}}\frac{\delta_{pr}}{\delta_{pr}^2 + 1}\frac{\left(\frac{I_p}{I_p^{th}} + 2\right)}{\left(\frac{I_p}{I_p^{th}} + 1\right)^2} \tag{2.36}$$

Eq. (2.34) and Eq. (2.36) show a pump-power functional dependency that is nontrivial in the sense that you may expect an increase in the nonlinear susceptibility. This is owed to the fact that the total susceptibility increased with the pump laser [32].

The reason why the susceptibility decreased can be explained by the fact that the nonlinear susceptibility is proportional to the higher moments of the charge density distribution. When the pump field is turned on, the charge distribution is altered and the charge density is modified. The pump field depletes the ground state from carriers that may participate in the other transitions (i.e. probe, signal). Fig. 3 shows the dependency of the normalized nonlinear susceptibility as the pump power is increased for the probe and the signal field.

In Fig. 3 we can see that the nonlinear susceptibility of the signal field become zero when the intensity of the pump is equal to the threshold pump intensity for population inversion. This is a nonlinear case of electromagnetically induce transparency [33]. The reason for the vanishing of the nonlinear susceptibility is simple, there is a long live upper energy level. As the intensity of the pump increases the system will reach a point where the population in the lower level is the same as in the upper level, and the system is bleach. At this point there is a reduction of the absorption with a consequent increased in the refraction through the KK relation. Classically in a two level system this will be the end of the story, but if another energy level comes into play then there is possible to invert the population, and the system will show optical gain, which is the case for the laser. However if a second laser is turn on such as to couple the level of the first transition to a third level then the absorption experience in the first transition can be switched off. Therefore changing the refractive index. Because the nonlinear refractive index follows the same KK dispersion relations then the same argument can also be applied to this case.

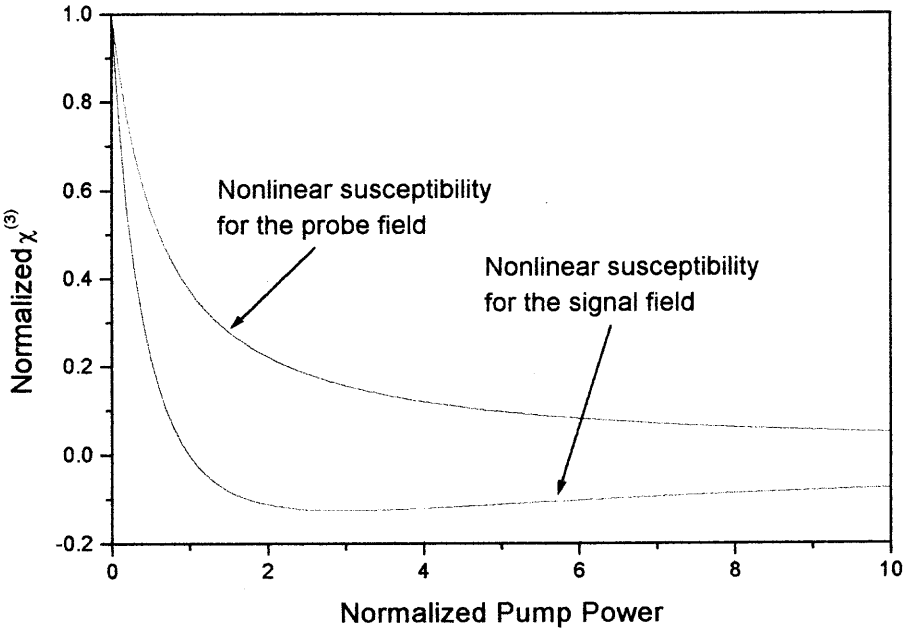

Figure 2.3 Decrease of the nonlinear susceptibility due to the presence of a pump field, in the case of the probe and the signal field.

CHAPTER 3

THE THEORY OF SELF-PHASE MODULATION

3.1 Self-Phase Modulation

When a high intensity optical pulse propagates in a nonlinear responding medium, it will experience phase modulation. This phenomena known as Self-Phase Modulation (SPM), was first observed [34] in the context of transient self-focusing of optical pulses propagating in a solution of a CS_2-filled cell. The observation of SPM in solids and glasses was done by Alfano and Shapiro using picoseconds pulses [35]. In optical fibers, the first experimental observation [36] of SPM was done using fiber with a core filled with CS_2. Stolen and Lin [37] performed a systematic study of SMP in silica glass fiber using picoseconds laser pulses.

Self-phase modulation is the process by which an ultrashort optical pulse propagating in a condensed medium changes the index of refraction of the medium. The medium in turn imposes a phase change on the optical pulse. SPM is a totally refractive phenomenon, and is due to the intensity dependent refractive index. This can be seen in the following form. When an optical pulse propagates in a solid medium, it suffers a phase change given by,

$$\delta\phi = \bar{n}k_o L = (n + n_2 I)k_o L \tag{3.1}$$

In the above equation, n_o is the refractive index of the system, n_2 is the nonlinear index of refraction, or Kerr coefficient, L is the medium length, I is the intensity of the pulse, and $k_o = 2\pi/\lambda_o$. The Kerr coefficient causes the frequency of the leading edge of the pulse to decrease or red-shifted while the frequencies of the trailing edge of the pulse

increases or gets blue-shifted. This can be seen in Fig. 3.1. In Fig. 3.2., the instantaneous frequency of the pulse has been plotted as a function of pulse width using the equation

$$\omega(t) = \frac{d\delta\omega}{dt} = \omega_o\left(1 - \frac{n_2 L}{c}\frac{\partial I(t)}{\partial t}\right) \tag{3.2}$$

assuming a Gaussian pulse shape.

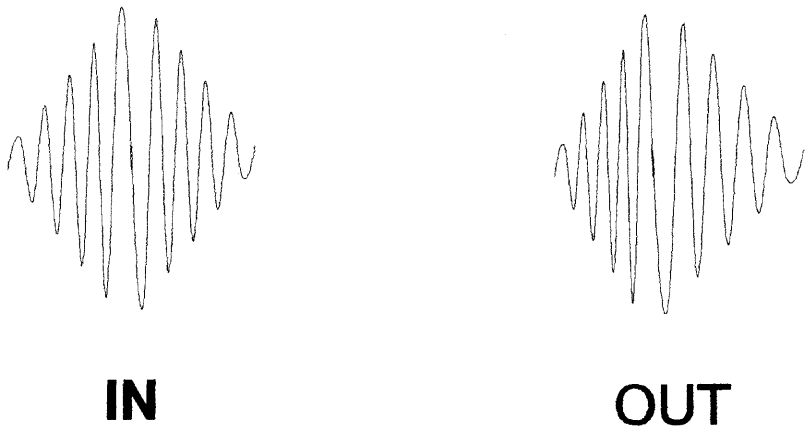

Figure 3.1 Self-phase modulated pulse before and after passing through an optical Kerr medium.

In order to understand self-phase modulation it is necessary to derive the equation that governs the optical pulse propagating in nonlinear media.

3.2 Nonlinear Wave Equation

To derive the nonlinear wave equation we will follow [38]. We start with the Maxwell equations for the electric and magnetic field ***E*** and ***H*** using Gaussians units

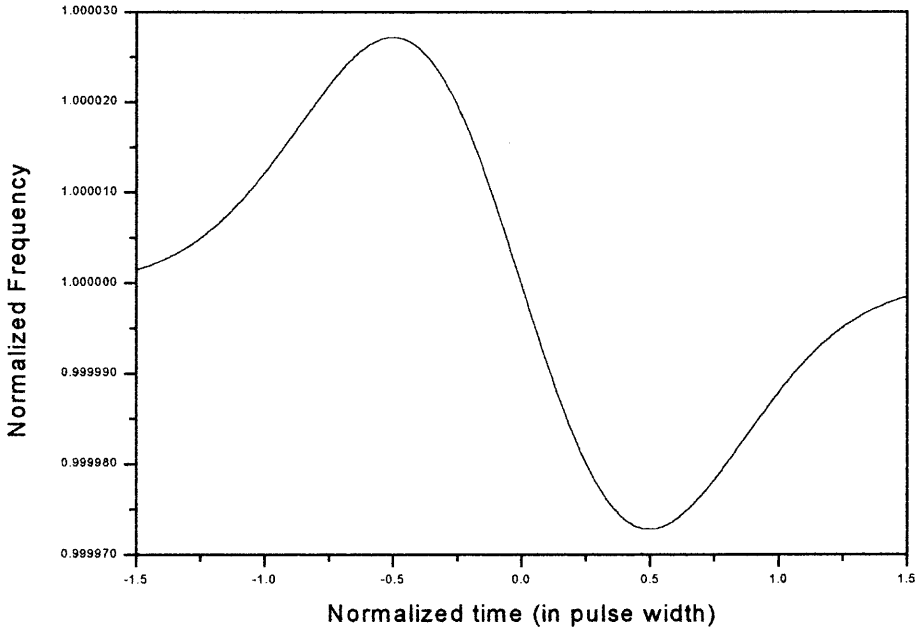

Figure 3.2 Effect of the intensity dependent refractive index n_2 on an optical pulse. The leading edge frequencies of the pulse decrease, while the trailing edge frequencies of the pulse increase.

$$\begin{aligned} \nabla \times E &= -\frac{1}{c}\frac{\partial B}{\partial t} \\ \nabla \times H &= \frac{1}{c}\frac{\partial D}{\partial t} + \frac{4\pi}{c}J \\ \nabla \cdot D &= 4\pi\rho \\ \nabla \cdot B &= 0 \end{aligned} \tag{3.3}$$

where $\boldsymbol{D}=\varepsilon\boldsymbol{E}$, $\boldsymbol{B}=\mu\boldsymbol{H}$, and $\boldsymbol{J}$ and ρ are the current and charge densities. In the case of nonmagnetic materials $\boldsymbol{B}=\boldsymbol{H}$. As was stated before, the refractive index of an isotropic material possessing an intensity-dependent nonlinear refractive index can be written as

$$n(\omega) = [\varepsilon(\omega)]^{1/2} = n_o(\omega) + n_2|E|^2 \tag{3.4}$$

To obtain the wave equation we used the identity $\nabla\times(\nabla\times\boldsymbol{E})=\nabla(\nabla\cdot\boldsymbol{E})-\nabla^2\boldsymbol{E} \approx -\nabla^2\boldsymbol{E}$ and neglected the $(n_2)^2$ term. In the absence of sources, Maxwell equations can be simplified into the wave equation. From Eq. (3.3) we get

$$\nabla^2 E(r,t)-\frac{1}{c^2}\frac{\partial^2 D_L(r,t)}{\partial t^2}=\frac{2n_o n_2}{c^2}\frac{\partial^2(|E|^2 E(r,t)}{\partial t^2} \tag{3.5}$$

because the pulse is confined in a single direction. Eq. (3.5) can be average over the x and y coordinates, assuming that the radial distribution is nearly constant, and neglecting second order spatial derivatives we get for the wave equation,

$$\frac{\partial^2 E(z,t)}{\partial z^2}-\frac{1}{c^2}\frac{\partial^2 D_L(z,t)}{\partial t^2}=\frac{2n_o n_2}{c^2}\frac{\partial^2(|E|^2 E(z,t)}{\partial t^2} \tag{3.6}$$

Using plane wave solution in Eq. (3.6) of the form

$$E(z,t)=A(z,t)\exp[i(k_o z-\omega_o t)] \tag{3.7}$$

where ω_o is the carrier frequency, k_o is the carrier wave number, and $A(z,t)$ is the pulse envelope function. Expressing the displacement vector in terms of Fourier transforms as,

$$\begin{aligned} D_L(z,t) &= \int_{-\infty}^{+\infty} n_o^2(\omega)\tilde{E}(z,\omega)\exp(-i\omega_o t)d\omega \\ \tilde{E}(z,\omega) &= \frac{1}{2\pi}\int_{-\infty}^{+\infty} E(z,t)\exp(i\omega t)dt. \end{aligned} \tag{3.8}$$

Using the above equation, the second derivative of the displacement vector can be written in the form

$$-\frac{1}{c^2}\frac{\partial^2 D_L(z,t)}{\partial t^2}=-\frac{1}{2\pi}\int_{-\infty}^{+\infty}\int_{-\infty}^{+\infty} k^2(\omega)A(z,t')\exp[i\omega(t'-t)]\exp[i(k_o z-\omega_o t')]d\omega\, dt' \tag{3.9}$$

We can arrive at the above equation by expanding $k^2(\omega)$ in a Taylor series around the carrier frequency ω_o or

$$k^2(\omega) \approx k_o^2 + 2k_o k_o^{(1)}(\omega-\omega_o) + k_o k_p^{(2)}(\omega-\omega_o)^2 + \cdots, \quad (3.10)$$

where $k_o^{(1)} = 1/v_g$ is the inverse of group velocity, and $k_o^{(2)}$ is the inverse of the group velocity dispersion. Substituting Eq. (3.10) into Eq. (3.9) and using the following properties of the Dirac Delta function

$$\begin{aligned} &\frac{1}{2\pi}\int_{-\infty}^{+\infty}(\omega-\omega_o)^n \exp[i(\omega-\omega_o)(t'-t)]d\omega = \delta^{(n)}(t'-t) \\ &\int_{-\infty}^{+\infty}\delta^{(n)}(t-t_o)f(t)dt = \left.\frac{d^n f(t)}{dt^n}\right|_{t=t_o} \end{aligned} \quad (3.11)$$

Eq. (3.9) becomes

$$\left[k_o^2 A + i2k_o k_o^{(1)}\frac{\partial A}{\partial t} - k_o k_o^{(2)}\frac{\partial^2 A}{\partial t}\right]\exp[i(k_o z - \omega_o t)] \quad (3.12)$$

Neglecting the second derivatives of the envelope function (slowly varying envelope approximation), we get for the first term on the left-hand side of Eq. (3.6)

$$\frac{\partial^2 E(z,t)}{\partial z^2} \approx \left[-k_o^2 A(z,t) + 2ik_o\frac{\partial A(z,t)}{\partial z}\right]\exp[i(k_o z - \omega_o t)] \quad (3.13)$$

and for the term on the right hand side of Eq. (3.6),

$$\frac{n_o n_2}{c^2}\frac{\partial^2 |E|^2 E}{\partial t^2} \approx -\frac{n_o n_2 \omega_o^2}{c^2}|A|^2 A\exp[i(k_o z - \omega_o t)], \quad (3.14)$$

Inserting Eqs. (3.12) to (3.14) into Eq. (3.6), we get the wave equation for the evolution of the pulse envelope

$$i\left(\frac{\partial A}{\partial z} + \frac{1}{v_g}\frac{\partial A}{\partial t}\right) - \frac{1}{2}k_o^{(2)}\frac{\partial^2 A}{\partial t^2} + \frac{\omega_o}{2c}n_2|A|^2 A = 0 \quad (3.15)$$

Eq. (3.15) is known as the Nonlinear Schrödinger Equation (NSE)[39]. The first two terms describe the envelope evolution at the group velocity υ_g; the third term determines the temporal pulse broadening due to group velocity dispersion; the fourth term describes the second order of the nonlinear polarization. This term is responsible for self-phase modulation and spectral broadening of the pulse.

Eq. (3.15) can be further simplified by defining normalized variables such, as

$$\tau = \frac{\left(t - z/\upsilon_g\right)}{T_o}, \qquad A = \sqrt{P_o}\exp(-\alpha z/2)U \tag{3.16}$$

where T_o and P_o are related to the width and peak power of the pulse. Defining $\gamma = n_2\omega_o/cA_{eff}$ and using the Eq. (3.16) into Eq. (3.15), we obtain

$$i\frac{\partial U}{\partial z} = \pm\frac{1}{2L_D}\frac{\partial^2 U}{\partial \tau^2} - \frac{1}{L_{NL}}e^{-\alpha z}|U|^2 U \tag{3.17}$$

where L_{NL} = nonlinear length = $1/\gamma P_o$, and L_D = dispersion length = $\frac{T_o^2}{|\beta_2|}$. The sign of Eq. (3.17) depends on dispersion regime. In the case of normal dispersion or $\beta_2 > 0$, the + sign is chosen, or minus in the case of anomalous dispersion or $\beta_2 < 0$. Depending on the relative magnitude of the fiber length L compared with L_D and L_{NL}, Eq. (3.17) describes different regimes.

If the fiber length is such that $L \ll L_{NL}$ and $L \approx L_D$, the nonlinear term can be neglected and the system is in the dispersion-dominant regime. In this case, the pulse broadens. In the case of a simple unchirped Gaussian pulse, $U(0,\tau)=\exp(-\tau^2/2)$, the pulse broadens by a factor of $(1+z^2/L_D)^{1/2}$ as it propagates along the fiber. The dispersion-dominant regimen is relevant when the condition below is such that

$$\frac{L_D}{L_{NL}} = \frac{\gamma P_o T_o}{|\beta_2|} << 1 \tag{3.18}$$

The nonlinear-dominant regime is such that $L << L_D$, while $L \geq L_{NL}$. In this case, the dispersion term can be neglected and we obtain from Eq. (3.17),

$$i\frac{\partial U}{\partial z} = -\frac{1}{L_{NL}} e^{-\alpha z} |U|^2 U \tag{3.19}$$

This equation admits solutions of the form

$$U(z,\tau) = U(0,\tau)\exp\left[i\phi_{SPM}(z,\tau)\right], \tag{3.20}$$

where

$$\phi_{SPM}(z,\tau) = \phi_o + \left(\frac{1-e^{-\alpha z}}{\alpha L_{NL}}\right)|U(0,\tau)|^2 \tag{3.21}$$

The above two equations implied that as the pulse propagates in the nonlinear medium, the pulse enveloped does not change its shape. The second equation tells us that because of the nonlinear index, the pulse suffers a phase modulation or phase change. This additional phase change is the shift experienced by the pulse as it propagates from the point 0 to z in the nonlinear medium.

Fig. 3.3 shows the spectra for a Gaussian pulse obtain by taking the Fourier transform of Eq. (3.20) in the case of zero absorption, and z=10L_{NL}. It can be seen that the pulse spectrum increases as the pulse propagates in the nonlinear medium.

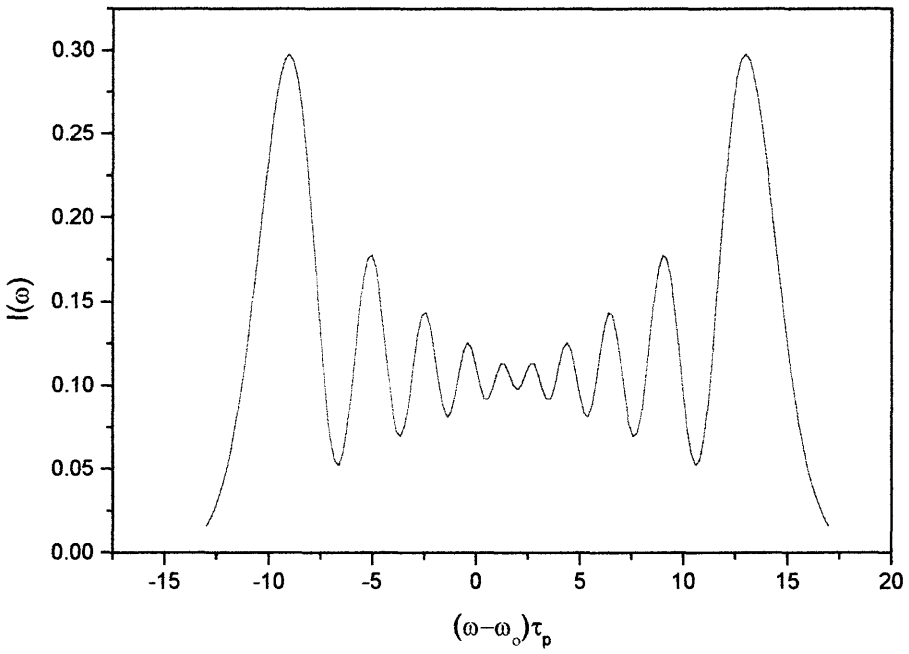

Figure 3.3 Calculated spectrum for a Gaussian pulse of width τ_p at a distance $z=10L_{NL}$. The SPM is calculated by taking the Fourier transform of Eq. (3.20).

In the case that the fiber length is longer than the two-length scales of the system L_D and L_{NL}, dispersion and nonlinearities act together as the pulse propagates along the nonlinear medium. When the group velocity dispersion is compensated by the self-phase modulation, Eq. (3.17) admits solitons solution or nondispersive energy solutions.

3.3 Another Point of View of the NLS Equation

Eq. (3.17) is also known in quantum field theory as the *Gross-Pitaeveskii equation* [40]. In quantum field theory, it is used to describe the breaking of the gauge invariant in superfluity and superconductivity [41]. The envelope function is the condensate wave function or the order parameter in a Bose-Einstein system. It represents the amplitude to

annihilate a particle at any point **x**. This amplitude is proportional or of the order of $N^{1/2}$, and it is expressed as

$$\psi(x) = \langle N-1|\hat{\Psi}(x)|N\rangle = O(N^{1/2}) \tag{22.0}$$

where N is the number of particles in the ground state, represented by $|N\rangle$. This condition is called in condensed matter physics "off-diagonal long range order" (ODLRO), and was introduced by Yang [42]. The *Gross-Pitaeveskii equation* can be easily derived by assuming that in a condensate, particles interact through a δ-function potential of strength g. In this case, each atom feels an additional potential proportional to the local density of the condensate. This additional interaction can be included in the Schrödinger equation to account for the atom-atom interaction. The *Gross-Pitaevskii* (GP) was introduced originally to explain some of the properties of the Bose condensation state at T=0 temperature. The equation can be written as

$$-\frac{1}{2m}\nabla^2\psi + g\psi^*\psi^2 = i\hbar\frac{\partial\psi}{\partial t} \tag{3.12}$$

Today there are very active areas of research in condensed-matter physics in the field of Bose-Einstein condensation in diluted gases [43].

This close similarity with the NSE may allow one to use some of the results in the solid state physics in the field of optics. It is remarkable that the structure of the excitations predicted by Eq. (3.12) such as solitions and vortices can also be found in Eq. (3.17), but in the temporal domain. When we discuss temporal solitons in the NSE in the GP equation, we talk about spatial solitons and vortices. There is a vast amount of research in terms of solving analytically and numerically the GP equations that can be applied to optics. One intriguing aspect is the formation of multiple solitons and self-

steepening of optical pulses propagating in a nonlinear media. Here, modulation instabilities may affect the pulse shape and produce a transition to infinity of the bandwidth of the pulse. This phenomenon can be called an *optical phase transition.* It will be interesting to study this matter under the scope of the GP equation.

CHAPTER 4

TWO-BEAM COUPLING IN A SLOW RESPONDING MEDIUM

4.1 Two-Beam Coupling

Under certain circumstances, when two beams intercept in a nonlinear medium, energy can be transferred from one beam to the other. Two-beam coupling is a process that is automatically phase matched. The central argument in a two-beam coupling experiment is that the refractive index change experienced by one beam is modified by the intensity of the other beam.

There are several physical mechanisms that cause energy transfer, such as; nonlinear response of a two-level system to pump-probe fields, stimulated Brillouin scattering, and stimulated Raman scattering. In the next section, it will be shown that in photorefractive material, energy transfer can be accomplished by the formation of an intensity-dependent grating.

The intensity dependent refractive index is not the only mechanism through which grating formation is possible. There are separate physical processes that can give rise to index gratings. These include the photorefractive effect mentioned above, Drude refractive index gratings, and absorption gratings [44]. An interesting point to consider for the cubic and ferroelectric oxides is that no energy is transferred for long delays, compared to the pulse width. However in the case of semiconductors, there is an absorption background that persists even for long pulse delays long compared to the pulse width [45]. This occur in semiconductors because the mechanisms to produce free carrier grating is stronger in semiconductors than in the oxides, due to the large drift

carrier mobility and long recombination lifetimes [46]. In two-beam coupling, all the processes described can be present.

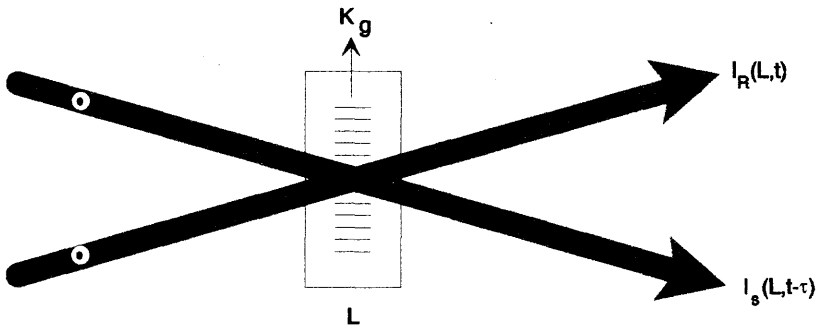

Figure 4.1 Beam geometry for two-beam energy coupling experiment. The intersection angle in the crystal is 2θ. Both beams are polarized perpendicular to the plane of the figure.

The effect of grating formation analyzed by S. L. Palfrey *et al* [47] will be described in detail. In this case, phase gratings are associated with the real part of the third-order nonlinear susceptibility, while amplitude gratings are associated with the imaginary part of the third-order nonlinear susceptibility (absorption gratings). The difference between the absorption grating and the phase grating can be understood as follows: when the pulses are mutually coherent in the sample, they set up a spatial modulation in the medium's optical properties. This induced grating can scatter radiation in the probe direction, affecting the probe intensity. For transformed limited pulses, the scattered radiation will be in phase with the probe if the grating comes from the modulation of the absorption coefficient (amplitude grating). On the other hand, if the grating is formed from a modulation in the refractive index (phase gratings), then the

scattered light will be in quadrature with the probe, unless the pulses forming the grating have some degree of phase modulation [47].

When two beams are combined in a medium, the optical susceptibility of the medium is modified by the presence of the beams. At the same time, the beams are modified by the susceptibility change. Because the fields cannot act instantaneously and the change in the susceptibility can only influence the field at later times (causality), the third-order nonlinear polarization at frequency ω is given by

$$P_i^{(3)}(t) = E_j(t)\int_{-\infty}^{\infty} dt' E_k^*(t') E_l(t')\left[A'_{ijkl}(t-t') - iA''_{ijkl}(t-t')\right] \tag{4.0}$$

In the above equatio, A_{ijkl} are the real and imaginary components of the third-order nonlinear susceptibility tensor. In the pump-probe measurement, the total electric field E consists of the sum of the pump field E_1 and the probe field E_2 Using the optical theorem, the rate of energy loss due to this polarization for the probe beam is

$$W = \mathrm{Im}\left\{\int_{-\infty}^{\infty}\int_{V} E_2^* \cdot P^{(3)} dt dr\right\} \tag{4.1}$$

If the angle between the probe and pump beam is small, and assuming that the fields are polarized along the x-direction, the only term that contributes to the total energy is the A_{xxxx}. Out of the 2^4 combination of the fields i,j,k,l=1,2, the terms with i=1 (2^3) describe the change of the pump intensity which are not measured. From the remaining combinations, 8 are integrated over the small area along the y-direction and can be neglected. The term with 2222 is a selfmodulation of the probe, which is a small effect. Therefore the only terms are 2211 and 2112. Eq. (4.1) can be written as:

$$W = \mathrm{Im}\left\{\int_{-\infty}^{\infty} E_2^*(r,t) E_1(r,t) \int\int_{-\infty V}^{t} E_1^*(r',t') E_2(r',t') \times \left[A'(r-r',t-t') + iA''(r-r',t-t')\right] dr'\, dt'\, dt\right\}$$

$$+\mathrm{Im}\left\{\int_{-\infty}^{\infty} E_2^*(r,t)E_2(r,t)\int_{-\infty V}^{t}\int E_1^*(r',t')E_1(r',t')\times[A(r-r',t-t')+iA''(r-r',t-t')]dr'\,dt'\,dt\right\} \quad (4.2)$$

In the case of the pump-probe experiment, the probe beam is just a replica of the pump beam delayed by τ seconds, expressed as

$$E_1(t)=E(t) \quad (4.3)$$

and

$$E_2(t)=E(t-\tau)e^{i\omega\tau} \quad (4.4)$$

Substituting Eq. (4.3) and Eq. (4.4) into Eq. (4.2), the second term in Eq. (4.2) can be expressed as

$$S_2 = \int_{-\infty}^{\infty}\int_{-\infty V}^{t}\int |E(t')|^2 |E(t-t')|^2 A''(t-t')dtdt'\,dr \quad (4.5)$$

Eq. (4.5) is called the incoherent term. As can be seen, it depends on the convolution of the intensity autocorrelation function of the electric field with the response function A'' for the induced bleaching or absorption. The response function for this term can be expressed as

$$A''(t-t') = a_{pop}\exp\left(-\frac{t-t'}{\tau_{pop}}\right) \quad (4.5a)$$

In the above equation, a_{pop} is proportional to the absorbing carrier density, and τ_{pop} is the effective reorientational diffusion time. We will touch on this later to prove that in the case of oxides like $BaTiO_3$, $KnbO_3$ this term is very small compared with the case of GaAs:Cr or CdMnTe:V, where a constant background can be observed in a two-beam coupling experiment. Any phase information that may be contained in the pulse is lost through this term. It is worth noting that this term will persist as long as the material

response persists. This mean that it is not necessary for the pulses to be overlaped in time. The incoherent term is, strictly speaking an absorption term, because it depends on the imaginary part of the nonlinear susceptibility (see Apendix A for details).

The first term can be broken into two terms; the fist term is given by

$$S_1'(\tau) = \mathrm{Re}\left\{\int_{-\infty}^{\infty}\int_{-\infty}^{t}\int_{V} E^*(t-\tau)E(t)E^*(t')E(t'-\tau)A''(t-t')dtdt'\,dr\right\} \qquad (4.6)$$

and the second term by

$$S_1(\tau) = \mathrm{Im}\left\{\int_{-\infty}^{\infty}\int_{-\infty}^{t}\int_{V} E^*(t-\tau)E(t)E^*(t')E(t'-\tau)A'(t-t')dtdt'\,dr\right\} \qquad (4.7)$$

it is interesting to see that both terms will give you phase information. Both terms are called the coherent contribution. In the case of pure refraction, the first term will be equal to zero. The term in Equation (4.6) is symmetrical around the delay time τ, because if τ is substituted with $-\tau$, the term remains the same.

In the case considered here, the contribution of the first term in the coherent contribution can be neglected. Since the grating generated by the first term is a fast responding grating which depends entirely on population differences, it is faster than the pulse maximum delay time T. Secondly, the refraction grating (which can be thermal or photorefractive in origin) is the consequence of many pulses accumulated over many T periods. This is called a slow-responding medium. After many T periods, the grating is formed and is driven into a steady state. In this case, the analysis of Kukhtarev [48] can be applied.

To simplify the second term, assume a model for the response function of the medium. In the case of a slow responding medium, it is possible to assume that the real component can be expressed as

$$A'(r-r',t-t') = a_{ph} e^{\left(\frac{t-t'}{\tau_{ph}}\right)} \delta(r-r') \tag{4.8}$$

in Eq. (4.8) τ_{ph} is mostly due to the photorefractive effect, which is long compared to the period of the train of pulses. For most commonly known slow responding material, the grating response time is of the order of milliseconds or longer (even for the case of semiconductors). The next step is to substitute into Eq. (4.8) the value for the electric field. This is given by

$$E(r,t) = \sum_{m=-\infty}^{\infty} E(t+mT)\exp(i[k\cdot r - \omega(t+mT)]) \tag{4.9}$$

and for the delay pulse

$$E(r,t-\tau) = \sum_{m=-\infty}^{\infty} E(t+mT-\tau)\exp(i[k\cdot r - \omega(t+mT-\tau)]) \tag{4.10}$$

substituting Eq. (4.8), Eq. (4.9), and Eq. (4.10) into Eq. (4.7), performing the volume integration, and making the following assumptions;

- Consider only the energy transfer to pulse m=0.
- Discard all the contributions from non-overlapping pulses. This will eliminate the double sum in the t' integration.
- The pulse period T is much smaller than the decay grating time τ_{ph}. Since the only relevant time in the response function $A'(t-t')$ is mT, it can be taken out of the t' integration, but not out of the sum.

- The limit of the t' integration can be extended up to infinity because the current pulse is testing the grating made by previous pulses.

Using the above assumptions, Eq. (4.7) becomes

$$S_1(\tau) = \mathrm{Im}\left\{ a_{ph} \sum_{m=-\infty}^{0} e^{-\left(\frac{T}{\tau_{ph}} m\right)} \int_{-\infty}^{\infty}\int_{-\infty}^{\infty} E^*(t-\tau)E(t)E(t'-\tau)E^*(t')dt'\,dt \right\} \qquad (4.11)$$

The sum over m is easy to perform. It will give an enhancement factor as a consequence of the accumulation effects of the grating. In the above equation, the Im expression can be dropped. There is an i factor, because the induced nonlinear polarization is $\pi/2$ out of phase with the pump-probe field. With this in mind, the following equation is obtained:

$$S_1(\tau) = a_{ph}\left(\frac{\tau_{ph}}{T}\right)\left|\int_{-\infty}^{\infty} E^*(t-\tau)E(t)dt\right|^2 \qquad (4.12)$$

This expression can be normalized to 1 when τ=0. By assuming a normalization condition, all information about the physics underlining the grating effect is lost. Eq. (4.12) will provide phase information if the incoming pulse has a time-dependent phase. If the phase in the incoming pulse is time-independent, then the above expression is just a normal autocorrelation [49] measurement of the pulse.

The result of Eq. (4.12) looks identical to the case of Levine *et al* [50]. Originally the expression was used to study phase distortion in nonlinear media, particularly chirped pulses and Self-phase modulated pulses [51]. In our case, we will use it as medium characterization. In [50], it was proved that the same expression could be used for several types of geometries such as three-beam coupling, two-beam coupling, and self-diffraction as are shown in Fig. 4.2. In general, the expression inside the integral sign is commonly

known as correlation function [49]. They are basically a mix of *n* distinct, or the same replicas of light pulses. In the first case the correlation function are called *cross-correlations*, and in the second case they are called *auto-correlations.*

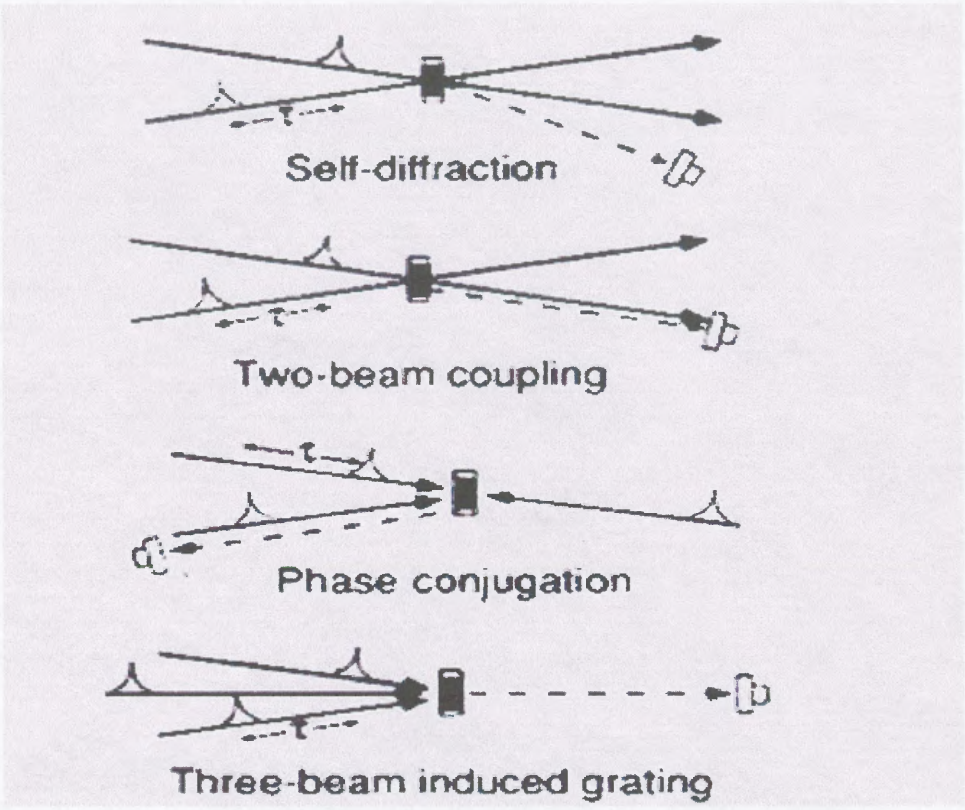

Figure 4.2 Several Geometries for performing IGA experiments [50].

Because the optical pulses are creating a grating from which a secondary pulse or the same pulse can be diffracted off, the experimental setup was called Induced-Grating Autocorrelation or IGA [50,51,52]. Depending on the time response of the medium, it is classified into fast-IGA, slow-IGA, and ultraslow-IGA. Fast-IGA has been applied to measure the third order intensity autocorrelation: It has the advantage of detecting pulse asymmetries [54,55]. On the other hand IGA-slow provides the same phase information as in interferometric Second Harmonic autocorrelation (ISHGA). In the next section, we will prove that the energy detected when two-beams intersect in a slow-responding

medium-like a photorefractive crystal is proportional to the electric field autocorrelation function. It will also be showed that the normalization constant is proportional to the material parameters.

4.2 The Photorefractive Effect

The photorefractive effect is the change of the refractive index on an optical material that results from the optically induced redistribution of charges (holes or electrons). The photorefractive effect is quite different from the other nonlinear effects in the sense that it cannot be described by a nonlinear susceptibility $\chi^{(n)}$ for any order of n. The reason for this effect is that under a variety of steady state conditions, the photorefractive effect is intensity independent [56].

For many electro-optic crystals with typical band gap energy of 2-3 eV, there are energy levels deep in the band-gap region which originate from various imperfections and impurities in the crystal. The index of refraction of some of these crystals may be spatially modulated through photoionization and spatial rearrangement of bound charges in these energy levels or trap-sites. The spatial modulation is due to the light field. The subsequent response of the crystal is the formation of a static space charge electric field. The essential steps involved in the photorefractive process are as follow [57]:

- When two mutually coherent light beams intersect inside a photorefractive crystal, a light intensity pattern is created due to the beams interference. Charges are liberated from trap-sites via photoionization in the regions where the light intensity is nonzero.
- The resulting charges can be moved around in the conduction band via diffusion until they recombine with other ionized or empty traps at other sites. There is a net

migration from regions of high intensity to those of low intensity. This creates a pattern of charges, which follow that of the light intensity pattern.

- An electric field is induced by the charge pattern according to the Poisson equation:

$$\nabla \cdot \vec{E} = \frac{\rho}{\varepsilon_o} \tag{4.13}$$

This electric field pattern mimics the charge and light intensity pattern, but is shifted by $\pi/2$.

- Finally, the space charge electric field induces a spatial modulation of the refractive index through the *linear electro-optic effect*. This is a second-order nonlinear optical response in which the index of refraction at a particular position in the crystal is linearly proportional to the value of the static electric field at that point. It is given by

$$\Delta n_i = \frac{1}{2} n_i^3 r_{ij} \Delta E_j^{sc} \tag{4.14}$$

In the above equation, r_{ij} is the electro-optic coefficient, n_i is the refractive index, and ΔE_j is the space charge field created by the intersection of the two beams.

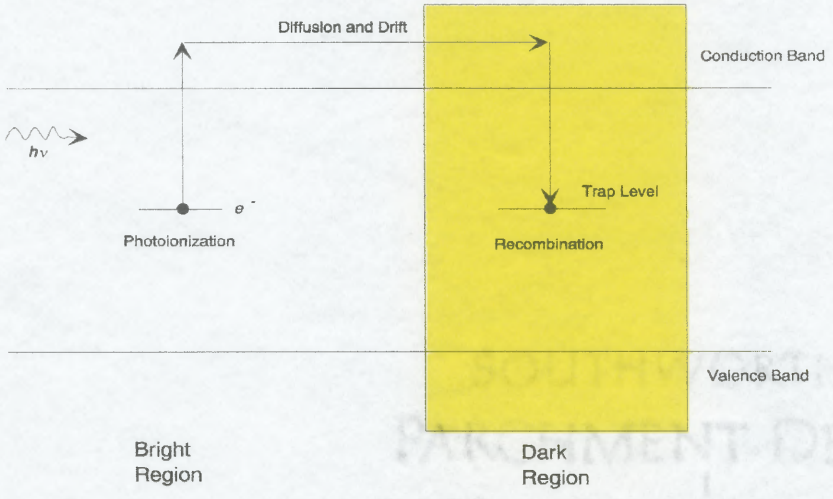

Figure 4.3 Band Trap Model of the photorefractive effect due to *Kukhtarev et al* [48].

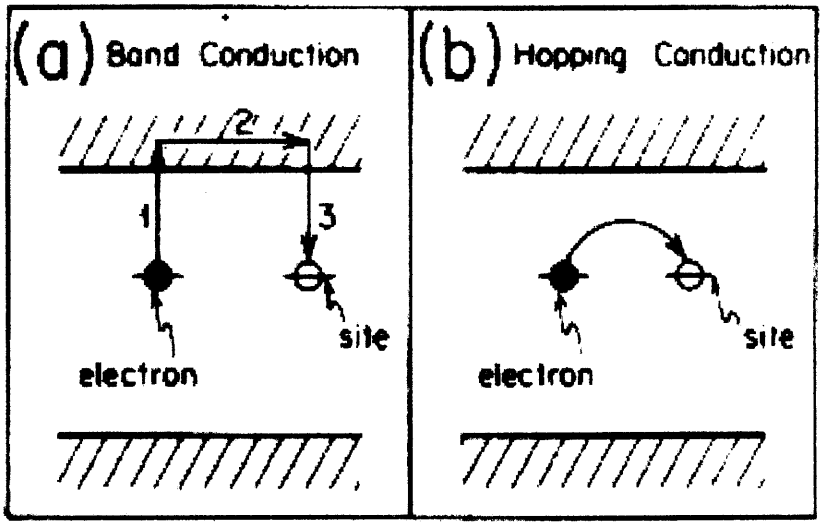

Figure 4.4 Two mechanisms for photoconduction. (a) Band conduction (b) Hopping, which is a single process [57].

The above process is shown in Fig. 4.3. Fig 4.4 shows an alternative mechanism for photorefraction. It is based on the hopping of the carries between traps, and is a single process whereby based on carriers hop between sites through photoassisted tunneling. Depending on the recombination time, both models can give different or the same result [57].

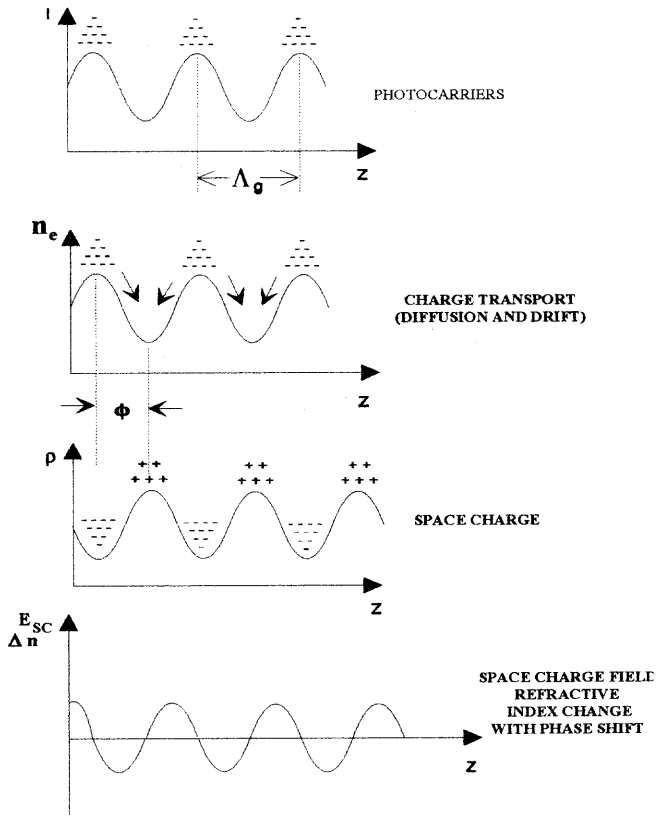

Figure 4.5 Grating formation in a photorefractive material. The space-charge field is in general out of phase with the incident irradiance.

4.3 Theory of Two-Beam Coupling in a Photorefractive Crystal

Here we will consider the coupling of mode-locked laser pulses in a photorefractive crystal [11]. The reason to use photorefractive crystal is that in general, photorefractive materials tend to show long grating formation time, and therefore can be considered as slow-responding media. The time dependent space-charge field is governed by

$$\frac{\partial E_{sc}(r,t)}{\partial t} + aI_o(t)E_{sc}(r,t) = ibE_1(r,t)E_2^*(r,t) \tag{4.15}$$

where the constant a,b are complicated functions of material parameters [58]. The E_{sc} is the magnitude of the space charge field, and E_1, and E_2 are the slow varying complex optical-field envelopes interacting in the medium. In Eq. (4.15) I_o(t) is proportional to the total intensity.

Eq. (4.15) indicates that the space charge field is been driven by the interference term $E_1(r,t)E_2(r,t)$, and is erase by the uniform intensity I_o. There are two limitations to Eq. (4.15). First, it is valid only in the case that the carrier recombination time is much less than the pulse width, and spatial variations can be ignored. Otherwise, Eq. (4.15) must couple with other equations that describe these variations or introduce these variations phenomenologically by assuming a constant background free carrier absorption. Second, fluctuation of the laser pulse in phase or amplitude must be taken into account. In our case, because the pulses generating the grating come for the same laser source these fluctuations can be ignored or assumed they show some degree of correlation.

For a static case situation, the solution to Eq. (4.15) can be averaged over time and be written as

$$E_{sc} = \frac{ib}{a} \frac{\left\langle E_1(r,t)E_1^*(r,t)\right\rangle}{\left\langle \left|E_1(r,t)\right|^2 + \left|E_2(r,t)\right|^2 \right\rangle} \tag{4.16}$$

where the $\langle\rangle$ denotes an average over time T (repetitions rate):

$$\left\langle f(t)\right\rangle = \frac{1}{T}\int_{-T/2}^{T/2} f(t)dt \tag{4.16a}$$

Considering the fact that one pulse is delayed with respect to the other by a time τ_d, Eq. (4.16) can be written as

$$E_{sc} = \frac{ib}{a} \frac{\left\langle E_1(r,t)E_2^*(r,t-\tau_d)\right\rangle}{I_o} \tag{4.17}$$

The next question is to verify that Eq. (4.17) is indeed a steady state solution we numerically integrated Eq. (4.15) using a fourth-order Runge-Kutta method, a transform limited Gaussian pulse in time, and assuming that we have a periodic train of pulses. Fig.

4.6 and Fig. 4.7 show the variation of the space charge field from its steady state solution, for the arrival of a new pulse after the grating has been formed.

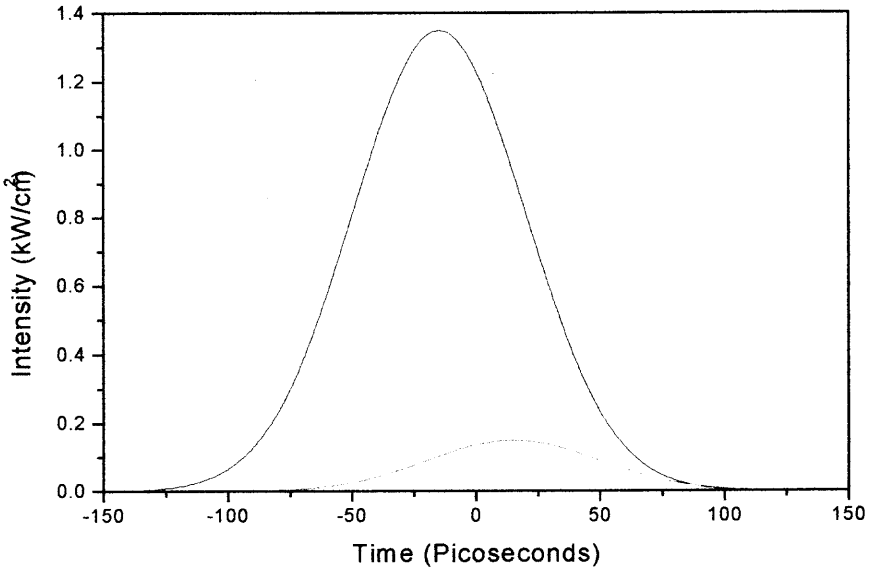

(a)

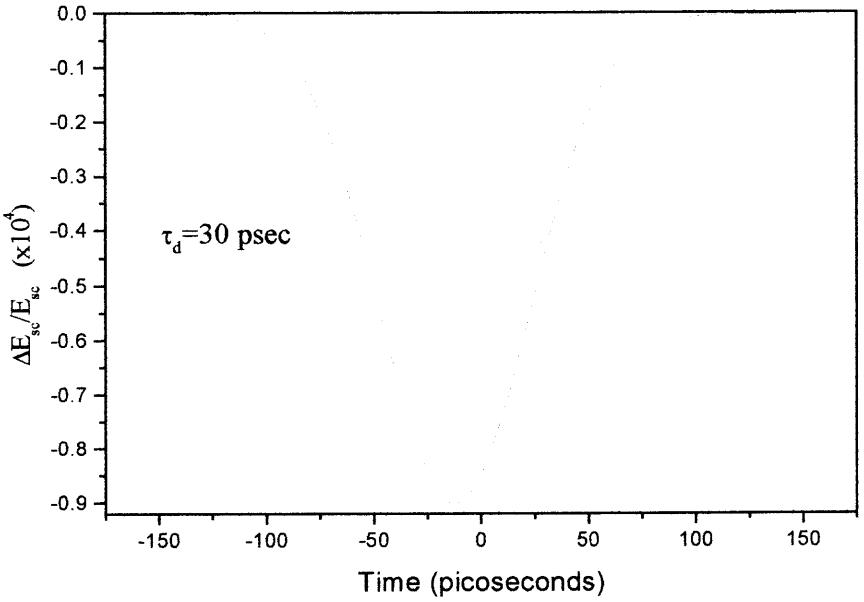

(b)

Figure 4.6 (a) A strong optical beam leads a weak beam by 30 psec. (b) When the two pulses overlap, the space charge field momentarily deviates from its steady state value by 1 part in 10^5.

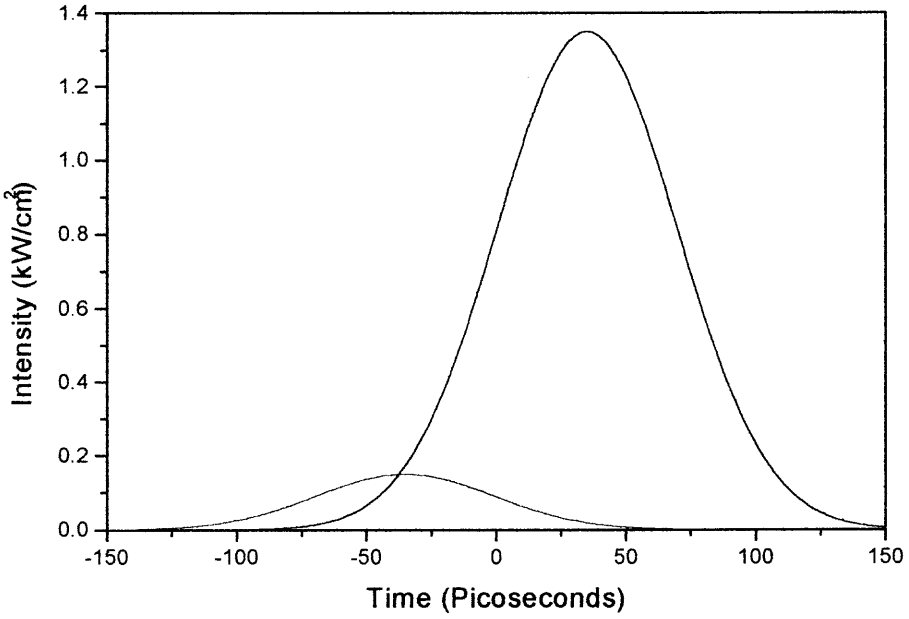

(a)

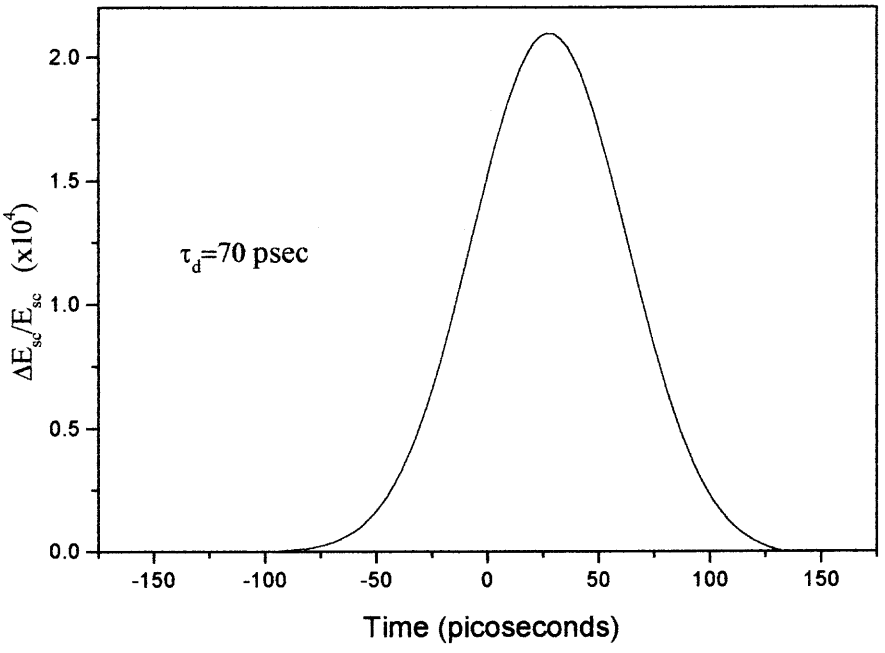

(b)

Figure 4.7 (a) A strong optical beam leads a weak beam by 70 psec. (b) When the two pulses overlap, the space charge field momentarily deviates from its steady state value by 1 part in 10^5.

The interference of the two beams in a photorefractive crystal eventually will produce a quasi-steady state space charge field given by Eq. (4.15). This creates a refractive index grating. We will discuss next how the optical beams are coupled and affected by this grating. To derive the wave equation, we assumed that there are no free currents in the system. Maxwell's equation can be written as

$$\nabla^2 \mathcal{E}(r,t) - \mu_o \frac{\partial^2 \mathcal{D}(r,t)}{\partial t^2} = 0 \tag{4.18}$$

where $\mathcal{E}(r,t)$ is the total electric field inside the crystal, and $\mathcal{D}(r,t)$ is the displacement vector. If we let the total electric field be written as the sum of the two optical beams of the same frequency ω_o, wave vector $\mathbf{k}_1$ and $\mathbf{k}_2$, and polarization ε_1 and ε_2 we have the following equation

$$\mathcal{E}(r,t) = \mathrm{Re}\{[e_1 E_1(r,t)\exp(ik_1 \cdot r) + e_2 E_2(r,t)\exp(ik_2 \cdot r)]\exp(-i\omega_o t)\} \tag{4.19}$$

for the electric displacement, we have

$$\mathcal{D}(r,t) = \mathrm{Re}\{[e_1 D_1(r,t)\exp(ik_1 \cdot r) + e_2 D_2(r,t)\exp(ik_2 \cdot r)]\exp(-i\omega_o t)\} \tag{4.20}$$

and

$$D_i(r,t) = \varepsilon_o \varepsilon(r) \cdot e_i E_i(r,t), \qquad i = 1,2. \tag{4.21}$$

The interference pattern must have periodicity $\cos(\mathbf{k}_g \cdot \mathbf{r})$ and $\mathbf{k}_g \equiv \mathbf{k}_1 - \mathbf{k}_2$. In Eq. (4.21) ε_o is the permittivity of free space, and $\varepsilon(r)$ is the relative dielectric tensor of the medium. The modulation of the electric dielectric tensor is then written as

$$\varepsilon(r) = \varepsilon_r + \mathrm{Re}(\Delta\varepsilon_r \cdot \exp(ik_g \cdot r)) \tag{4.22}$$

the space charge field E_{sc} of Eq. (4.15) will modulated the dielectric tensor by the electro-optic effect given by Eq. (4.17). Substituting Eq. (4.19), Eq. (4.20), Eq. (4.21), and Eq.

(4.22) into Eq. (4.15), we obtain the couple wave equation for the electric field envelopes E_1, and E_2:

$$\frac{\partial|E_1(z,t)|^2}{\partial z} = 2\,\mathrm{Re}(\eta_{12})\left|\left\langle E_1(z,t)E_2^*(z,t-\tau_d)\right\rangle\right|^2 \tag{4.23}$$

$$\frac{\partial|E_2(z,t)|^2}{\partial z} = 2\,\mathrm{Re}(\eta_{21})\left|\left\langle E_1(z,t)E_2^*(z,t-\tau_d)\right\rangle\right|^2 \tag{4.23a}$$

$$\frac{\partial\left\langle E_1(z,t)E_2^*(z,t)\right\rangle}{\partial z} = \frac{\left\langle E_1(z,t)E_2^*(z,t)\right\rangle}{I_o}\left(\eta_{12}|E_1|^2 + \eta_{21}|E_2|^2\right) \tag{4.23b}$$

Assuming that the intensity of the two beams are equal Eq. (4.23b) can be solved to yield

$$\left\langle E_1(z,t)E_2^*(z,t)\right\rangle = \left\langle E_1(0,t)E_2^*(0,t)\right\rangle \exp\left(\frac{I_o}{4}(\eta_{12}-\eta_{21})z\right) \tag{4.24}$$

Substituting Eq. (4.24) into Eq. (4.23), we get for the change in transmission of beam 1

$$\left\langle|E_1(z,t)|^2\right\rangle - \left\langle|E_1(0,t)|^2\right\rangle = \frac{4\eta_{12}}{(\eta_{12}-\eta_{21})}\left|\int_{-t}^{t} E_1(z,t)E_2^*(z,t-\tau_d)dt\right|^2\left[\exp\left(\frac{1}{2}(\eta_{12}-\eta_{21})z\right)-1\right] \tag{4.25}$$

Eq. (4.25) is the central result of this calculation. It says that the transmission change in one of the beams after traversing a distance z in the photorefractive crystal is equal to the electric field autocorrelation function. This is the same result as in [50].

4.4 Photorefractive Crystals

Photorefractive materials such as $LiNbO_3$, $BaTiO_3$, and $Bi_{12}SiO_{20}$ have been investigated in the past for application in holography storage, optical data processing, and phase conjugation [59]. One of the limitations of cubic and ferroelectric oxides is the slow response time and poor efficiency for grating formation in the range 900 ~ 1500 nm. In the case of semiconductors such as GaAs and CdTe, these materials have sensitive [60]

and fast [61] responses However, because of the inherent energy band gap, they are limited to operate in wavelengths longer than ~ 900 nm. In the present work, the photorefractive crystal used is CdMnTe:V. This semiconductor has shown fast response time for grating formation (in the order of msec), and larger sensitivity [62] in the range of 900-1500-nm which is significant for experiments in the fiber communications wavelengths. In the following paragraph we discuss some of the properties of the photorefractive crystals used in experiments described in the next chapters.

4.4.1 $BaTiO_3$

Barium Titanate is a ferroelectric crystal with tetragonal symmetry. The crystal has a pale yellow color. The active material or deep levels are well know to be Fe [63]. $BaTiO_3$ has an absorption spectrum that extends from the 800-nm up to the band edge at 410-nm. Fig. 4.8 shows the absorption as a function of wavelength.

$BaTiO_3$ is known to have one of the highest electro-optic coefficients amount inorganic crystals. The crystal has a large index modulation without an applied electric field in the visible, select dopants are used to enhance the photorefractive properties. The mobility of $BaTiO_3$ is on the order of < 2-cm^2/V-sec, and a mobility-lifetime product < $2x10^{-10}$-cm^2/V [64]. Table 4.1 summarized some of the physical properties of $BaTiO_3$ as well as other photorefractive semiconductors

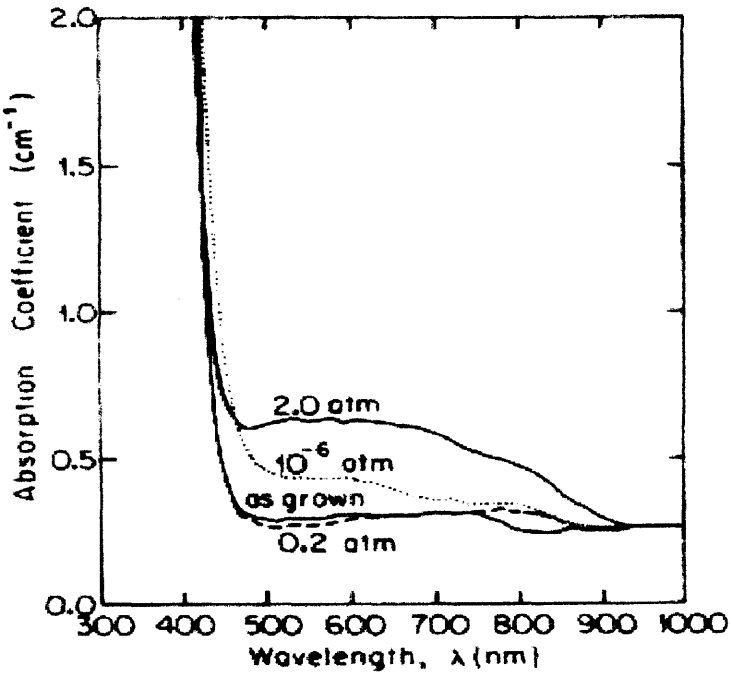

Figure 4.8 $BaTiO_3$ absorption spectrum as a function of Wavelength.

4.4.2 GaAs:Cr

This semiconductor has very fast response time for grating formation. It is known that the deep levels come from intentionally doped with Cr. These deep levels can also arise from stoichiometric defects [46]. The dominant defect in undoped material is a donor called EL2 that is located 0.8 eV below the conduction band. The absorption spectrum is shown in Fig. 4.9. GaAs:Cr exhibit a long tail in the absorption edge compared to InP:Fe also shown in the same figure .

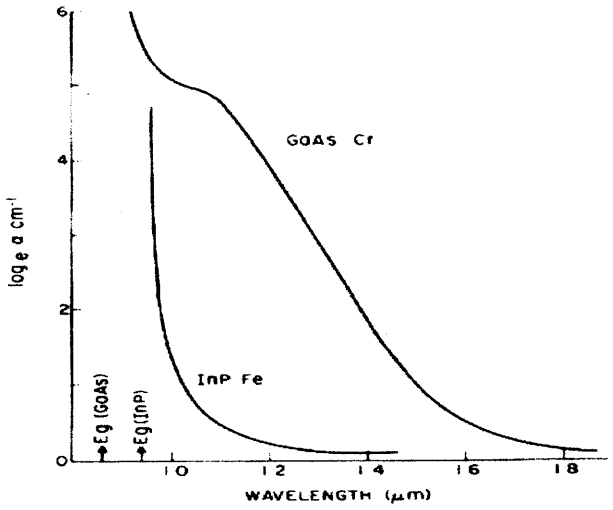

Figure 4.9 Optical Absorption Spectra for GaAs:Cr (~10^{16} cm^{-3}).

GaAs:Cr has excellent response in the IR, but it becomes very absorbing in the visible. GaAs:Cr has very small electro-optic coefficient, and a large mobility of the order of 5000 cm^2/V-sec.

4.4.3 CdMnTe:V

Most of the experiment performed here were done with CdMnTe:V. The bandgap of this material is about 2.1 eV, but it can be modified through band gap engineering, in fact the band gap of $Cd_{1-x}Mn_xTe$:V varies with mole fractions as 1.53 + 1.26x eV [65]. The grow CdMnTe is not difficult. The challenging task is to make then photorefractive. The major reason is the incorporation of Vanadium deep centers that act a recombination and trap centers for photorefraction. The transmission spectrum is shown in Fig. 4.10.

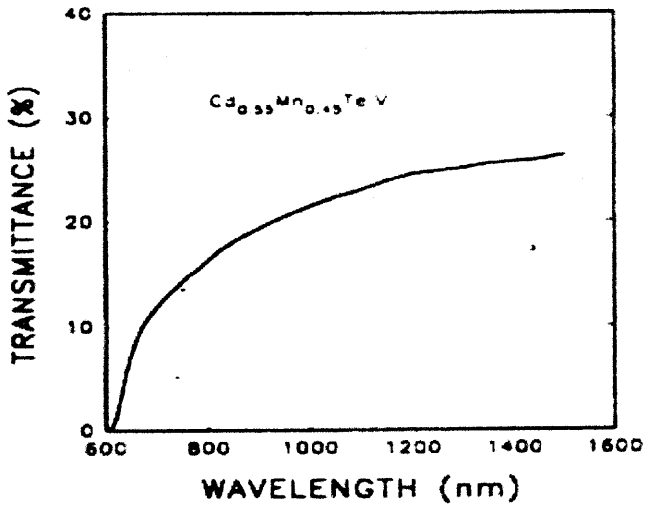

Figure 4.10 Transmission spectrum of $Cd_{0.55}Mn_{0.45}Te$:V

In the above figure we see that the absorption tail extend from 0.6 μm to beyond 1.5 μm. It is known that only one type of carrier act in the photorefraction of this semiconductor. Fig. 4.11 shows the schematic energy level diagram for CdMnTe:V.

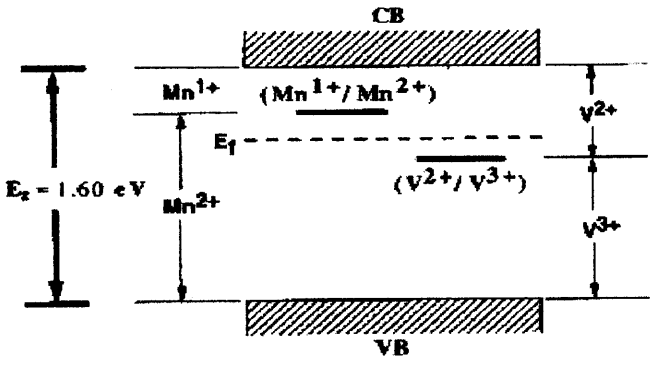

Figure 4.11 Energy level diagram depicting the positions of the ionization levels. For vanadium and Manganese [66].

CdMnTe:V possess a small electrooptic coefficient comparable with GaAs:Cr. The mobility is 5 order of magnitude smaller than in GaAs, but it shows a fast response time in the order of msec, most importantly it shows a broad range wavelength response for photorefraction. Fig. 4.12 shows a graph of grating formation time as a function of grating spacing.

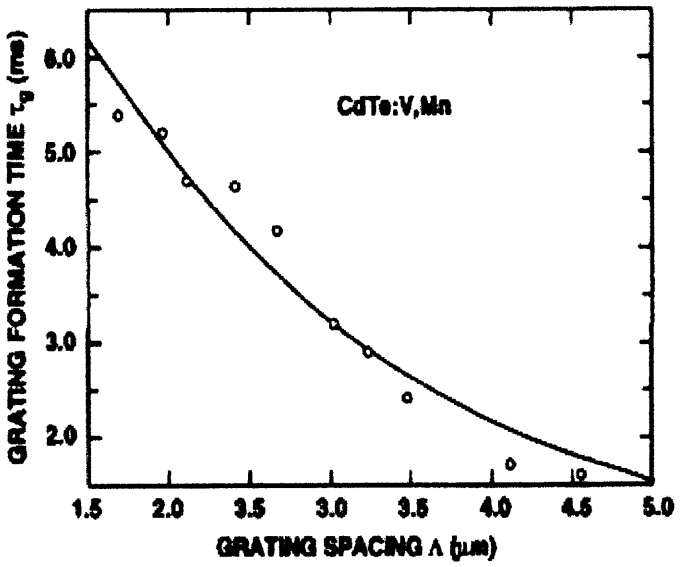

Figure 4.12 Grating formation time as a function of grating spacing [66].

Table 4.1 summarized some of the properties of the three photorefractive materials described here. There are few point to be mention, semiconductors tend to have short grating time formation, while oxides tend to have long grating time formation. The advantage of the semiconductor over the oxides is that their band gap can be tailored through bandgap engineering. Moreover the wavelength response of the semiconductor surpasses the oxides and can be extended from the visible up to the IR.

It is worth mentioned here that in the process of forming an index grating in a two beam coupling experiment the semiconductor tend to develop at the same time an

absorption grating due to their long recombination time. There are two relevant time scales in this process, one is the diffusion time which is related to the mobility, and the other the recombination time, which is the time for a carrier through recombination be trap by a deep level. In the oxides the diffusion time is of the order of 10^4 psec, while in the semiconductors it is of the order of 1-2 psec. On the other hand, for the oxides the recombination time is around 0.1 nsec, and for semiconductors ~10-30 nsec. For semiconductor because of the long recombination time, the carriers can diffuse long distance before they get trap. In the oxides the carriers will get trap before they will be able to diffuse away. This is the reason why in experiments perform with photorefractive semiconductors there is and absorption background in top of the two beam coupling time delay trace. In the oxides this constant absorbing background disappear (see apendix A for details).

Table 4.1 Comparison for the three photorefractives described above.

Parameter	**$BaTiO_3$**	**GaAs:Cr**	**CdMnTe:V**
Electro-optic coefficient (pm/V)	r_{13}=24, r_{33}=80	r_{41}=1.4	r_{41}=2.8
Mobility, μ (cm^2/V sec)	< 2	5800	1000
Recombination time, τ_r (nsec)	< 0.1	38	10
Mobility-life time product $\mu\tau_r$	$< 2x10^{-10}$	$2.2x10^{-4}$	$1.0x10^{-5}$
Diffusion time, τ_d (1 μm) (psec)	$\sim 10^4$	~2.0	~3
Effective trap density, N_t (cm^{-3})	10^{17}	10^{15}	$1.2x10^{15}$

The data for GaAs:Cr and $BaTiO_3$ is from Ref. [64]. The data for CdMnTe:V come from Ref. [65] and Ref. [67].

CHAPTER 5

EXPERIMENTAL MEASUREMENT OF n_2 USING INDUXED GRATING AUTOCORRELATION

5.1 Background

In Chapter two and Chapter three we present the theoretical background necessary to calculate the nonlinear index of refraction for optical fibers and semiconductor films. In the first sections of this chapter, a description of the experimental setup will be given. We will argue that TBC-IGA is useful when the researcher is in possession of a well-characterized pulse envelope. In practice TBC-IGA provides the phase of the pulse. After characterizing the pulse envelope we will then show how TBC-IGA can retrieve the phase of a pulse that has been self-phase modulated in an optical fiber. We will characterize the nonlinearities of three different optical fibers. Silica-Glass polarization preserving fiber, Erbium-doped fiber, and Ytterbium-doped fiber. Finally we will be extending the technique to measure changes on the nonlinearities of the Erbium and Ytterbium fibers due to a pump laser.

5.2 Experimental Setup

The experiments were performed with a harmonically mode-locked Quantronix Nd:YAG laser, model 416 operating at a wavelength of 1.064-μm and running at a repetition rate of 100.468 MHz, which produces a pulse every 10-nsec. The model 416 is a solid state laser [68] consisting of a Neodymium doped Yttrium Aluminum Garnet (Nd:YAG) crystal rod. Parallel to the rod there is a high pressure Krypton lamp. Both the crystal and the lamp are located at the focal point of an elliptical gold reflector. Most of the energy in this laser is converted to heat and must be removed by water-cooling. The laser uses a 352-quantronix mode locker. This is an acousto-optic modulator acting as a very fast

optical gate. The mode locking technique implies that laser resonator modes will have a coherent phase relationship. The proper modulation frequency for the laser to generate pulses that grow to a stable value is given by

$$f_o = \frac{1}{2T} = \frac{\Delta f}{2} = \frac{c}{4L} \tag{5.1}$$

in the above equation f_o stands for modulation frequency where L is the total length of the resonator, and c is the speed of light. The frequency must be adjusted such that the length of the cavity must be half the resonator mode spacing.

The width of the output pulse is such that the width of the pulse ($\Delta\tau_p$) is determined by the number of resonator modes that are phase coherent or mode-locked. In the case of a Gaussian pulse the pulse/bandwidth product is be given as the following relationship

$$\Delta\nu_p \Delta\tau_p \approx 0.5 \tag{5.2}$$

The first set of experiments were performed to characterized the pulse envelope from our Nd:YAG laser. A second harmonic generation technique was used; the experimental setup is shown in Fig 5.1. The laser output is send to a modified Michelson interferometer through a 50/50 beam splitter, one of the arms is held fixed while the other can be changed in length and consequently in delay by a Klinger stepper motor controller, and by a translation stage. The translation stage has a 2-μm resolution and a 200-mm of travel for a total of 1500-psec delay. The translation stage is controlled with a GPIB-488 National Instrument card, and a LabView computer program.

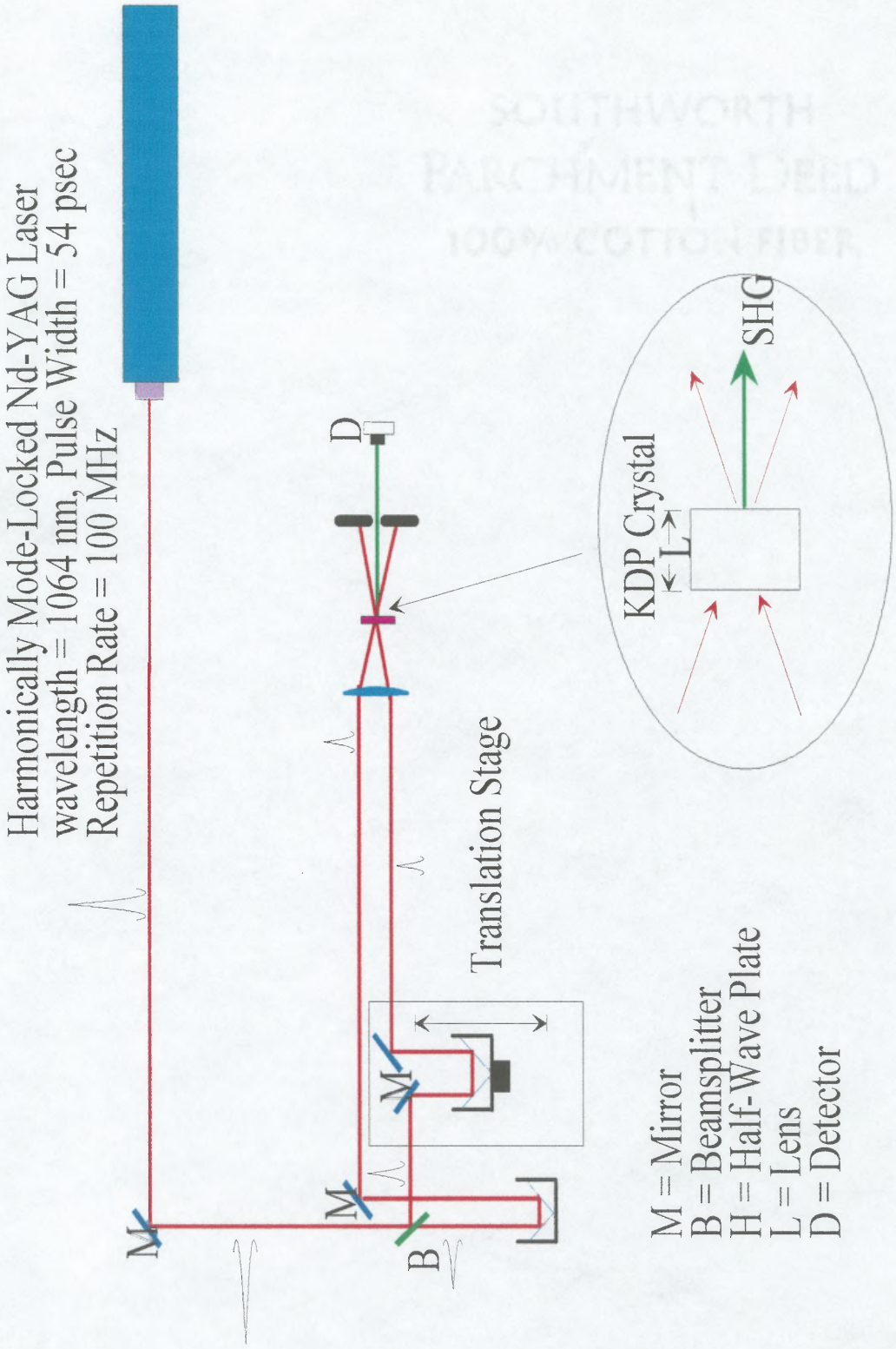

Figure 5.1. Second Harmonic Autocorrelation Lab Setup.

The two parallel, but noncollinear beams were focused with a 10-cm focal length into a 2-mm KDP crystal. The KDP crystal was cut for phase matching at 532-nm. The second harmonic generated signal is produced only when the two beams are temporally and partially overlapped into the crystal. The second harmonic signal is generated in the bisecting direction of the two focused beams. This type of autocorrelation is called "*background free*". The two 1.064-μm beams emerging from the KDP crystal were eliminated with a 720 ND filter. The 532-nm signal is collimated with a pinhole and detected with a THORLABS silicon photodetector model PDA50. This photodetector has a bandwidth up to 10 MHz, an active area of 5-mm^2, and a spectral responsivity from 400-nm to 1100-nm. One of the arms of the Michelson interferometer was chopped at 2 kHz and detected with an EG&G 5209 looking amplifier.

The data was collected with a computer LabView program in pairs corresponding to the delay time and the signal strength. The computer program gives the user the ability to average each point at the same location *N*-times or by *N*-runs. Averaging the data over many run helps to decorrelate the noise level and laser fluctuations. The averaging is done in order to increase the signal/noise ration, especially when the signal level is very weak.

Second harmonic generation (SHG) takes place due to the presence in the KDP crystal of a second order nonlinearity. The energy detected in the photodetector is proportional to the intensity of the SHG signal. The second harmonic signal is proportional to the square of the complex amplitude of the total incident field in the sample. It is given by

$$E_2(t) \propto \left[E_1(t) + E_1(t+\tau)e^{i\omega\tau}\right]^2 = E_1^2(t) + E_1^2(t+\tau)e^{2i\omega t} + 2E_1(t)E_1(t+\tau)e^{i\omega t} \quad (5.3)$$

The total energy of the detected SHG signal will be proportional to its intensity. It is given by a second order autocorrelation function express as

$$G_2^2(\tau) = \int_{-\infty}^{\infty} I(t)I(t+\tau)dt = \int_{-\infty}^{\infty} \left\langle E_1^*(t)E_1(t+\tau)E_1(t)E_1^*(t+\tau)\right\rangle dt \qquad (5.4)$$

Fig. 5.2 shows a typical autocorrelation trace for our Nd:YAG laser, and the corresponding fitting to a Gaussian beam profile of the form here:

$$E_1(t) = E_o \exp\left(-2\ln 2\left(\frac{t}{\tau_p}\right)^2 + i(\omega t + k\cdot r)\right) \qquad (5.5)$$

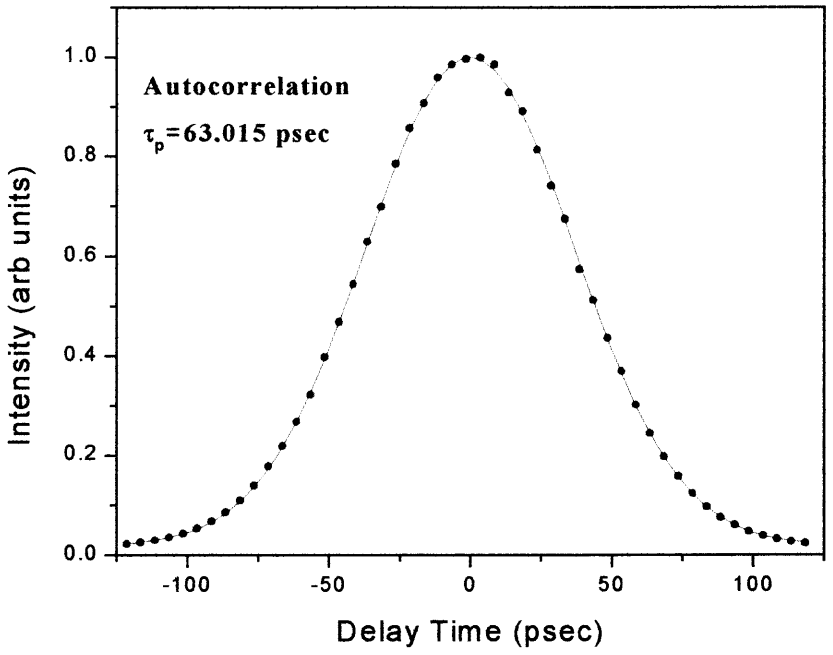

Figure 5.2. SHG Autocorrelation measure of the pulse width

The FWHM of the pulse in this particular trace is equal to τ_p=63.015 psec. Fig. 5.3 shows the same graph in a log scale. It can be seen that the pulse corresponds to a well

behaved transform limited Gaussian pulse. Even at the wings of the pulse, the fitting is extremely good.

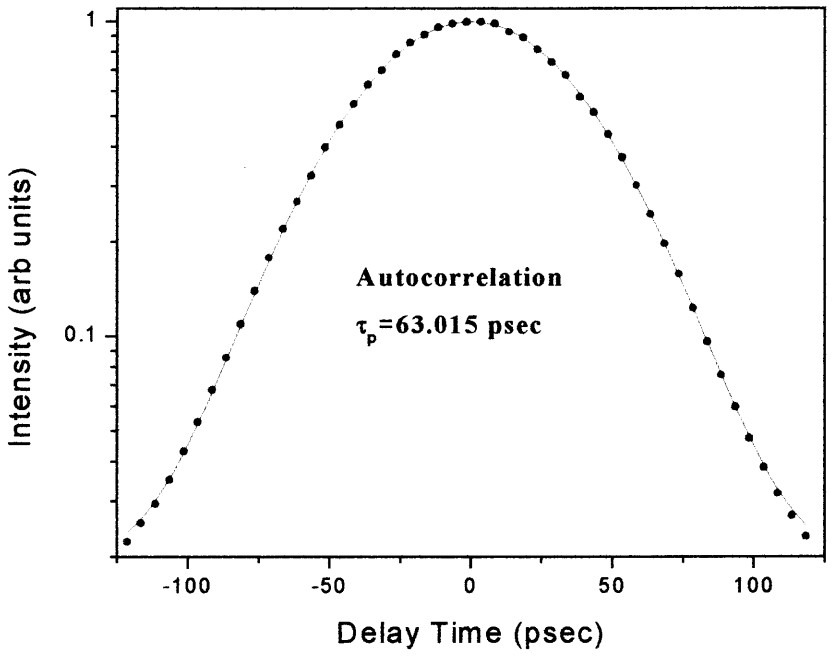

Figure 5.3. Same autocorrelation as in Fig. 5.3. but in a log scale.

In all of the traces taken in the experiments the pulse width varies between 50 to 70 psec. A common experimental procedure was to take several autocorrelations traces at the beginning of every experiment. This ensures that the correct pulse parameters were used at the end. To confirm the fact that the pulse was a transform limited, we took spectral measurements of the pulse before it had been coupled into the fiber. We were limited by the optical spectrum analyzer 0.1-nm resolution. To measure the spectral width of the laser pulse, some of the light coming out the Nd:YAG laser was coupled into an optical fiber head run through an Advantes-Q8381A optical spectrum analyzer. Fig. 5.4 shows the spectrum of our pulse, it is easy to see that the analyzer limits the resolution. Using Eq. (5.2) we found for the pulse/bandwidth product ,as seen here:

$$\tau_p \frac{c\Delta\lambda}{\lambda^2} = 63.015x10^{-12} \frac{3x10^8(0.878x10^{-9})}{(1064x10^{-9})^2} = 14.6$$

This product should be of the order of 0.5. The bandwidth of the pulse can be resolved in an optical spectrum analyzer with a resolution of the order of 0.01-Å.

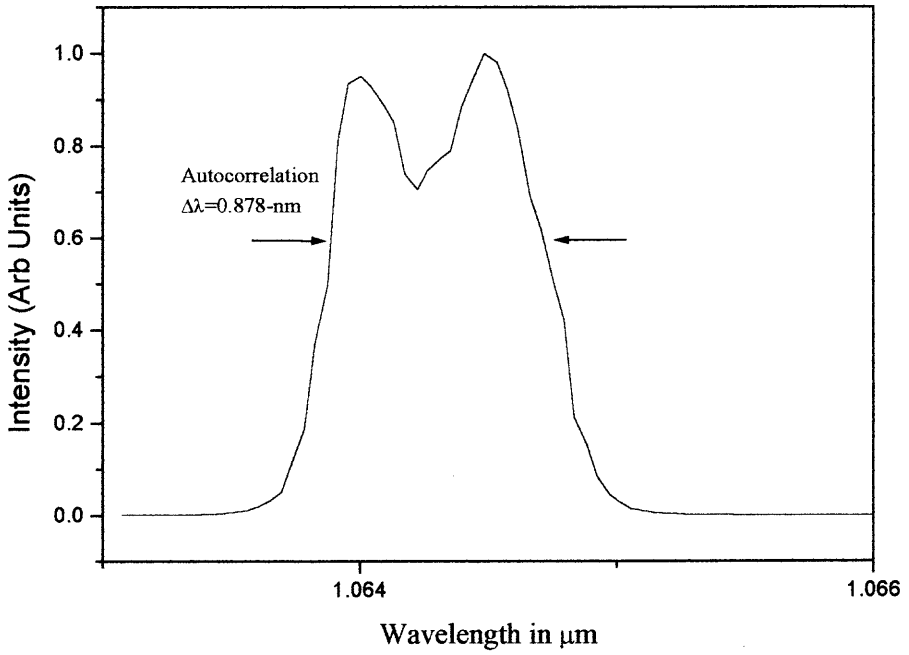

Figure 5.4. Spectral bandwidth of the output pulse of the Nd:YAG laser.

5.3 Measure of n_2 in Optical Fibers

5.3.1 Fiber Nonlinearities

Fiber nonlinearities may limit the amount of information that can be transmitted in high-bit-rate transmission systems. There are several processes that contribute to the fiber nonlinearities. It is well known for example that about 18% of the fiber nonlinearities come from Raman effect [69]. This constitutes a non-instantaneous, nonlinear response

that can be observed in the femtosecond regime. Other contributions are electronic and nuclear nonlinearities, electrostriction, and thermal effects. In the picosecond regime all these nonlinearities contribute to the total nonlinear refractive index of optical fibers. The control of the nonlinear properties of optical fiber is of fundamental importance for system design, particularly for high-power optical amplifiers and soliton systems. Therefore it is of fundamental importance to have a reliable method available for measuring the nonlinear refractive index of optical fibers.

The technique presented here will provide the researcher another experimental tool for measuring the nonlinear refractive index of optical fibers. There are Two advantages to this technique: first, that it is based on pure refraction, and second that it can be implemented with short lengths of fibers, something which is of paramount importance for fiber design and development. The new demands and challenges imposed on optical fibers by the rapid increase in the telecommunication industry cause fibers in to carry more wavelengths over greater distances, often at higher bit rates and power levels [70]. The distance over which the signal must travel can vary from 300-m facility premises to several thousand of kilometers in submarine cable systems. The bit rate per wavelength may only be 10 Mb/s on premises, but can be up to 10 Gb/s in long haul systems. The frenzied demand of bandwidth for internet access, CATV, and data networking has driven the development of the entire telecommunication industry. Optical fibers entering young adulthood are fundamental elements of the telecommunication infrastructure.

An integral part of most optical networks is that optical amplifiers are used to reduce the need for optoelectronic regenerators. Signals must travel longer distance

before they are amplified. The combination of longer distances and high optical powers from optical amplifiers give rise to the potential for fiber nonlinear effects that must be controlled and characterized. Fiber nonlinearities can be classified in two categories: stimulated scattering and refractive index fluctuations. Depending on the power level, each of these effects will play a different role and produce different effects.

The importance of the nonlinear effects in optical fibers can be understood on their waveguiding properties. In general, silica-based fibers show very low nonlinear properties [71]. The third order nonlinear susceptibility is two to three order of magnitude less than that of traditional nonlinear material such as CS_2. However in general the efficiency of the nonlinear process is not only determined by the nonlinear coefficient, but also by the product of the pump power density and the interaction length. This can be understood as follows: in the case of bulk media the laser light is focused into a spot size of radius r_0. Because of diffraction, the size of the spot size changes or diffracts as it propagates through the media according to the formula shown here:

$$r(z) = r_o\sqrt{1+\left(z\lambda/2\pi n r_o\right)^2} \tag{5.6}$$

The product of power density and distance expressed as the following:

$$A_{bulk} = \int_{-L/2}^{L/2} \frac{P}{\pi r^2(z)}dz \le \int_{-\infty}^{+\infty} \frac{P}{\pi r^2(z)}dz = P\frac{2\pi n}{\lambda} \tag{5.7}$$

where P is the average power in the medium, and L is the length of the medium it can be seen that in bulk media the product of the pulse density and the interaction length is

independent of the degree of focusing. In the case of an optical fiber, because the transverse dimension is constant the product is given by the equation,

$$A_{fiber} = \frac{PL}{\pi a^2} = \left(\frac{P}{\pi a}\right)\left(\frac{L}{a}\right) \tag{5.8}$$

where a is the radius of the fiber core. In an optical fiber $a \sim \lambda$, then, we see that

$$A_{fiber} = A_{bulk}\left(\frac{L}{a}\right) \tag{5.9}$$

the ratio of fiber length and fiber radius can be of the order of 10^9-10^{10} for a typical 1-km fiber. Such a great advantage over the bulk counterpart significantly reduces the threshold for the observation of nonlinear process in optical fibers. The above process is shown in Fig. 5.5.

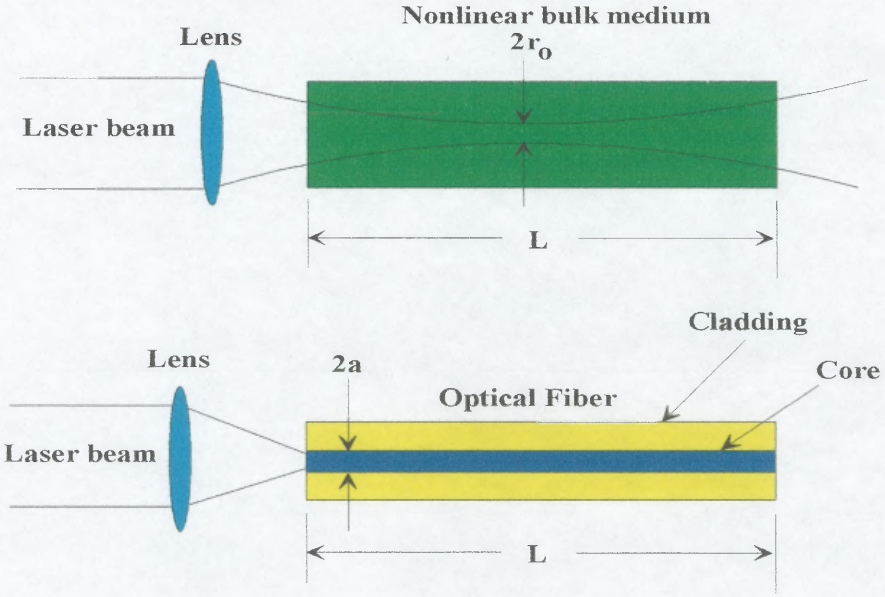

Figure 5.5 Experimental geometry for pumping light in a nonlinear bulk material (top), and optical fiber (bottom).

Several power thresholds can be calculated for different nonlinear processes. This will help us to identify the regime where pure self-phase modulation is the dominant mechanism.

5.3.2 Nonlinear Optical Powers Thresholds for Several Nonlinear Processes

To identify the regime where TBC-IGA can be applied, it is necessary to calculate the power levels needed it to excite or stimulated different nonlinear processes. In the first case let us calculated the effective length of a typical silica glass fiber. For silica fibers the absorption coefficient at 1.55-μm has a value of α=0.048-km^{-1}, and for a typical fiber length, L=20-m, used in TBC-IGA experiments, we get for the effective length, L_{eff}, as

$$L_{eff} = \frac{1 - e^{-\alpha L}}{\alpha} = 19.99\ m$$

As can be seen the effective length is equal to the fiber length. With the above result lets determine if we are the dispersion-dominant or nonlinear-dominant regime by using Eq. (3.18). Using a pulse width of 61 ps and a fiber dispersion β_2=0.06 ps^2/m we can find the dispersion effective length

$$L_D = \frac{T_o^2}{|\beta_2|} = 62\ km$$

therefore our fiber length is much smaller than the effective length of the dispersion regime. To determine if in our case the nonlinear regime is more relevant than the disperse regime, we need to calculate the effective nonlinear length given by Eq. (3.18).

For a typical fiber we have A_{eff}=50 μm^2, γ=2.0x10^{-5} cm^{-1}-W^{-1}, then we find the nonlinear effective length, assuming a P_{avg}=0.2 W

$$L_{NL} = \frac{1}{\gamma P_o} = 15.25\ m$$

It is evident from the above number that we are in the nonlinear dominant regime. Therefore we can neglect any dispersion in the fiber and use Eq. (3.19) to describe the propagation of the pulse in the fiber.

The next step is to find what types of nonlinear effects we can observed at an average power of 0.2 W and at 20 m length of fiber. The most important nonlinearities in optical fibers are stimulated Raman scattering, self-phase modulation, and stimulated Brillouin scattering:

Stimulated Raman Scattering: stimulated Raman scattering is a nonlinear effect in which light in the fiber interacts with molecular vibration (optical phonons) and in which scattered light is generated at a wavelength longer than that of the incident light [72]. There is a power threshold defined such that at this power the Raman scattered light will deplete the pump signal by about 50% [69,73], and it is given by

$$\frac{g_r L P_{peack}}{A_{eff}} = 16 \qquad (5.10)$$

where g_r is the Raman gain coefficient. It can be express as g_r=(4.7/$\lambda_{\mu m}$)x10^{-12} cm/W [78] L is the fiber length, A_{eff} is the effective area defined as

$$A_{eff} = 2\pi \frac{\int_0^\infty |E(r)|^2 r dr}{\int_0^\infty |E(r)|^4 r dr} \tag{5.10}$$

A_{eff} can be obtained by computer analysis from the index profile of the fiber. It has been shown that A_{eff} can be approximated by the Namihira relation [74,75],

$$A_{eff} \approx 0.944\left(\frac{\pi}{4}\right) MFD^2 \tag{5.11}$$

where *MFD* is the mode field diameter of the fiber. It is important to note that for a Gaussian intensity profile the effective area corresponds to $\pi\omega_o^2$, where ω_o is the $1/e$ width of the field. The Raman gain coefficient is at its maximum at a pump-Raman separation of about 500 cm^{-1}. For silica glass it takes a value of the order of 4.4×10^{-12} cm/W at 1.064 μm. Using the same value for A_{eff}=50 μm^2, we can use Eq. (5.10) for the case of ps pulses if the length of the fiber is substituted by an effective length that takes into account the walk-off length. This length is expressed as $L_{eff}=\pi^{1/2}L_W=\pi^{1/2}T_o/|d|$ where d is the walk-off parameter which is of the order of 2-6 ps/m, for a 54-ps pulse, the effective length is L_{eff}=47.85 m. We find a peak power threshold of the order of P_{peak}=379.97 W, this correspond to a average power of 2 W. In the case of polarization preserving fibers, the critical power is twice small, because the gain coefficient is two times higher. As we can see the critical power is high compared to the power used in the experiment performed here.

Stimulated Brillouin Scattering: Stimulated Brillouin scattering is similar to SRS except that it involves the interaction of light with a acoustical phonon or sound waves. The gain coefficient for SBS is over two orders of magnitude larger (g_b=4x10^{-9} cm/W) than the gain coefficient in SRS, and wavelength independent. The maximum gain in SBS occurs for a shifting of about 200 cm^{-1}. One of the main differences between SRS and SBS is that for phase matching conditions the SBS signal propagates in the opposite direction from the pump. The critical or threshold power is given by the equation

$$P_{cr} = \frac{21A_{eff}}{g_b L} = 1.3\,W \tag{5.12}$$

which corresponds to an a average power of 7.0 mW. For polarization preserving fibers this value is 3.5 mW. As can be seen, SBS is the dominant nonlinear process that takes place in fibers. The only advantage of SBS is that because the pump propagates in the opposite direction of the scattering wave, the interaction length is short.

Self-Phase Modulation: Self-phase modulation has been explained in chapter 3. The threshold power for the signal to develop a nonlinear phase shift of one rad at the fiber output is the following

$$P_{cr} = \frac{\lambda A_{eff}}{2\pi n_2 L} = 16.2\,W \tag{5.13}$$

This corresponds to an average power of 87 mW.

From the above analysis we conclude that the experiment performed here can be analyzed in the self-phase modulated regime. Because of the short fiber length we can

neglect GVD. Because of the low power needed to generate self-phase modulation, we neglect SBR, and SRS as well. It is self-phase modulation the effect that we will use to measure the nonlinear refractive index in three types of fibers, silica-glass fiber, Erbium-doped fiber, and Ytterbium-doped fiber.

5.4 Two Beam Coupling with a Self-Phase Modulated Pulse

In chapter three we developed the equation used to described the propagation of an optical pulse in a medium where self-phase modulation is the dominant nonlinear effect. In the previous section we have shown that in optical fibers of short length (L<20 m) and low power (P_{avg}<300 mw) this regime can be applied, and GVD, SRS, SBS can be neglected. We also showed in chapter four that in a two beam coupling experiment the energy scatter of one beam along the direction of the other beam was proportional to the electric field autocorrelation function. We also pointed out that any time dependent phase contained in the pulse, will be retrieved by a two beam coupling experiment perform in a slow responding media (photorefractive crystal). This phase retrieval technique [73] will be used now to characterize the medium where the self-phase modulation was originated.

Let us recall some of the main results of chapter three and chapter four. If we assumed that the input pulse into the fiber is a transformed limited Gaussian pulse, as in Eq. 5.5, then the solution to Eq. (3.19) can be expressed as:

$$A(z,t) = U_o \exp\left(-2\ln 2\left(t/\tau_p\right)^2\right)\exp\left(i\left(\omega_o t + k\cdot r + \phi_{spm}(t)\right)\right)$$
$$\phi_{spm}(z,t) = \frac{2\pi\omega_o^2}{k_o c^2}\chi^{(3)}\left|A(z,t)\right|^2 z = \frac{\omega_o n_2}{c}\left|A(z,t)\right|^2 z \qquad (5.14)$$

To test if the above equation is correct, we performed a series of experiments using the autocorrelation function technique (as described in section 5.2) of the pulse propagating through the fiber and without propagating to the fiber. According to Eq. (5.14) the intensity-intensity autocorrelation function must look the same. In other words the shape of the pulse must remain the same. The experiments were performed in a 20 m length of (polarization preserving) Silica-glass optical fiber. The experimental setup is the same as described in section 5.2, except that in one of the experiments the pulse is sent to the fiber and then to the modified Michelson interferometer. Fig. 5.6 shows two autocorrelation traces of the same pulse. One of the pulses has been propagated in the optical fiber. As can be seen, the pulse shaped does not change and can still be approximated by a Gaussian pulse of the same width.

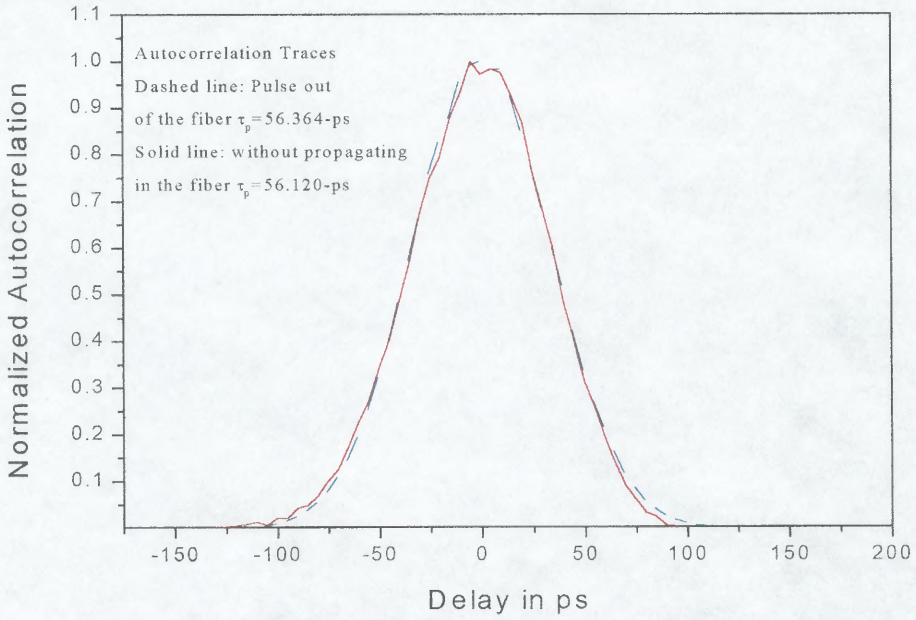

Figure 5.6 Autocorrelation of a pulse that has been self-phase modulated in an optical fiber in comparison with one that has not been.

If Eq. (5.14) is substituted into Eq. (4.12) and the integral normalized the such that when the delay time is zero the electric field autocorrelation function is equal to 1, we can obtain the phase of the pulse. Any nonlinear time-dependent phase in the pulse can be retrieve. In other words a linear time dependency will be cancel out in the complex conjugated operation in the integral. The final equation is given by

$$W_{\mathrm{det}}(x) = N\left|\int_{-\infty}^{\infty}\exp\{-2\ln 2\cdot u^2 - i\omega_o\tau_p Q\exp[-4\ln 2\cdot u^2]\}\exp\begin{Bmatrix}-2\ln 2\cdot(u+x)^2 - i\omega_o\tau_p Q\\ \times\exp[\exp-4\ln 2\cdot(u+x)^2]\end{Bmatrix}\right|^2 \tag{5.15}$$

In Eq. (5.15) $u=t/\tau_p$ is the normalized time with respect to the pulse width, and $x=\tau/\tau_p$ is the normalized delay. The normalization constant N is such that when $x=0$ the integral is equal to $1/N$. Because Eq. (5.15) has no analytical solution for the case of a Gaussian self-phase modulated pulse then the integration must perform numerically. Defining the self-phase modulation strength as (see appendix B for derivation)

$$SPMS = \omega_o \tau_p Q = \frac{\omega_o n_2}{c} z U_o^2 = \frac{\tau_r L P_{avg}}{n A_{eff} \tau_p c \lambda} \left(32\pi^2 \sqrt{\frac{\ln 2}{\pi^2}} \times 10^7 \right) \qquad (5.16)$$

the nonlinear index of refraction n_2 in cm^2/W is given by

$$n_2 = \frac{n A_{eff} \tau_p c \lambda}{\tau_r L} \left(32\pi^2 \sqrt{\frac{\ln 2}{\pi}} \times 10^7 \right)^{-1} \left(\frac{\omega_o \tau_p Q}{P_{avg}} \right) \qquad (5.17)$$

Fig. 5.7 shows a series of IGA traces for pulses that have experience different self-phase modulation strengths (SPMS = 5, 10, 15). It can be seen that as the self-phase modulation strength increases the pulse develops a series of oscillations in the wings that are reminiscence of an interference pattern. At the bottom of these oscillations the IGA trace must go to zero. There are some critical values of the self-phase modulation strength at which two new oscillations are added to the trace. The IGA trace develop a new oscillation every time the self-phase modulation strength increases by π. This is in contradiction where the reported values given in [73]. The correlation function must also be symmetric and real for a pulse whose intensity is a real even function.

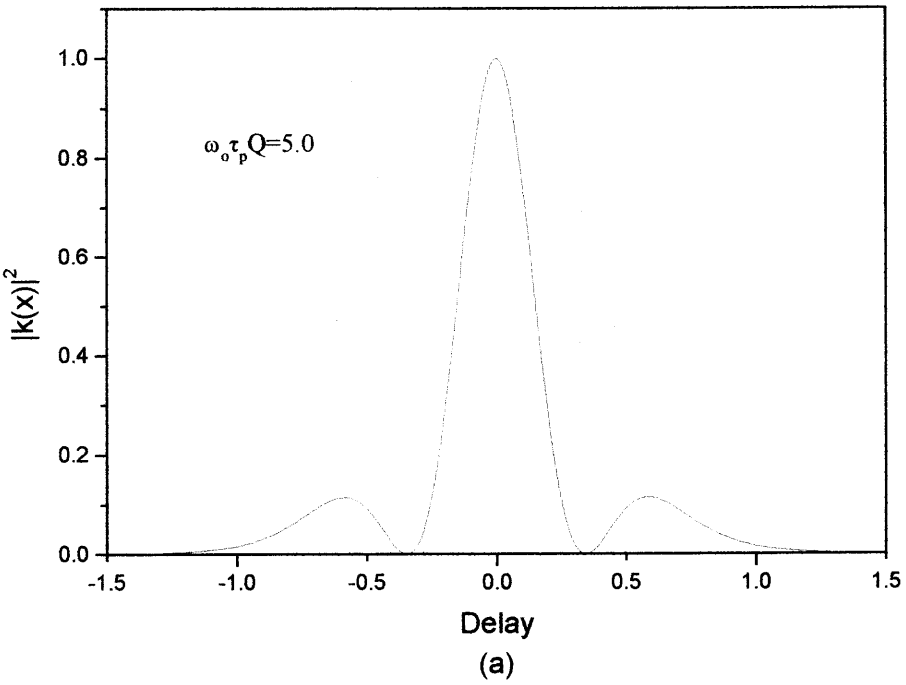
$\omega_o\tau_pQ$=5.0
$|k(x)|^2$
1.0
0.8
0.6
0.4
0.2
0.0
-1.5
-1.0
-0.5
0.0
0.5
1.0
1.5
Delay

(a)

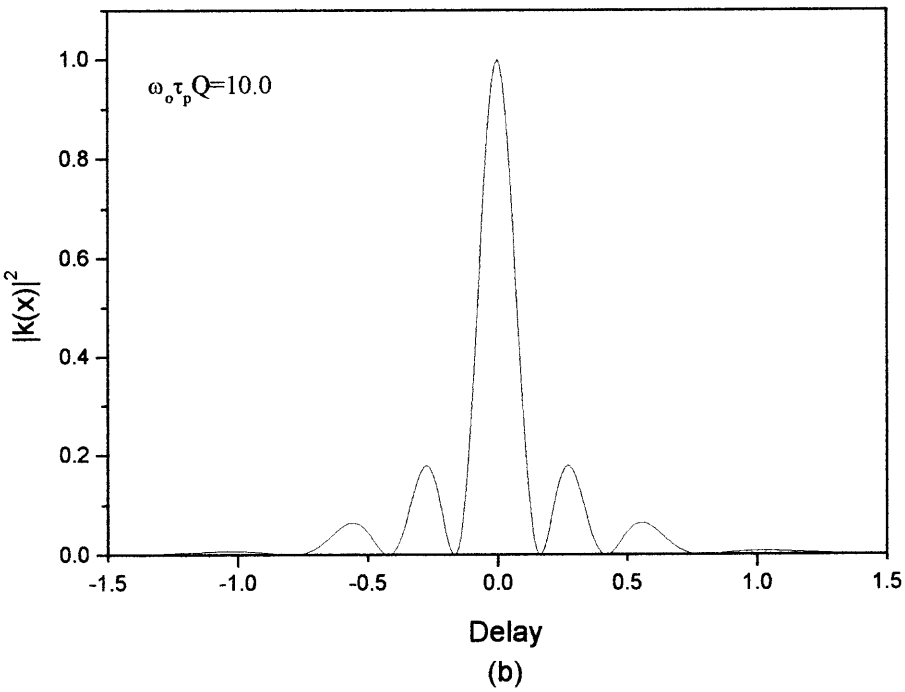
$\omega_o\tau_pQ$=10.0
$|k(x)|^2$
1.0
0.8
0.6
0.4
0.2
0.0
-1.5
-1.0
-0.5
0.0
0.5
1.0
1.5
Delay

(b)

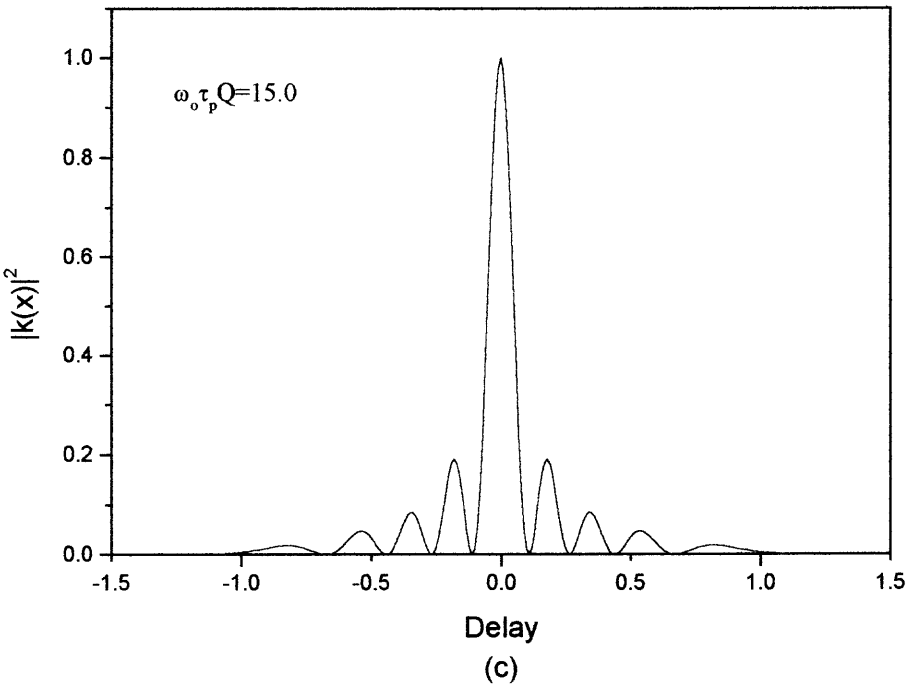

Figure 5.7 Theoretical IGA-traces for several values of SPMS.

5.5 TBC-IGA Experimental Setup

To obtain self-phase modulated pulse we couple the output of our Nd:YAG laser into an optical fiber, and the output pulse of the fiber is sent to a 50/50 beam-splitter and into a modified Michelson interferometer. One of the pulses is sent to a variable delay composed of a stepper-motor-retroreflector combination, controled by a Klinger stepper motor controller CM100 with a 2-μm resolution. The two beams are then focus by a pair of 10-cm focal-length in a CdMnTe:V photorefractive crystal. This crystal acts as a slow responding medium forming a grating with a period given by

$$\Lambda = \frac{\lambda}{2\sin\theta} = \frac{1.064\,\mu m}{2\sin(17.5)} = 1.76\,\mu m \tag{5.18}$$

where θ is the angle of intersection of the two beams. One of the beams is chopped, and the transfer modulation is detected in the direction of the other beam with a THORLABS silicon photodetector model PDA50 and an EG&G locking amplifier. The time constant in the locking amplifier is generally set to 100-ms.

The data is collected with a LabView interface program, this program has an internal time constant of 4 times the time constant in the locking amplifier. The program collects data in two different modes, locally or by swept. In the first case N data points are collected and average at the same location. This is less time-consuming, but the signal-to-noise ratio can be low, especially if your laser system has intensity fluctuation. The reason for such low signal-to-noise ratio can be understood in that laser fluctuations are time correlated at the same point, and show in your detector as signals. The second method consists of taking N swept collecting a single data point each location, and averaging at the end. This method decorrelates noise and laser fluctuations, improving the signal-to-noise figure.

The data is recorded as a function of delay and saved in data files for later analysis. Each experimental section consists of first recording a SHG-autocorrelation trace of the pulse, then switching to the IGA-setup using mirrors on kinematics mounts. Fig. 5.8 shows the experimental setup for the IGA-TBC experiment, and Fig. 5.7 shows a typical IGA-TBC trace for the case of 20-m of polarization preserving Silica-Glass fiber.

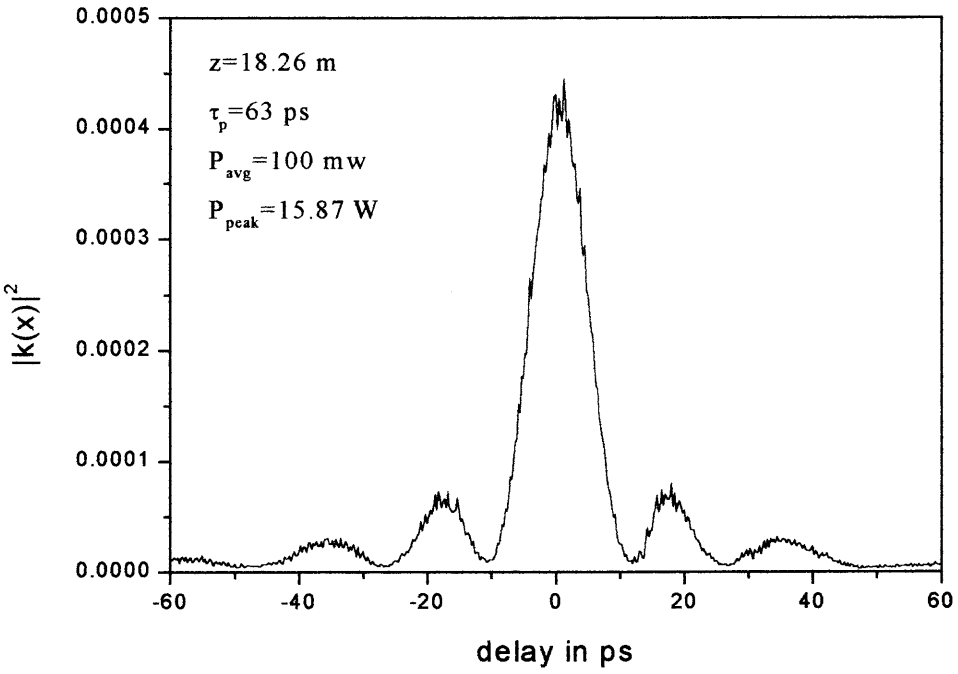

Figure. 5.8 Typical autocorrelation trace for 18.2 m of polarization maintaining fiber.

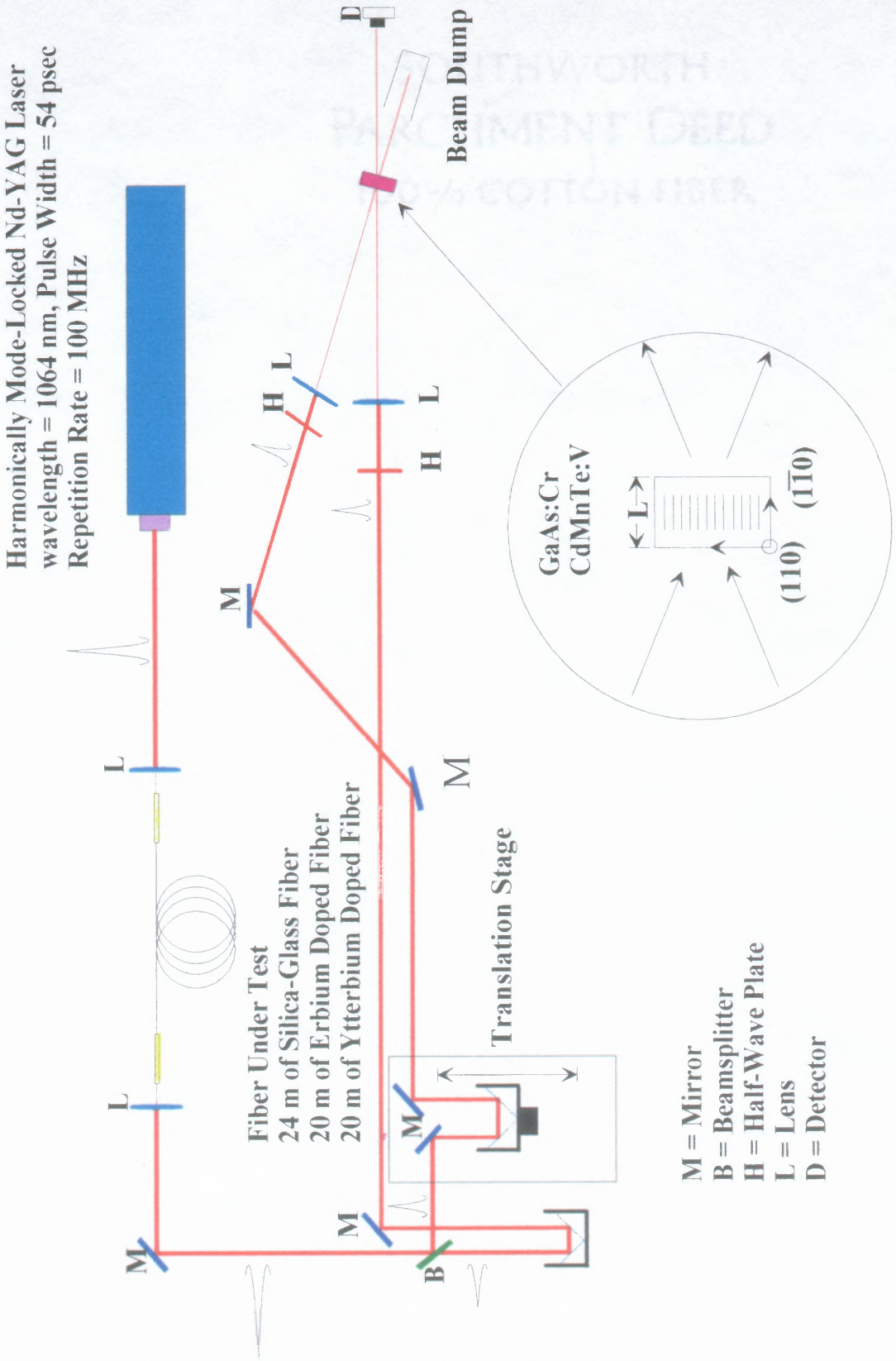

Figure. 5.9 Experimental Setup for TBC-IGA.

The analysis of the data uses only a single fitting parameter. The single parameter is the self-phase modulation strength. A series of nonlinear numerical recipes were used to fit the normalized experimental data [77] (see appendix C for details). The experimental data is normalized such that at zero delay $|k(0)|^2$ equals to 1. The time delay is also normalized with respect to the pulse width.

For each fiber a set of IGA traces were taken at different power levels. The self-phase modulation strength is found as a fitting parameter, and the nonlinear index of refraction is equal to the slope of the graph of the SPMS, up to a multiplicative constant, as a function of average power.

The maximum average power couple into the fiber should be taken such that the SRS peak is minimum. If the power in the fiber is strong enough to generate SRS, the pulse will suffer both shape, and phase distortion. Fig. 5.10 shows the SHG-autocorrelation as well as the TBC-IGA traces of a pulse that have propagated in 20 m of silica glass fiber with an average power of 1.5 W. The distortion is evident, recalling that the critical power for the generation of SRS is around 1 W in silica-glass fiber. TBC-IGA must always be performed with average power at least 1/3 of the SRS critical power.

In the next 3 sections we will describe the experiment performed with three types of optical fibers. Some of the results will be compared with the ones available in the literature. The result for silica-glass fiber is well established; this is not the case for Er-doped as well as Yb-doped optical fiber.

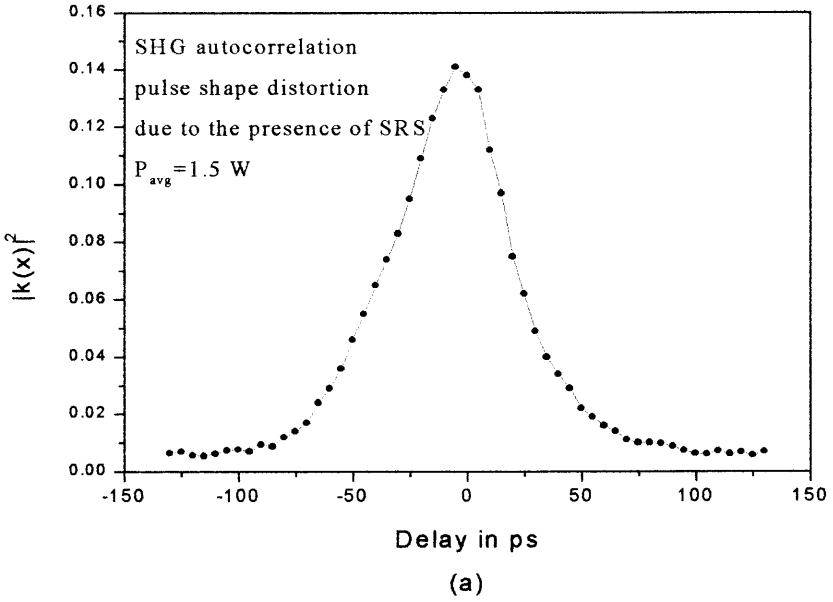

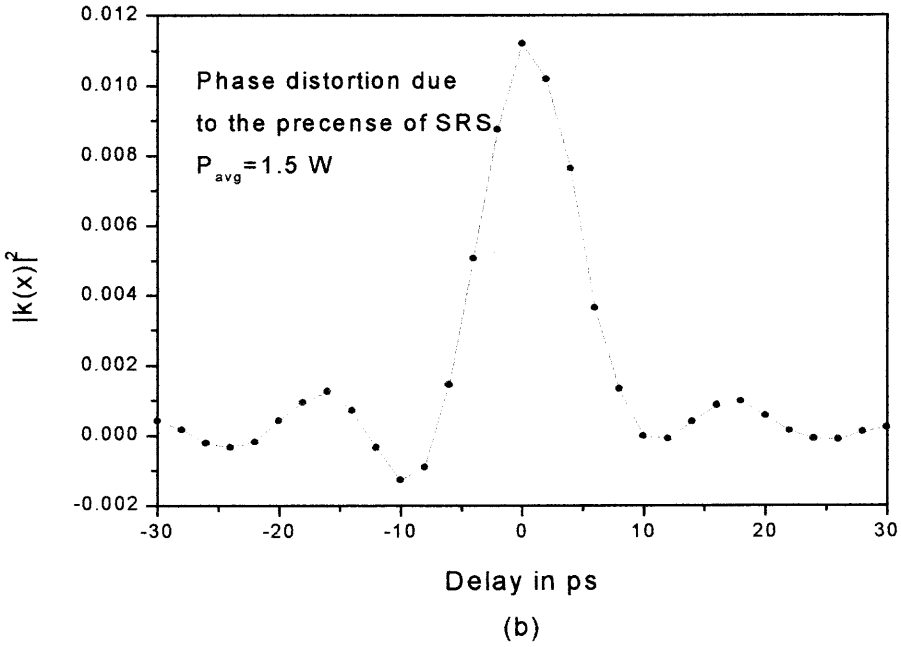

Figure 5.10 Shaped distortion (a), and phase distortion (b) experience by a pulse in the presence of SRS.

5.6 Measure of n_2 in Silica-Glass Fiber

A 24 m length silica-glass fibers was used in the first set of experiments. The composition of this fiber is unknown. The fiber has a deformation along one direction of the core making it elliptical in shape. This shape breaks rotational symmetry and maintains the fiber polarization. The introduction of this asymmetry is done with the purposed of minimizing polarization rotation due to modal birefringence. The fiber effective core area is A_{eff}=5x10^{-7} cm^2. A series of IGA traces were taken, varying the average power couple into the fiber. The average power was varied from 0.25 to 1.4 W. The average power was measured with a power meter locate in from of the fiber output. The light loss in the output focal lens must be taken into account.

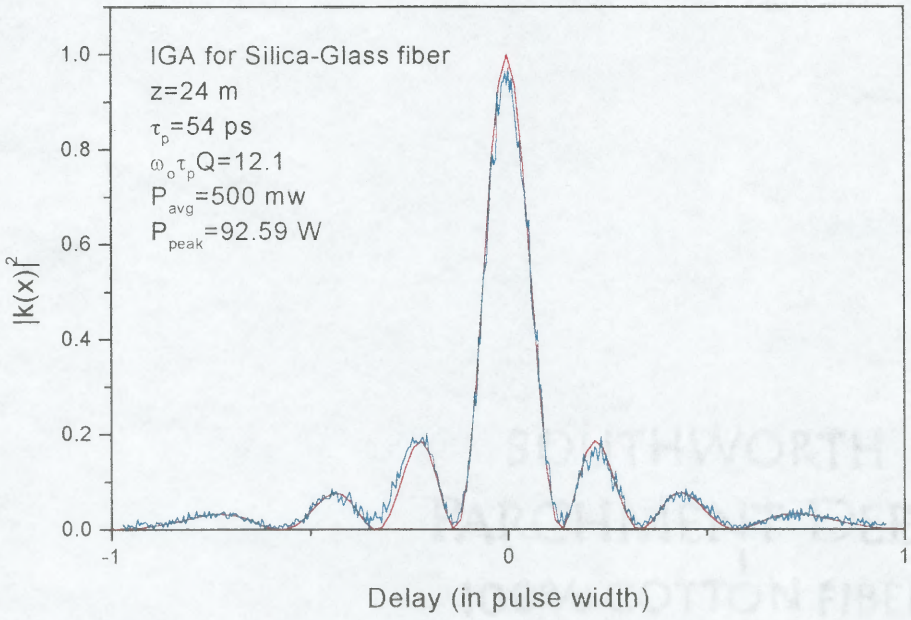

Figure 5.11 Experimental IGA-trace and their corresponding Theoretical IGA-trace using Eq. (5.15).

Fig. 5.11 shows a 0.5 W average power TBC-IGA trace and their corresponding nonlinear fit, with the best SPMS found. Fig. 5.12 present the result of several IGA traces and the corresponding SPMS plotted as a function of average power. Using the slope found on the graph and the parameters for the fiber given in table 5.1. The slope of Fig. 5.12 is $(\omega_o \tau_p Q/P_{avg})$=22.54±0.8443, and we get for the nonlinear index of refraction

$$\boldsymbol{n_2 = (2.44\pm0.0914)\times10^{-16}\ cm^2/W = (0.85\pm0.03184)\times10^{-13}\ esu\ cm^2}$$

this is within 5% of the value reported by Stolen, *et al.* [78].

This is remarkable because we need only one fitting parameter, more importantly the length of the fiber is short compared with hundreds of meter used by Stolen [78]. TBC-IGA is ideal for fiber development and design because the nonlinear properties of optical fibers can be characterized with only a few meters with psec pulses or few cm with fs pulses.

Table 5.1 Parameters used to calculate the n_2 for silica-glass fiber.

Parameter	Value
Effective Area, A_{eff}	5×10^{-7} cm^2
Length, L	24 m
Index of Refraction, n	1.46
Speed of Light, c	3×10^{6} cm/s
Wave length, λ	1.064×10^{-4} cm
Pulse Width, τ_p	54×10^{-12} s
Repetition Rate, τ_r	10×10^{-9} s

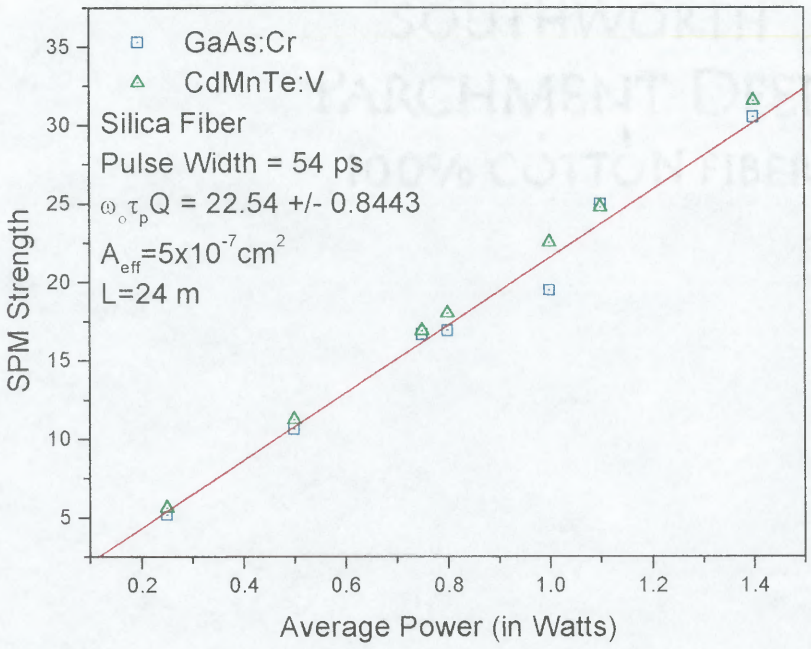

Figure 5.12 SPMS as a function of average power for Silica-glass fiber.

5.7 Measure of n_2 in Erbium-Doped Fiber

Erbium-doped fibers are of fundamental importance in today telecommunication industry. Erbium-doped fiber is widely used in optical amplifier for their high-gain and broad laser transition in the 1.53 μm window [79]. Glass fibers with Erbium-ion doping are use in optical communication as laser or as in-line optical amplifiers.

Erbium amplifiers provide advantages over regenerative repeaters because of the complexity and high-speed electronics needed in electronic repeaters. The complexity increases as the bit rates increases. Erbium-doped fibers, on the other hand, do not require high-speed electronics, and the optical gain of the amplifier does not change with the bit rate (bit rate transparency) [80]. Despite of all the research work done in Erbium-doped

fibers, there are only few papers reporting the measure of n_2 and the study of the nonlinear optical properties of Erbium-doped optical fibers [81,82,83,84]. The reported value for n_2 in Erbium-doped fibers is very inconsistent, and most researches assume that the same value found in silica-glass fibers can be extrapolated or use in the case of Erbium-doped fibers. What is worse is the lack of a systematic study of the effect of doping concentration on the nonlinear optical properties of Erbium-doped fibers.

Table 5.2 EDF-MP980 fiber parameters

Parameter	**Value**
Cutoff wavelength	880 nm
Core Radius	1.63 μm
Refractive index diff (Δn)	0.0146
Numerical aperture	0.207
Peak absortption (near 1.53 μm)	5.20 dB/m
Peak absorption (near 980 nm)	4.22 dB/m
MFD at 1.55 μm	6.17 μm
Estimated erbium concentration	$8x10^{24}$ m^{-3}
Effective Area	$1.24x10^{-7}$ cm^2

The fiber used in this research is an EDF-MP980 made by Lucent Technologies. Some of the parameters for this fiber are shown in Table. 5.2. Fig. 5.13 shows the emission and absorption cross section for this fiber as a function of wavelength.

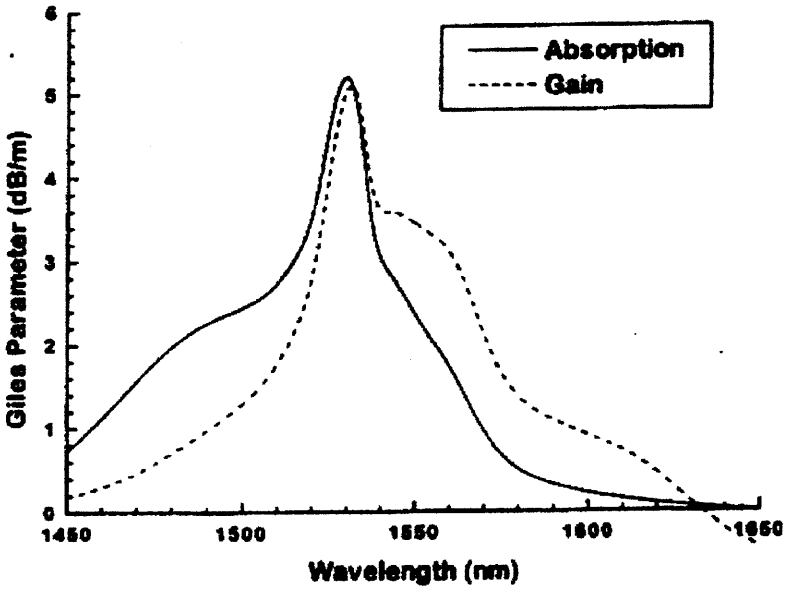

Figure 5.13 Experimental absorption and emission cross-section for the EDF-MP980 fiber used in these experiments.

It was found that the fiber turn blue and greenish as the power was increased. The power level was keep below 400 mW, because the power threshold for SRS power was found to be of the order of 500 mW at 1064 nm. Fig. 5.14 shows three peaks at 600 mW average power in the fiber. The first peak is located at 1064 nm corresponding to the center wavelength of the laser. The second peak located at 1116 nm correspond to a Raman shift of $\Delta\nu$=437.92 cm^{-1}. The third peak located at 1332 nm correspond to a parametric mixing of the Raman peak and the $2\omega_{1116}$-ω_{1064} which has totally been depleted.

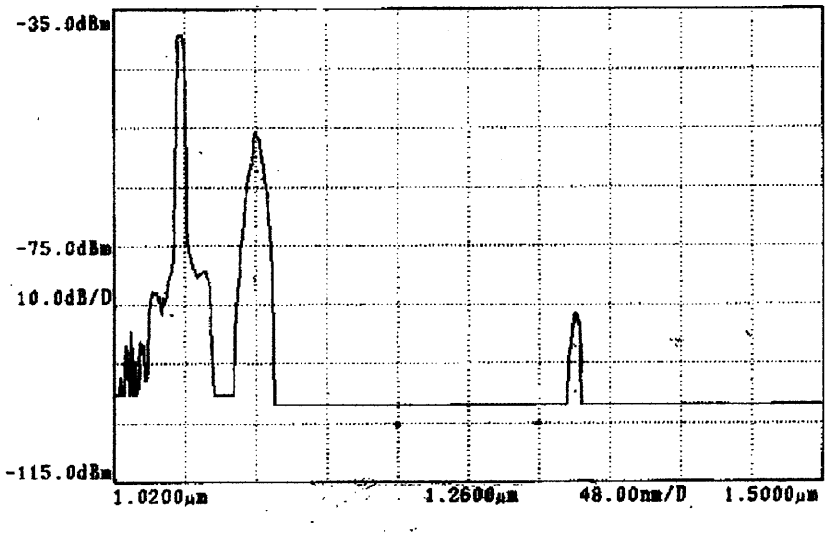

Figure 5.14 Spectrum of nonlinear processes in EDF-MP980 erbium-doped fiber for power level above 600 mW.

A series of IGA-TBC traces in a L=10 m length Erbium-doped fiber were taken. The maximum average power couple into the fiber was 300 mW corresponding to a maximum peak power of 55 W. Fig. 5.15 shows two traces corresponding to the minimum and maximum power use, the traces are shown with their corresponding fit. The effective area was determined by its index profile to have a value of A_{eff}=1.24x10^{-7} cm^2 [85]. Fig. 5.16 shows the graph of the self-phase modulated strength as a function average power. Using the value found for the sloped on Fig. 5.16 we get for the nonlinear refractive index of our Erbium-doped fiber

$$\mathbf{n_2=(3.416\pm0.01714)x10^{-16}\ cm^2/W=(1.191\pm0.00597)x10^{-13}\ esu}$$

Once again, the value is within 5% of the reported value [81]. This is remarkable because in this case only 10 meters of fiber were used.

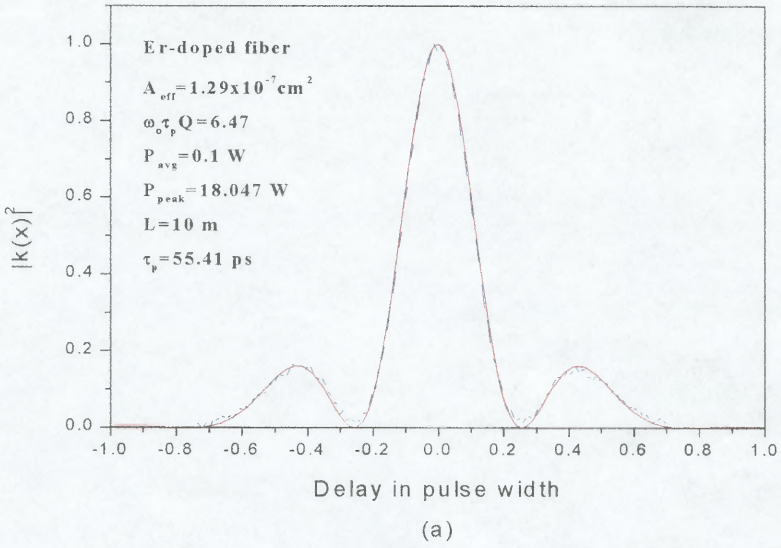

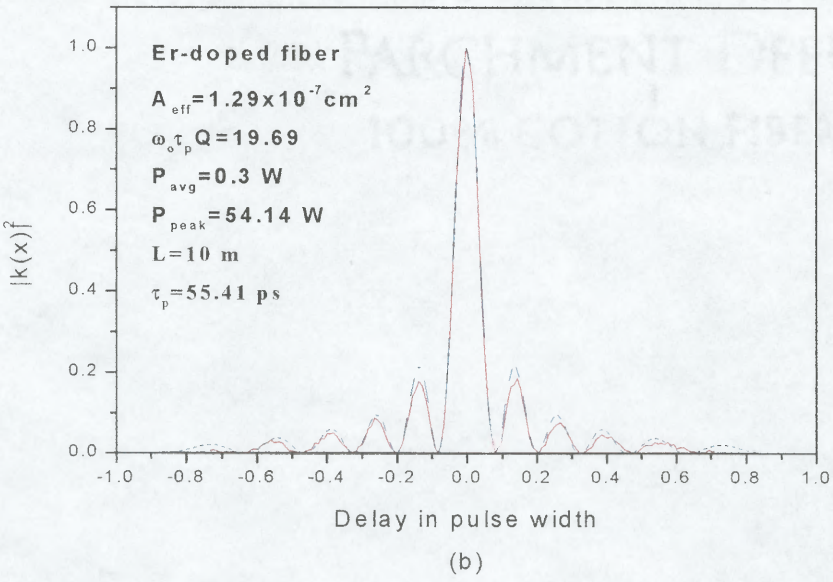

Figure 5.15 IGA-TBC traces for Er-doped fiber for different power levels.

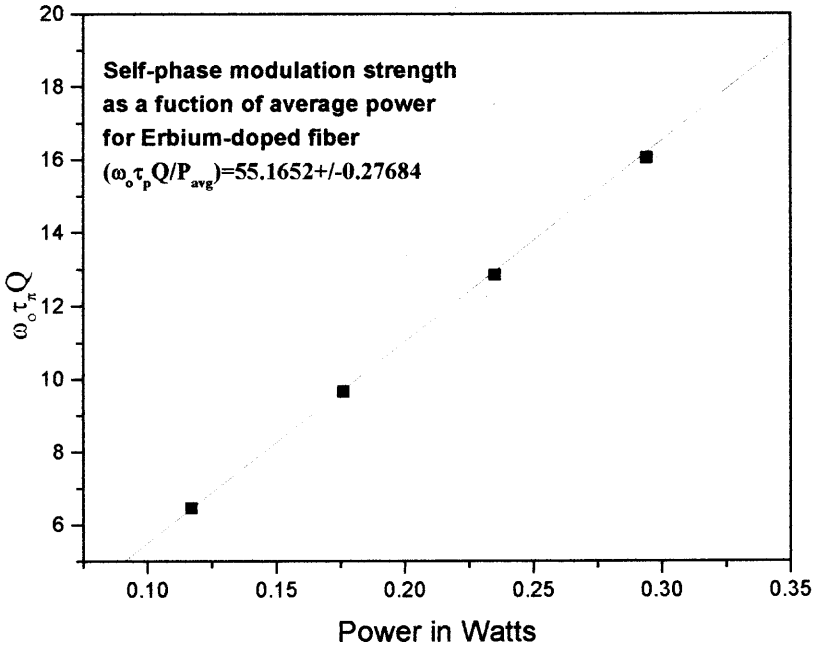

Figure 5.16 Self-phase modulated strength as a function of average power for Er-doped fiber.

5.8 Measure of n_2 in Ytterbium-Doped Fiber

Another rare-earth doped element that had lased in glass is Ytterbium [86]. Ytterbium doped fibers had been used as high power fiber lasers [87] that can be used as high power pump in optical amplifiers. Also Yb-doped fibers are used in cascaded Raman resonator laser with outputs up to 8.5 W at 1472 [87]. Cascaded Raman resonators are fabricated by writing a UV induces grating in the fiber where each Raman pulse pumps the subsequent Stokes emission [88].

Ytterbium-doped fibers offered a number of interesting aspects. For example, there is an absence of exited state absorption (ESA), since apart for the laser energy level transitions all the other energy levels are in the UV region [89]. Also the laser transitions

show broad spectral range that allow for significant tuning range. The fluorescence shows a wavelength covered from 1.015 to 1.40 μm, which exceeds that covered by the Nd fiber laser [89]. Fig. 5.17 shows the energy level diagram of Yb in silica host and the fluorescence spectrum after [89].

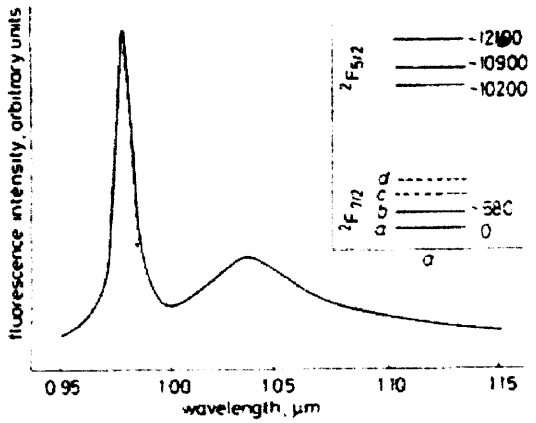

Figure 5.17 Energy levels and fluorescence of Yb in silica host [89].

In spite of all the applications of Yb-doped fibers there is a lack of information about its nonlinear properties. There is no literature available about the value of the nonlinear index of refraction.

We measured n_2 using 20 meters of Yb-doped fiber. The fiber use in this experiments was obtain from researches at Lucent Technologies in Murray Hill. There is a little of information about the technical specification of the fiber. In Table 5.3 we summarized the information that we posses about this fiber.

Table 5.3 Parameters used in the case of Yb-doped fiber

Parameter	Value
Core Radius	2.25 μm
Peak absorption (near 1064 nm)	1 dB/m
Peak Absorption (near 980 nm)	270 dB/m
Length, L	20 m
Refractive index diff (Δn)	0.01
Ytterbium concentration	Low

The Raman peak starts to appear around 400 mW of average power or 74 W peak power. The experiments were performed with an average power range of 100-320 mW. Fig. 5.18 presents the output spectrum of the fiber when pumped with 1064 nm. The graph is not at scale. The peak at 1332 nm correspond to the parametric mixing of the signal at 1198.4 nm and the signal at 1062.8 or $2x\omega_{1332} - \omega_{1062} = \omega_{1332}$. The signal at 1198.4 nm can be identified as the Stokes Raman peak. The 665 nm to a parametric mixing, and the 532 nm may possible correspond to upconversion. There is an interesting point to make, when the fiber was pumped with 980 nm a peak corresponding to amplified spontaneous emission (ASE) located at 1032 nm appear in the spectrum. Therefore the 1064 nm laser is located at the tail of the absorption peak in this fiber.

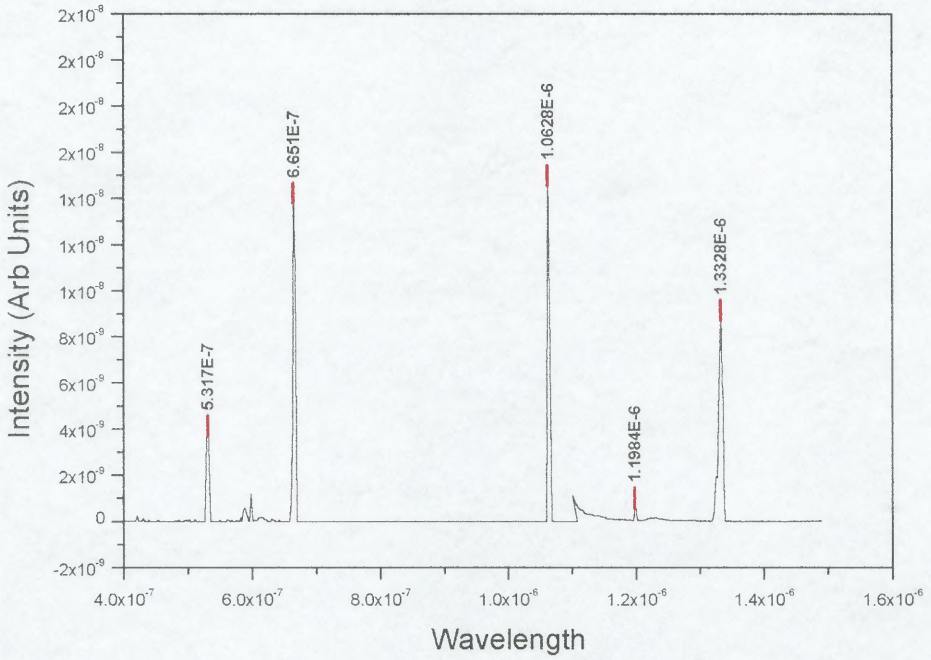

Figure 5.18 Spectrum of the Yb-doped fiber when pumped with 1064 nm.

Several traces were taken, and recorded with different power for analysis. There is not reference to compared the experimental results, except for bulk glass crystal made of Yb^{3+}:KYW, which has a value of $n_2=8.7\text{x}10^{-16}$ cm^2/W at 1080 nm [90]. Fig. 5.19 correspond to the IGA traces for the maximum and minimum power levels. Fig. 5.20 to the graph of the self-phase modulate strength as a function of average power. Although the value of the effective area is unknown, we calculate the nonlinear index/effective area ratio as

$$n_2/A_{eff} = (5.173\pm0.0123)\text{x}10^{-9}\ w^{-1}=(1.474\pm0.043)\text{x}10^{-7}\ cm^{-2}\ esu$$

This value is comparable with the Er-doped fiber case.

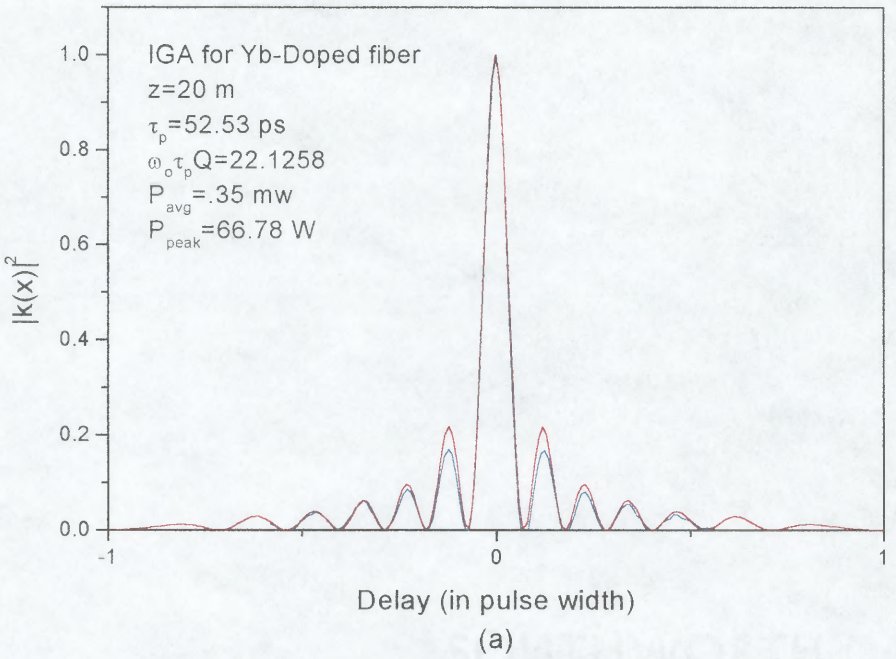

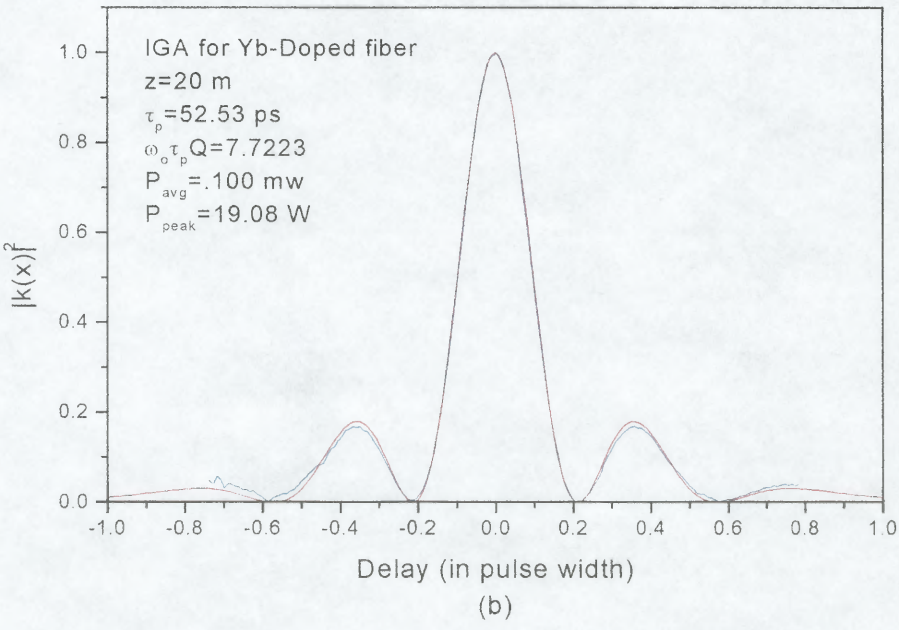

Figure 5.19 IGA traces for Yb-doped fiber for P_{avg}=0.1 and 0.300 W.

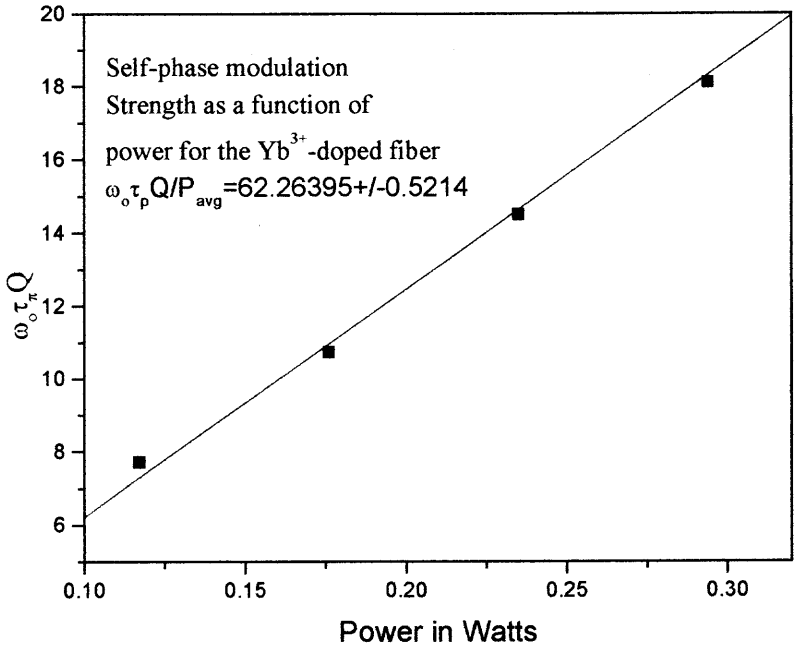

Figure 5.20 Self-phase modulated strength as function of average power for Yb-Doped fiber.

5.9 Measure of n_2 at 1064 nm in Yb-doped and Er-doped Fibers in the Presence of a 980 nm Pump Laser

The increasingly demanding application of Erbium-doped fiber amplifiers (EDFA) in telecommunication, ultralong soliton systems, and soliton laser sources, requires a deep understanding of the effects of the pump laser in the optical properties of the amplifier at the signal level. The amplification provides by EDFA is produced by optically pumping an absorption band to provide gain in the signal emission band. Promoting carriers to upper energy levels implies modification of the optical absorption coefficient of the system and consequently of the refractive index through the Kramers-Kronig relations.

There has been few studies on the pump induce refractive index change at the signal level in EDFA [91,92,93]. They all focus on the pump effects on the linear index of refraction, and none have address the effect of the pump on the nonlinear index of refraction n_2.

In chapter two the theory for the nonlinear susceptibility in the presence of a pump laser in a quasi-two-state system was developed. We found the most general expression for the nonlinear susceptibility when there was a probe beam and a pump beam in the system. In this section we use IGA-TBC to verify the results found in chapter two. The experiments were done in two steps; first an IGA trace with a nominal P_o signal average value, and no pump is recorded, then a series of IGA-traces varying the pump power and maintaining fix P_o are recorded. The change in the nonlinear refractive index is found from the variation of the self-phase modulation strength as the pump power is increased.

There is a difference between the Er-doped fiber and the Yb-doped fiber. In the case of the Erbium the average power at 1064 nm signal can be considered constant and only the power evolution of the pump laser must be model. For the Ytterbium the signal, as well as, the pump average power evolves in the fiber. In this case an effective power is defined as

$$P_{eff} = \frac{1}{L}\int_0^L P(z)dz$$

where $P(z)$ is the local average power of the signal, and L is fiber length.

5.9.1 Experimental Setup

The experiments were performed with the same fibers used in the measurement of the nonlinear index of refraction. The pump in the case of Er-doped fiber was couple counter propagating to the probe beam. The pump beam is a 980-nm diode laser with 80 mW maximum output power operating in cw-mode. SDL-2000-1 butterfly diode laser mount in a LDM-4980 model with temperature controller and current driver. In the case of the Er-doped fiber the pump was couple in the fiber with 10x microscope projector, counter propagating with respect to the 1064 nm probe beam. For the Yb-doped fiber the pump and the probe or signal copropagate in the fiber. The coupling is in free space with 10x-microscope projector in a 2x1 power combiner made by fusion splicing. Fig. 5.21 shows the experimental setup.

5.9.2 Er^{3+}-Doped System

lets us recall that in the case of the Erbium-doped fiber there is not signal field, the 1.064-μm laser is the probe beam. And the nonlinear susceptibility is given by

$$\chi_{pr}^{(3)}(\omega_{pr}) = \frac{n^2 \varepsilon_o N c^2 \sigma_{pr}^{peak}}{\omega_p \bar{I}_{pr}^{sat}} \frac{\delta_{pr}}{(\delta_{pr}^2 + 1)} \frac{\left(1 + \dfrac{I_p}{2 \cdot I_p^{th}}\right)}{\left(\dfrac{I_p}{I_p^{th}} + 1\right)^2} \tag{5.19}$$

The above equations give us the value for the nonlinear susceptibility in the case that the pump power is constant over the entire fiber length. In real experimental conditions the pump power changes over the length of the fiber, therefore one must refers to an effective susceptibility, which is the integral of the susceptibility over the fiber length divide by the fiber length.

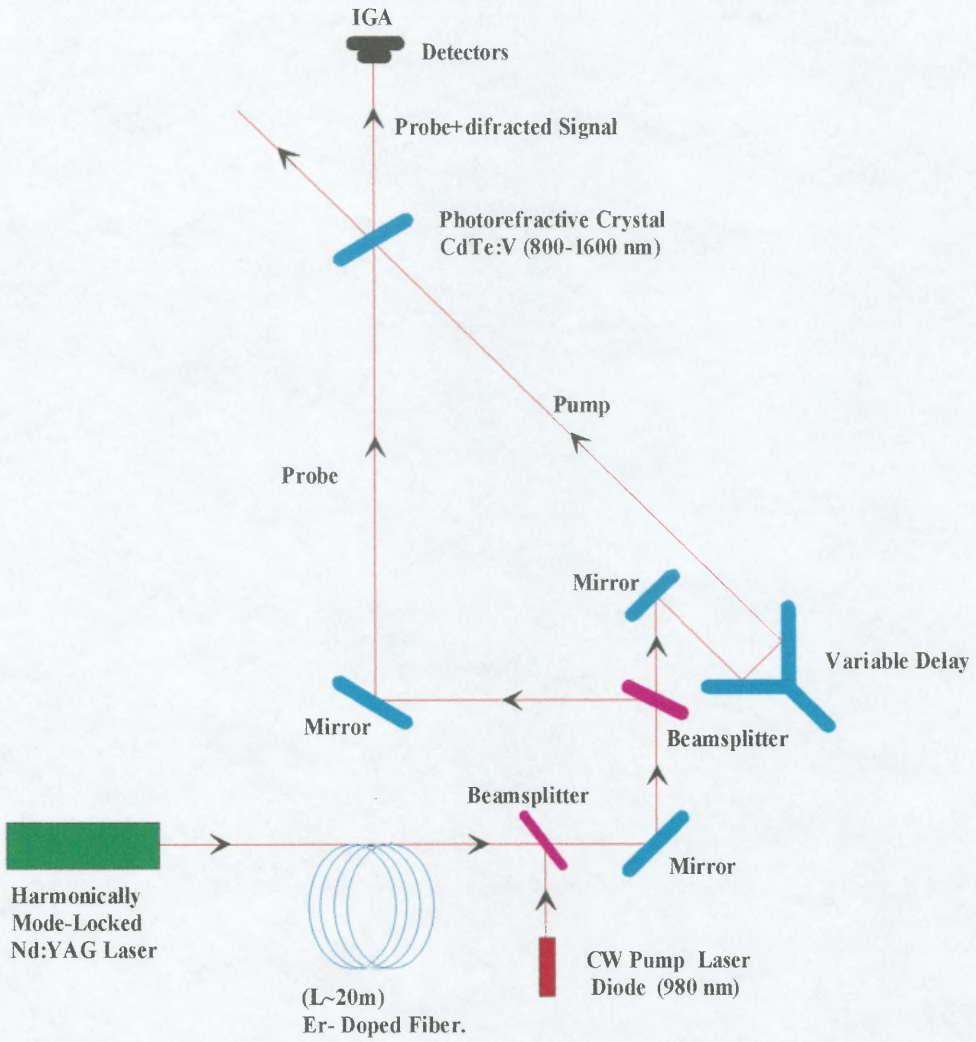

Figure 5.21 Counter propagating geometry for the measurement of the nonlinear refractive index in Er-doped fiber.

5.9.3 Yb^{3+}-Doped System

In the case of the Yb-doped fiber the probe beam is zero, the 1.064 μm is the signal beam. The real part for the nonlinear susceptibility is given as

$$\chi_s^{(3)}(\omega_s) = \frac{n^2 \varepsilon_o N c^2 \sigma_s^{peak}}{\omega_s \bar{I}_s^{sat}} \frac{\delta}{(\delta^2+1)} \frac{\left(1-\frac{I_p}{I_p^{th}}\right)}{\left(\frac{I_p}{I_p^{th}}+1\right)^2} \qquad (5.20)$$

The above equation has to be complemented with the power evolution along the fiber for the signal as well as the pump field.

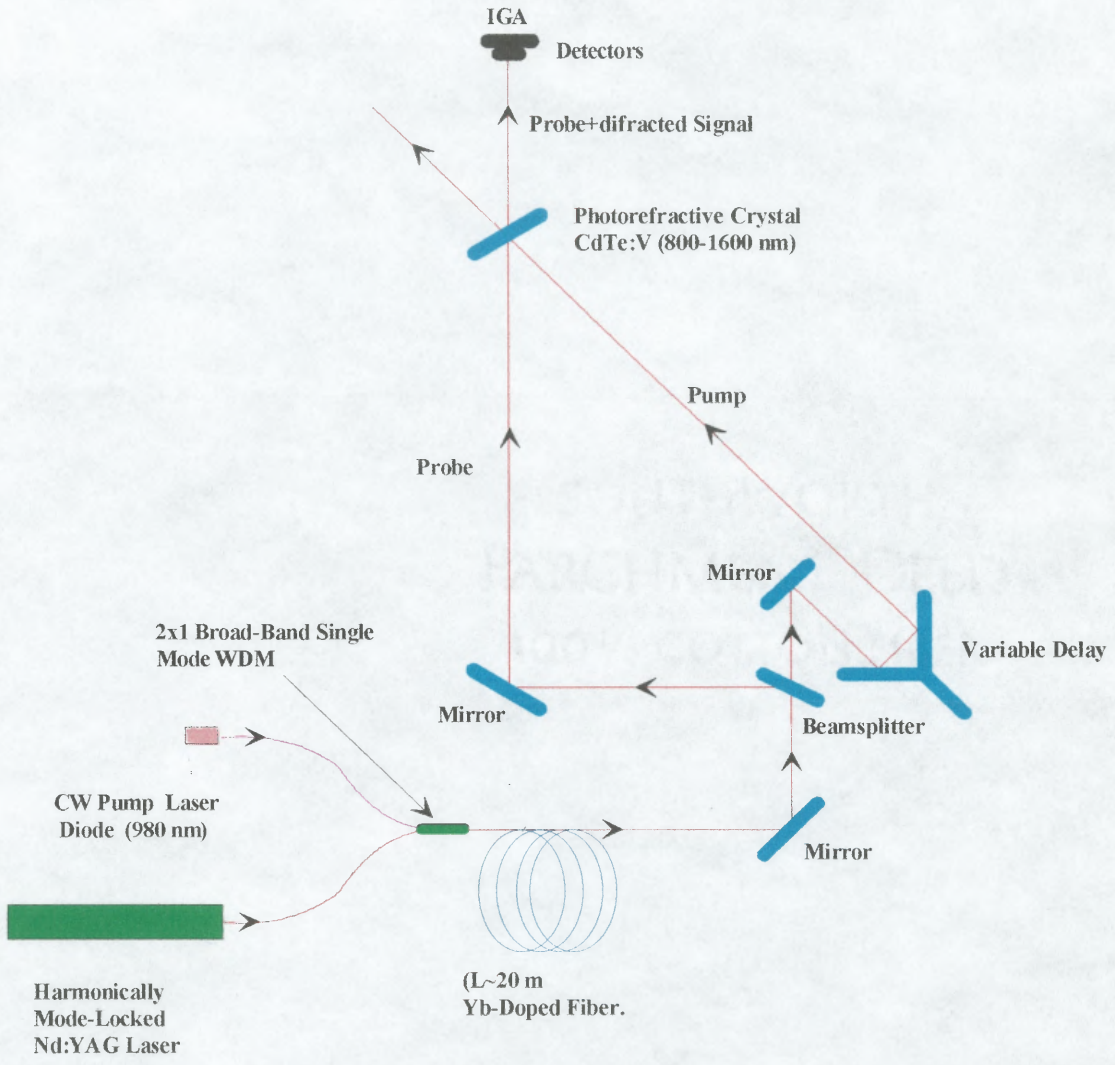

Figure 5.22 Copropagating geometry use to measure the nonlinear refractive index change in Yb-doped fiber.

5.9.4 Experimental Results

20 m of the EDF-MP980 Er-doped fiber with Erbium concentration of $8x10^{24}$ m^{-3}, and absorption coefficient of 4.22 dB/m, where used in this experiment. The pump threshold

power was P_p^{th}= 0.8-mw at 980-nm. Experiments were perform with different pump power levels from 0 to 10 mw, and 100 and 250 mw of 1.064 μm. The coupling geometry was counterpropagating. It is assumed that there is some exited state absorption in the system with an absorption coefficient of 4 dB/m. For the case of the Erbium doped fiber the probe beam intensity can be considered constant along the entirely fiber length.

The experiment is first performed with no pump present. An IGA-trace with a 100-mW or 250 mW is recorded as reference. After the reference trace is recorded a sets of traces are taken increasing the pump power with the same probe nominal power. The power of the pump beam is model as [82]

$$\frac{dP}{dz} = \frac{-P\alpha_{GS}}{1+\left(P/P_p^{th}\right)} + \frac{-P\alpha_{ES}}{1+\left(P_p^{th}/P\right)} \tag{5.21}$$

where α_{GS} is the absorption coefficient, α_{ES} is the excited state absorption coefficient ~ 4 dB/m. Fig. 5.23 shows the pump power evolution and the normalized nonlinear index of refraction in the fiber as a function of distance. From the graph we see that the nonlinear index remain constant at the beginning but when the probe beam interact with the pump beam the nonlinear index of refraction decreases. Because the change happens only at the last few meters of the fiber, what it is measure using IGA-TBC is an effective change in the nonlinear refractive index. The experimental change in the nonlinear refractive index is found by fitting the experimental IGA traces and recording the change in the self-phase modulating

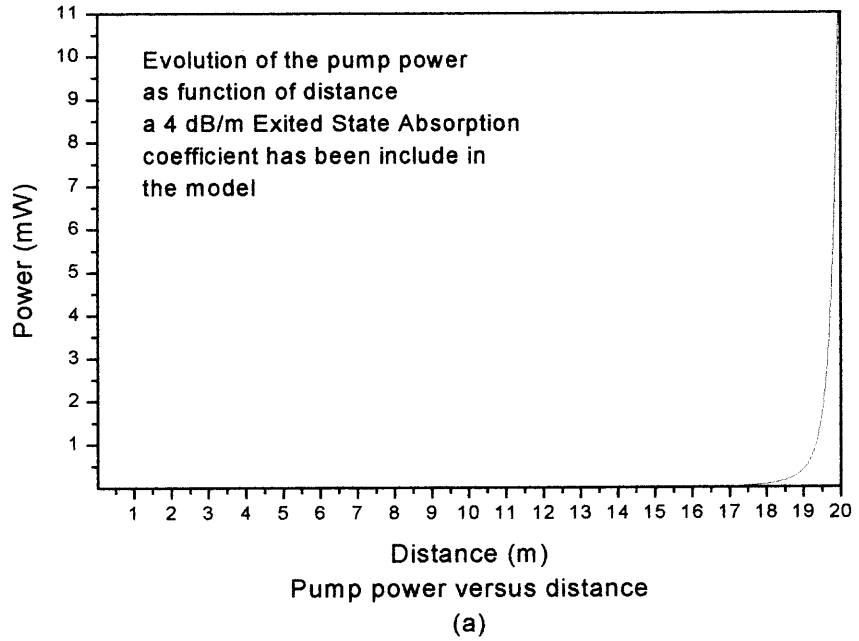

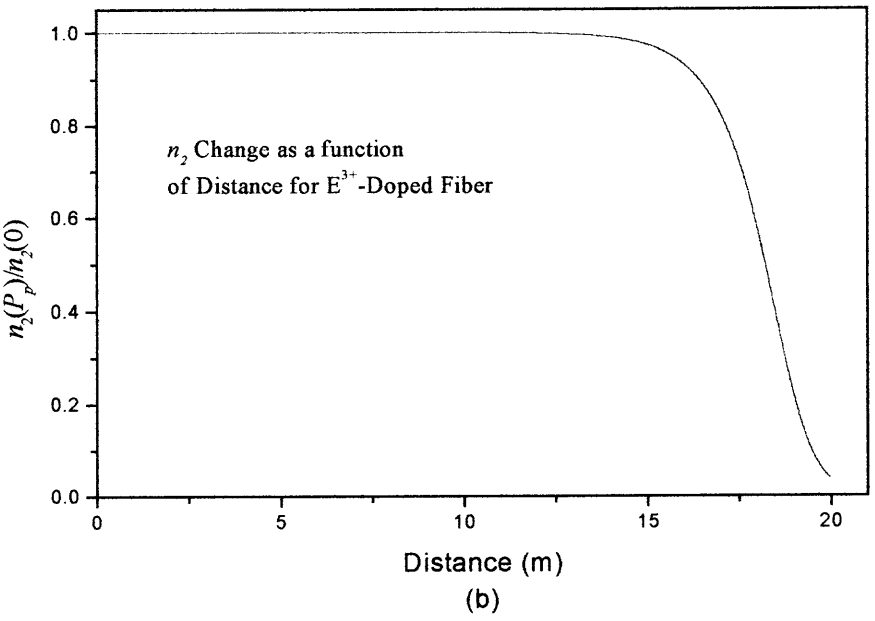

Figure 5.23 (a) Evolution of the pump power as a function of distance (b) decreased of the nonlinear refractive index.

strength. Fig. 5.24 shows an experimental IGA-trace with no pump present and one with 10 mW of pump power in the fiber. It is evident that the broadening of the central peak and the shifting of the oscillation are signature of the decreased of the nonlinear index of refraction.

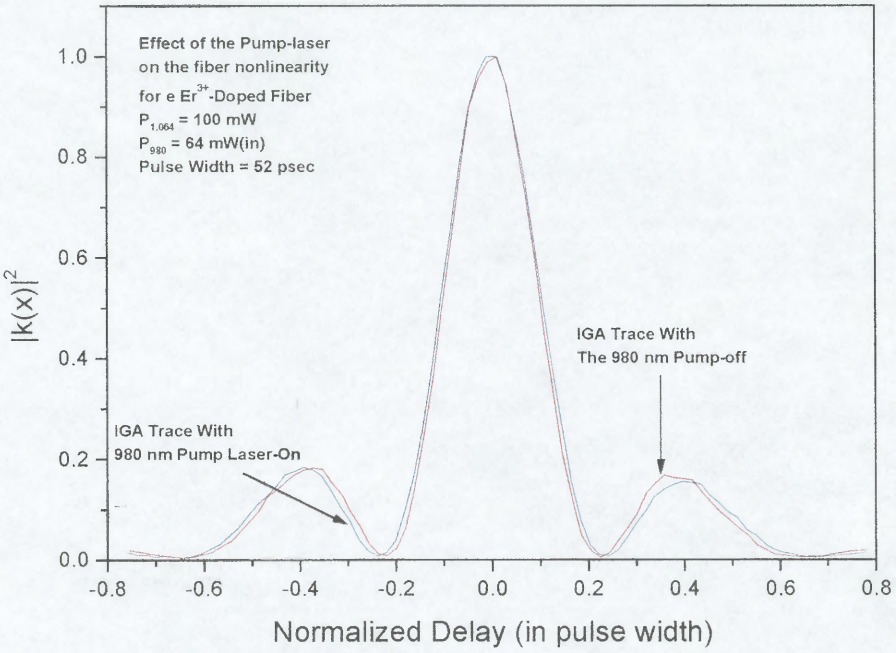

Figure 5.24 Shifting of the oscillation of the IGA trace when the pump Laser is turn on.

In Fig. 5.25 the change in the normalized nonlinear refractive index is plotted as a function of the pump power level. We have used the following relation to correlate the susceptibility given by Eq. (5.19)

$$n_2 = \frac{12\pi^2}{n_o^2 c}\chi^{(3)} \tag{5.22}$$

It is clear that the nonlinear index of refraction decreases because the self-phase modulation strength decreases. This decrease is predicted by Eq. (5.19). It can be understood as follows: the nonlinear susceptibility depends on the population difference between level $|1\rangle$ and level $|4\rangle$. As the pump is turn on carriers are removed from level $|1\rangle$ and promoted to level $|3\rangle$. As a consequence they do not contribute to the nonlinear susceptibility at 1.064-μm. For long haul communication this may be beneficial, but for systems were control of the nonlinear susceptibility is critical, such as long haul soliton systems this effect will be detrimental to soliton instability. Eq. (5.19) predicts a decrease of 7-9 % in the nonlinear susceptibility as it is observed in the experimental data.

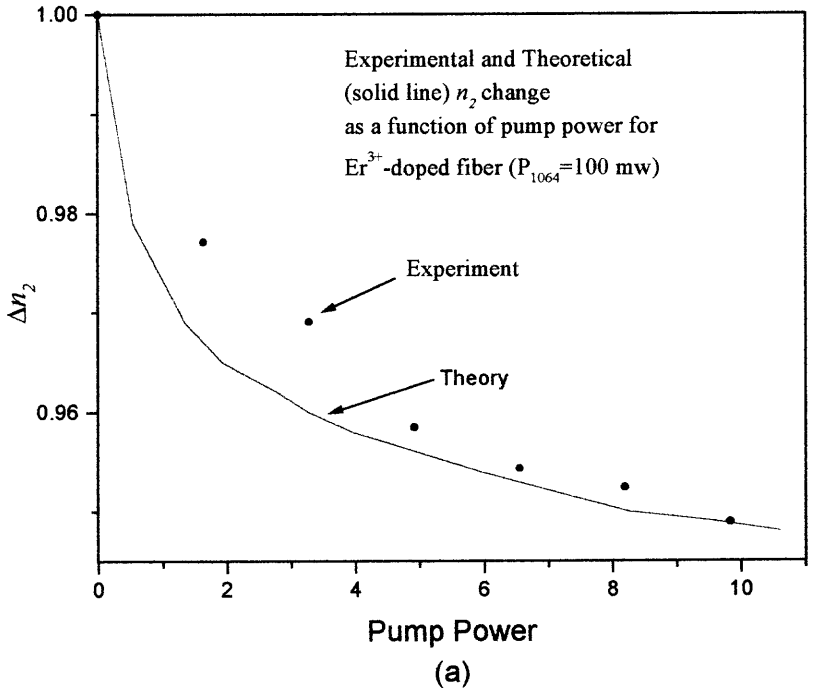

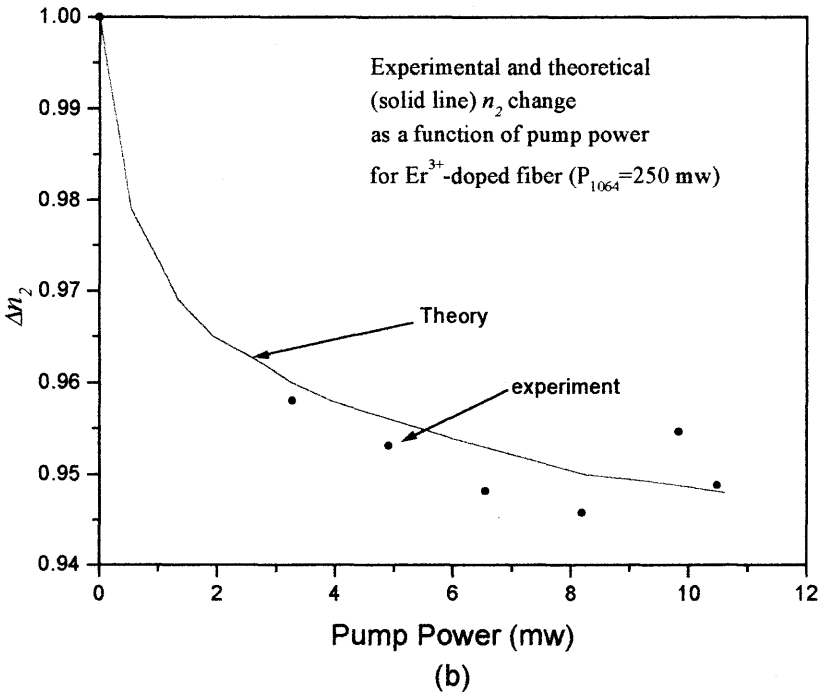

Figure 5.25 Decrease of the nonlinear index of refraction for (a) 100 mW of probe power, and (b) 250 mW of probe power as a function of pump power.

In the case of Yb-doped fiber the 1.064-μm laser experience gain. The signal beam acts as the probe, this is similar to the case of EDF-amplifiers. The power evolution of the signal and the pump laser has to be model in the analysis of IGA-TBC experiment. We assumed a saturate signal power of 1 mw for the 1.064-μm laser, and a 0.1 mw threshold power for the 980-nm. The analysis of the power evolution follows the same as in [94].

The erbium dopant assumed to be confined in the center of the core, the rate equation for the evolution of the pump (q), and signal (p) at wavelengths λ_p, λ_s, normalized to their respective intrinsic saturation powers take the form

$$-\frac{dq}{dz} = \pm\frac{\alpha_p}{D}\{U' p + 1\}q$$
$$\frac{dp}{dz} = \frac{\alpha_s}{D}\{Uq - 1\}p \tag{5.23}$$

with $D=1+q+p$ and $U=(\eta_s+\eta_p)/(1+\eta_p)$, $U'=(\eta_s-\eta_p)/(1+\eta_s)$, where the η's are the corresponding cross section radios. The α's are the absorption coefficients. Because the signal power changes along the fiber lets us defined an effective power defined by

$$P_{eff} = \frac{1}{L}\int_0^L P(z)dz \tag{5.24}$$

The experiment was done in two steps; first a trace with the pump on is take and recorded. This trace corresponds to the signal propagating in the fiber with an effective power P_{eff} with the pump off. The difference in the self-phase modulation strength of the two traces corresponds to the change in the nonlinear susceptibility. Physical parameters for the fiber are, α_p=270 dB/m, α_s=1 dB/m, L=20-m. Fig. 5.26 shows the evolution of the signal and the pump along the fiber. Fig. 5.27 the experimental IGA traces corresponding to the case of pump on and off. Finally Fig. 5.28 shows the decreased of the nonlinear index of refraction due to the presence of the pump compared with the theoretical model. Again the system shows a decreased on n_2 of the order of 9%.

In the model of the evolution of the pump power amplified spontaneous emission (ASE) is not included. The gain experience by the signal field is low The pump power couple in the fiber is about 10 mW, the signal experienced gain at the beginning of the fiber and is attenuated in the remaining length. The absorption peak of Yb is at 1032 nm, and not at 1064 nm. Therefore the 1064 nm laser is at the tail of the absorption band. This can be observed in Fig. 5.17.

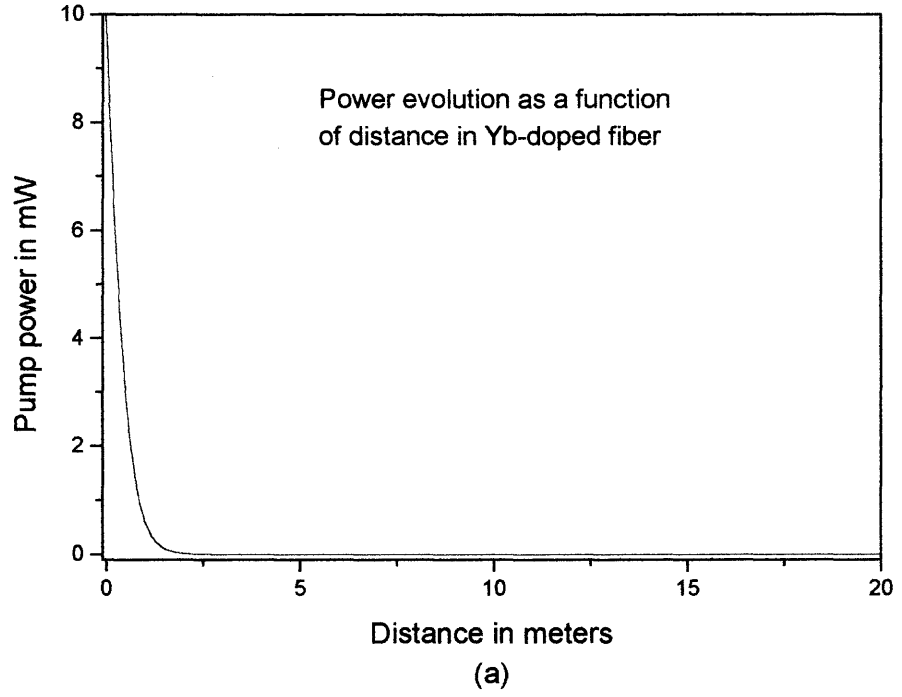

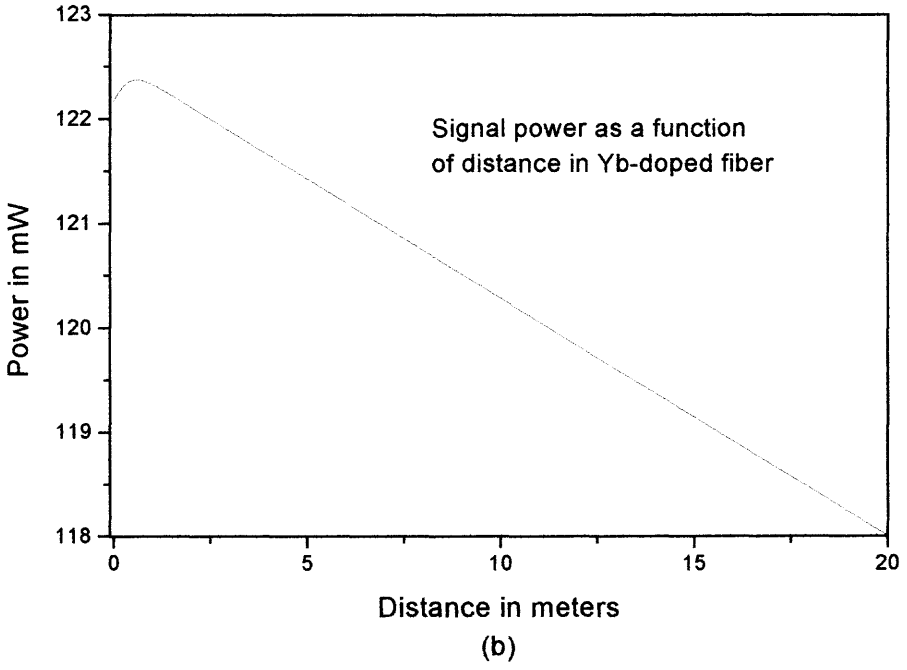

Figure 5.26 Evolution of the (a) pump power (b) signal power as a function of z from Eq. (5.23).

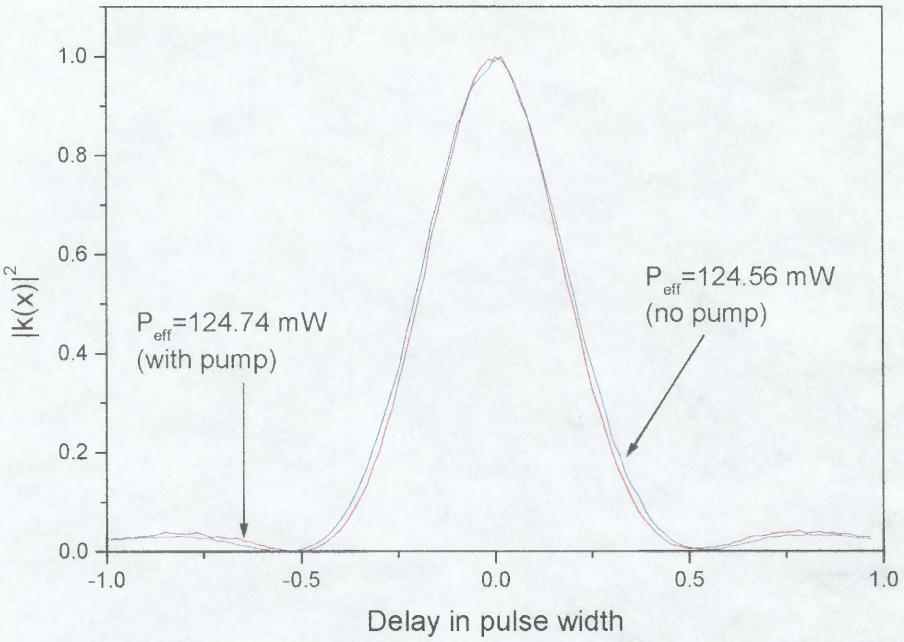

Figure 5.27 IGA traces for Yb-doped fiber with pump on and off.

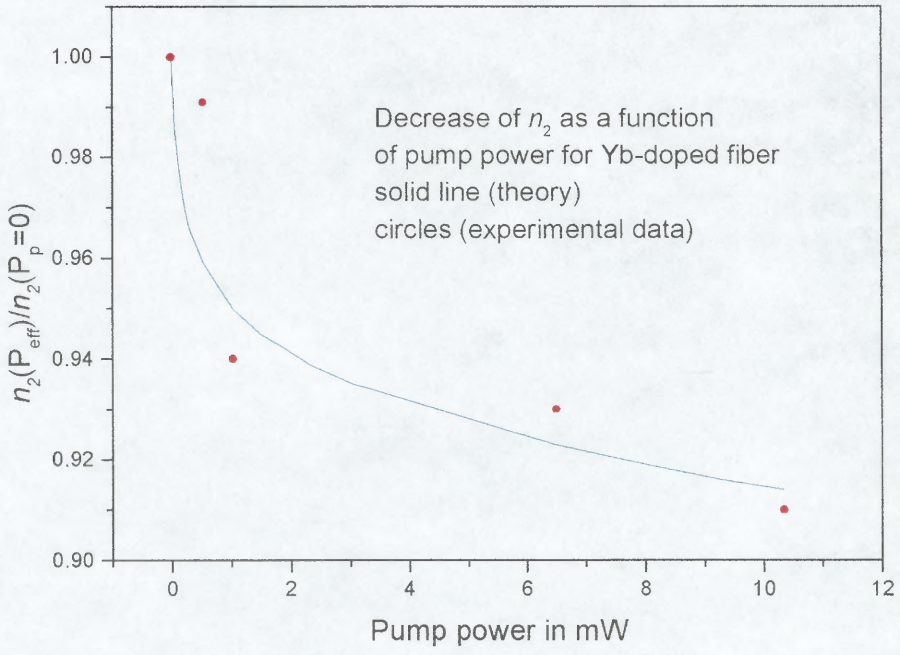

Figure 5.28 Decrease of n_2 as a function of pump power for Yb-doped fiber.

CHAPTER 6

MEASURE OF n_2 IN SEMICONDUCTORS USING TBC-IGA

6.1 Self-phase Modulation in Two Different Nonlinear Media

In section 3.2 we showed that in the nonlinear-dominant regime the wave equation describing the propagation of an optical pulse in a medium was given by

$$i\frac{\partial U}{\partial z} = -\frac{1}{L_{NL}}e^{\alpha z}|U|^2 U \tag{6.1}$$

Also we showed that Eq. (6.1) admits solution of the form

$$\begin{aligned} U(z,\tau) &= U(0,\tau)\exp\left(i\phi_{SMP}(z,\tau)\right) \\ \phi_{SPM}(z,\tau) &= \phi_o + \left(\frac{1-e^{-\alpha z}}{\alpha L_{NL}}\right)|U(0,\tau)|^2 \end{aligned} \tag{6.2}$$

in Eq. (6.2) ϕ_o represent an initial phase. Eq. (6.1) linear because any linear combination of solutions of Eq. (6.1) is also a solution of Eq. (6.1). This mean, in physical terms, that a pulse propagating in a set of N-nonlinear optical media will experienced a total self-phase modulation given by the sum of the self-phase modulation that the pulse experience in each of these media. This can be express as

$$\phi_{SPM}^{tot}(z,\tau) = \sum_i \phi_{SPM}^i(z_i,\tau) \tag{6.3}$$

If the pulse is a transformed limited Gaussian then the total self-phase modulation is given by

$$\phi(t) = \sum_i \frac{\omega_o n_2^i L_i}{2c} A_i^2 F_i^2(t) = \sum_i \omega_o \tau_p^i Q_i F_i^2(t) \tag{6.4}$$

In the case that the pulse propagates in two nonlinear media, the total self-phase modulation is given by

$$\phi(t) = \frac{\omega_o n_2^1 L_1}{2c} A_1^2 F_1^2(t) + \frac{\omega_o n_2^2 L_2}{2c} A_2^2 F_2^2(t) \tag{6.5}$$

where 1 and 2 represent each of the media.

In the case of TBC-IGA the above analysis mean that if a second medium is introduced in the path of a pulse that has been self-phase modulated, the total SPM experienced by the pulse is given by the sum of the contributions of each medium. This additional SPM produces narrowing or broadening of the initial IGA-trace, depending on the sign of n_2 in the second medium. If the first media is well characterized then the magnitude and the sign of n_2 in the second media can be found.

If the first medium is an optical fiber, the magnitude of n_2 in the second media is calculated by the change of the SPM strength when the second medium is introduced in the path of a pulse. If the second media is a semiconductor then the change in SPM is express as

$$\begin{aligned} &\omega_o \tau_p Q_{fiber} + \omega_o \tau_p Q_{semic} = \omega_o \tau_p Q_{tot} \\ &\omega_o \tau_p Q_{semi} = \omega_o \tau_p Q_{tot} - \omega_o \tau_p Q_{fiber} \\ &\omega_o \tau_p Q_{semi} = \Delta\omega_o \tau_p Q \end{aligned} \tag{6.5}$$

and n_2 is given by

$$n_2 = \frac{n_{semi} A_{eff}^{semi} \tau_p c \lambda}{\tau_r L_{semi}} \left(32\pi^2 \sqrt{\frac{\ln 2}{\pi}} \times 10^7 \right)^{-1} \left(\frac{\Delta\omega_o \tau_p Q}{P_{avg}^{semi}} \right) \tag{6.7}$$

The sign of n_2 is obtain by the increased/decreased of the total SPM strength when the semiconductor is place in the path of the optical pulse. If the total SPM increases, the nonlinear refractive index is positive on the other hand, if SPM decreases, the nonlinear refractive index of the semiconductor is negative.

One of the simplest and widely used approaches to the measurement of the nonlinear index of refraction in semiconductor films is the single beam Z-scan technique [95]. This technique measures the nonlinear phase distortion by measuring the transmittance of a Gaussian laser beam through the nonlinear medium and subsequently through a fine aperture in the far field. As the nonlinear medium is translated through the focus of the laser beam, the variance in the transmittance through the aperture is a consequence of the resultant intensity dependent nonlinear lens and hence a measure of n_2. Due to the confined mode of an optical fiber, the necessary spatial variation of the intensity dependent refractive index is precluded and thus *Z-scan cannot be applied to single mode fibers.* Although Z-scan is easy to implement, and requires little data manipulation, it is very sensitive to surface roughness and nonlinear absorption.

TBC-IGA is suitable for the measurement of n_2 in optical fibers [96,97] as well as semiconductor films [98]. The sign and magnitude can be extracted, and it is insensitive to surface roughness, and nonlinear absorption. TBC-IGA is totally base on pure nonlinear refraction. One of the limitations of TBC-IGA at the picosecond level is the need for high average powers in order to produce detectable changes in the SPM strength. This limitation can be overcome with fentosecond laser pulses. If fentosecond laser pulses are used the average power can be reduce to milliwatts.

6.2 Experimental Setup

Fig. 6.1 shows the experimental setup used to measure the nonlinear refractive index in semiconductor films. A train of 60.36-ps pulses generated by a cw mode-locked Nd:YAG laser running at 100-MHz repetition rate, were propagated in a 20-m Silica fiber, which generates SPM pulses. After propagating through the fiber the pulses were split in a

modified Michelson interferometer with a translation stage in one of the arms to produce time delay between the two pulses. The two beams were recombined in a photorefractive CdMnTe:V crystal (slow responding medium).

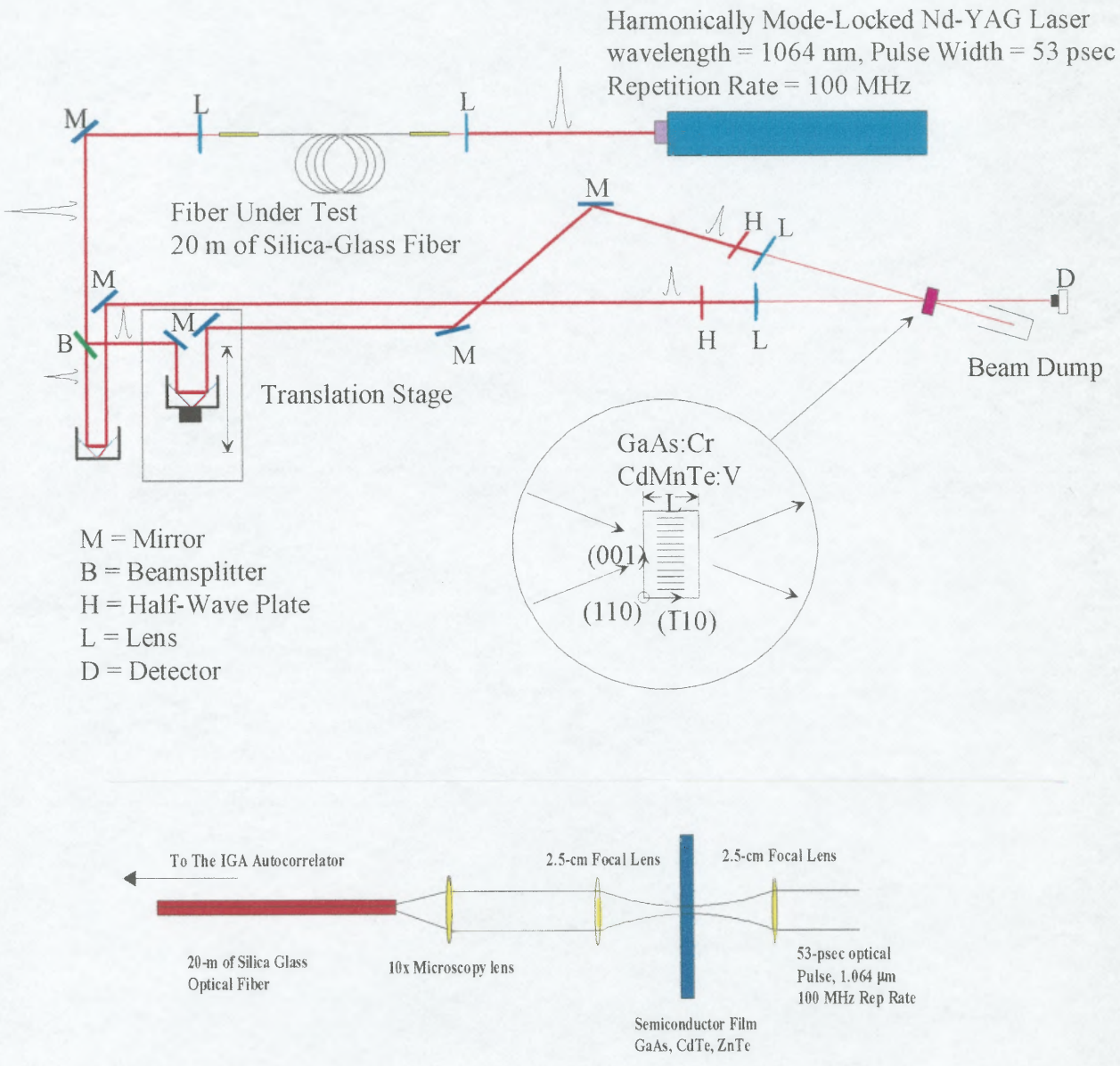

Figure 6.1 Experimental setup, the bottom figure shows the Setup for the case of the semiconductor.

The experimental procedure is as follows: first, an IGA trace is recorded as a function of time delay with an average power of 100 mW out the fiber. We call this trace the reference IGA-trace. Second, place the semiconductor in the path of the pulse, and before it is couple into the fiber as shown in Fig. 6.1. The average power couple into the fiber must be such that the output power is 100 mW. This second IGA-trace is recorded, and the observed shift in the oscillations must be proportional to the value for n_2 in the semiconductor. If the IGA-trace narrowed, the SPM-strength increases and the sign of n_2 in the semiconductor is positive. If the SPM-strength decreases, the IGA-trace broadens, and the sign of n_2 in the semiconductor is negative. The magnitude of n_2 is calculated from the increased (decreased) SPM-Strength due to the presence of the semiconductor film. Fig. 6.3 shows the experimental IGA traces for 1-mm thick samples of GaAs, CdTe and ZnTe. Table. 6.1 shows some of the parameters used in the calculation, and the experimental results for n_2 are shown in table 6.2. The results are also compared with values obtain using Z-scan [99].

Table 6.1 Experimental values used to calculated n_2.

	GaAs	**CdTe**	**ZnTe**
Effective Area	$1.0\text{x}10^{-6}$ cm^2	$1.0\text{x}10^{-6}$ cm^2	$1.0\text{x}10^{-6}$ cm^2
Average Power	3.04, 3.02 W	0.585 W	0.41 W
Thickness	1.0 mm	1.0 mm	3.0 mm
Index of refraction	3.48	2.84	2.79
Beam Diameter	0.3 cm	0.3 cm	0.3 cm
Pulse Width	60.36 ps	60.36 ps	60.36 ps
$\Delta\omega_o\tau_p Q$	1.894, 2.143	0.305	0.28

Table 6.2 Experimental values for n_2 obtaining by sing Z-scan [99] and TBC-IGA.

	GaAs	**CdTe**	**ZnTe**
Z-scan	-2700×10^{-13} esu	-2000×10^{-13} esu	830×10^{-13} esu
IGA-Two Beam coupling	-2830×10^{-13} esu	-1923×10^{-13} esu	825×10^{-13} esu

It can be seen inTable 6.2 that the IGA technique is within 5% of the accepted *Z-scan* value. It must be emphasized that although IGA is more involve in the implementation because it requires a two beam coupling arrangement, its advantage over Z-scan is that TBC-IGA can also be implemented in waveguide structures, like optical fibers were Z-scan is preclude. In regard to other conventional techniques to measure n_2, the experimental arrangements are more complicate and only the magnitude can be recovered. It is to the author's knowledge that only two techniques provide the sign information of n_2 they are Z-scan and TBC-IGA.

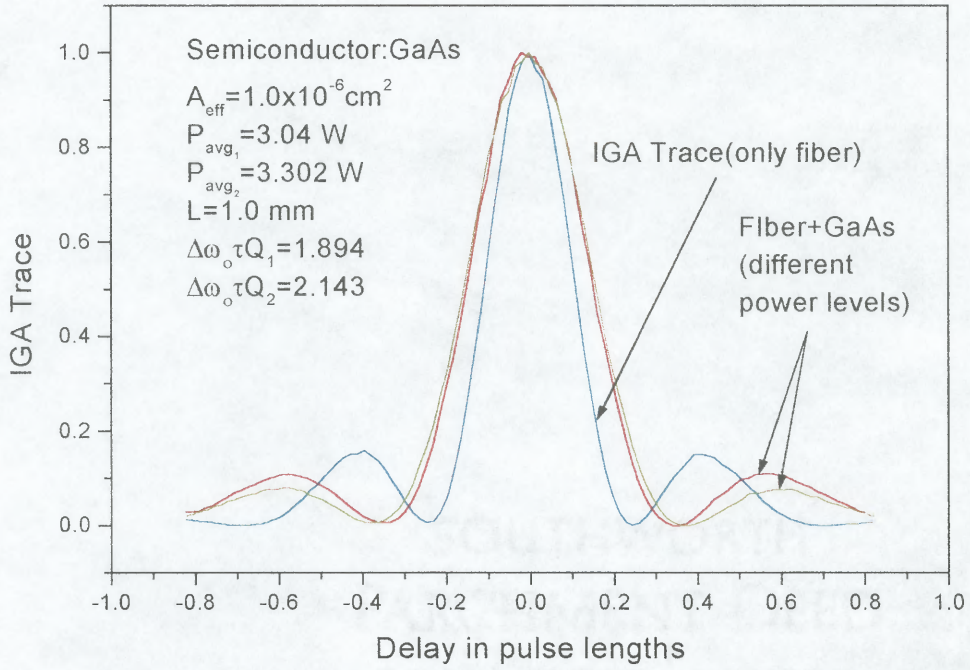
Semiconductor:GaAs
A_{eff}=1.0x10^{-6}cm^2
P_{avg_1}=3.04 W
P_{avg_2}=3.302 W
L=1.0 mm
$\Delta\omega_o\tau Q_1$=1.894
$\Delta\omega_o\tau Q_2$=2.143
IGA Trace(only fiber)
FIber+GaAs
(different
power levels)
IGA Trace
Delay in pulse lengths

(a)

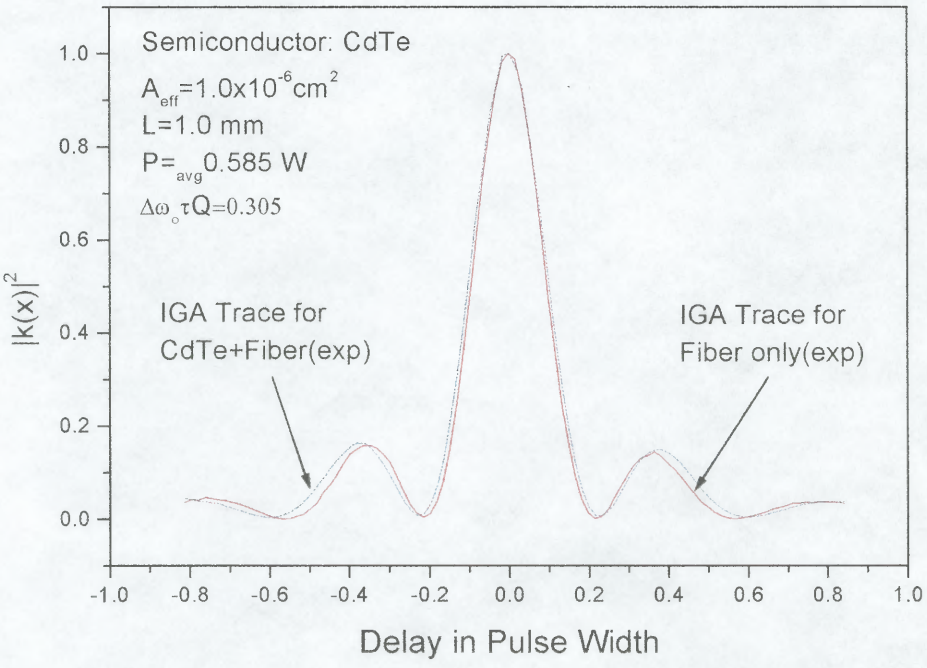
Semiconductor: CdTe
A_{eff}=1.0x10^{-6}cm^2
L=1.0 mm
P=$_{avg}$0.585 W
$\Delta\omega_o\tau Q$=0.305
IGA Trace for
CdTe+Fiber(exp)
IGA Trace for
Fiber only(exp)
$|k(x)|^2$
Delay in Pulse Width

(b)

Figure 6.2 Experiental IGA traces for (a) GaAs, and (b) CdTe.

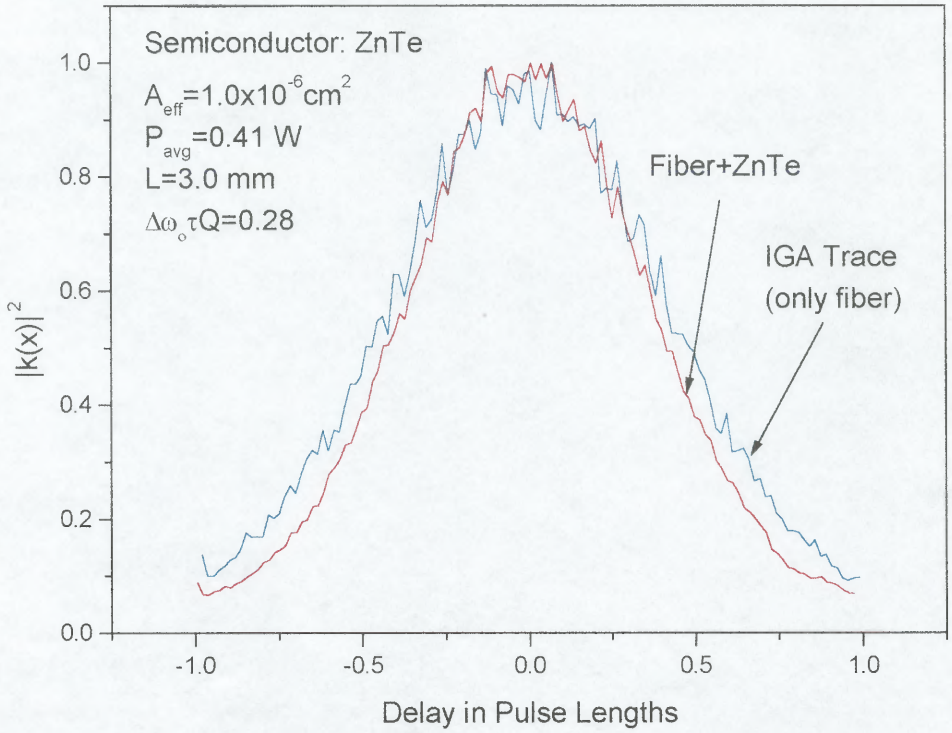

Figure 6.3 Experimental IGA-Traces with and without the semiconductor for for positive n_2 in ZnTe.

6.3 Conclusions

We have demonstrated theoretically and experimentally that the nonlinear susceptibility of optical fibers and semiconductors films can be extracted from a TBC-IGA trace of a picosecond pulse that has been self-phase modulated in the fiber or the semiconductor. This is a consequence of the fact that the energy detected in a TBC-IGA experiment is proportional to the electric field auto correlation function. This technique used to

characterized optical pulses, has been used here to characterized the medium where the pulse has propagates.

We also show that the results of Levine *et al* [50] were the same when the analysis was done using the space charge field analysis of two beam coupling in a photorefractive crystal [11]. We also found that the persistent absorption background present in the IGA trace of photorefractive semiconductors was due to the fact that semiconductors show long recombination times, as opposed to the short recombination times of the oxides. These long recombination times in semiconductors allow the formation of absorbing gratings whose duration were long than the laser repetition rates.

By identifying the dominant disperse and nonlinear effects in short length of fiber, we were able to find the correct experimental conditions for the case of pure self-phase modulation regime. The nonlinear index of refraction was experimentally determined for silica-glass, Erbium-doped, and Ytterbium-doped fibers. The values found for n_2 were in excellent agreement-within 5%- with the accepted values.

Using the density matrix approach we proved that the nonlinear index of refraction decreases in Er-doped and Yb-doped fibers in the presence of a pump laser. This decrease is the consequence of the charge redistribution when the pump laser is presence. This result beneficial for long haul communication systems may be detrimental for system where rigorous control of the nonlinear susceptibility is needed.

We also extended the technique to semiconductor films. We showed that the magnitude and the sign of n_2 could be determined in a semiconductor, because the total self-phase modulation experience by a pulse is the sum of the contribution of each of the nonlinear media that the pulse interact with. The values found were within 5% of the

values obtain from *Z-scan.* The advantage of TBC-IGA over *Z-scan* is that IGA is insensitive to surface roughness, and nonlinear absorption, because it is based on a pure refractive nonlinear phenomena.

TBC-IGA can be very useful in fiber development and design because it allows the characterization of the nonlinear optical properties of the fiber, especially of exotic optical fibers, and rare earth-doped fibers were production of long fibers is difficult.

Finally, this work should be try with fentosecond laser pulses. In this regime only few centimeters of fiber, and very low power levels are needed. In this case the pulse envelope must be modified to a sech type function. But in principle the same theory can also be applied. The technique at fentosecond level will be more attractive because of the low power needed to produce enough detectable self-phase.

APENDIX A

CALCULATION OF THE INCOHERENT TERM FOR A GAUSSIAN PULSE

The incoherent term in Eq. (4.22) can be analytical calculated for a transform limited Gaussian pulse. The incoherent term is

$$S_1(\tau) = \int_{-\infty}^{\infty}\int_{-\infty}^{\infty} |E(t)|^2 |E(t'-\tau)|^2 A''(t-t')dtdt' \tag{A.1}$$

assuming that the electric field is given by

$$E(t) = E_o \exp\left[-2\ln 2\frac{t^2}{\tau_p^2}\right]\exp(-i\omega t - ik\cdot r + i\phi) \tag{A.2}$$

and that the response function can be approximated as

$$A''(t-t') = a_{pop}\exp\left(-\frac{t-t'}{\tau_{pop}}\right) \tag{A.3}$$

In the above equations τ_p is the pulse FWHM, τ_{pop} is related to the population effects, also a_{pop} is related to the efficiency or deep of the population grating. Substituting Eq. (A.2) and Eq. (A.3) into Eq. (A.1), assuming that the pulses have the same average power and performing some arrangements we get

$$S_1(\tau) = I_o^2 a_{pop}\int_{-\infty}^{\infty}\exp\left(-4\ln 2\frac{t^2}{\tau_p^2}\right)\exp\left(\frac{-t}{\tau_{pop}}\right)dt\int_{-\infty}^{\infty}\exp\left(-4\ln 2\frac{(t'-\tau)^2}{\tau_p^2}\right)\exp\left(\frac{t'}{\tau_{pop}}\right)dt' \tag{A.4}$$

Completing the square in the first integral and regrouping terms we get from Eq. (A.4)

$$I_1(\tau) = \frac{\tau_p \exp\left(\frac{\tau_p^2}{16\ln 2 \cdot \tau_{pop}^2}\right)}{2\sqrt{\ln 2}} \int_{-\infty}^{\infty} e^{-u^2} du = \frac{\tau_p \exp\left(\frac{\tau_p^2}{16\ln 2 \tau_{pop}^2}\right)}{2\sqrt{\ln 2}} \sqrt{\pi} \quad \text{(A.5)}$$

and for the second term

$$I_2(\tau) = \frac{\tau_p \exp\left(\frac{\tau_p^2}{16\ln 2 \cdot \tau_{pop}^2}\right)}{2\sqrt{\ln 2}} \exp\left(-\frac{\tau}{\tau_{pop}}\right) \int_{-\infty}^{\infty} e^{-u^2} du = \frac{\tau_p \exp\left(\frac{\tau_p^2}{16\ln 2 \cdot \tau_{pop}^2}\right)}{2\sqrt{\ln 2}} \times \exp\left(-\frac{\tau}{\tau_{pop}}\right)\sqrt{\pi} \quad \text{(A.6)}$$

Replacing Eq. (A.5) and Eq. (A.6) into Eq. (A.4) we finally get

$$S_1(\tau) = \pi I_o^2 a_{pop} \frac{\tau_p^2 \exp\left(\frac{\tau_p^2}{8\ln 2 \cdot \tau_{pop}^2}\right)}{4\ln 2} \exp\left(-\frac{\tau}{\tau_{pop}}\right) \quad \text{(A.7)}$$

Eq. (A.7) describes the incoherent term due to the free carrier population; it is a function of the free carrier relaxation time, either by recombination or diffusion.

APENDIX B

DERIVATION OF THE RELATION BETWEEN THE AVERAGE POWER AND THE FIELD AMPLITUDE FOR A SELF-PHASE MODULATE GAUSSIAN PULSE

In the theory of self-phase modulation in a non-dispersive media, the self-phase modulation experience by the pulse can be written as

$$\phi_{spm}(t) = \frac{n_2 \omega_o L |A(t)|^2}{c} \tag{B.1}$$

assuming a Gaussian pulse envelope of the form

$$A(t) = U_o \exp\left[-2\ln 2\left(\frac{t}{\tau_p}\right)^2\right] \tag{B.2}$$

The total power per pulse is given by

$$P_{tot} = \int_{-\infty}^{\infty} |A(t)|^2 dt = \int_{-\infty}^{\infty} U_o^2 \exp\left(-4\ln 2\left(\frac{t}{\tau_p}\right)^2\right) dt = \frac{U_o^2 \tau_p}{2}\sqrt{\frac{\pi}{\ln 2}} \tag{B.3}$$

the peak intensity can be express as

$$I_{peak} = \frac{1}{2}\sqrt{\frac{\pi}{\ln 2}} U_o^2 \tag{B.4}$$

the peak intensity of the pulse can also be written in conventional unit as

$$I_{peak} = \frac{8\pi}{nc}\frac{P_{avg}\tau_r}{A_{eff}\tau_p} \times 10^7 \tag{B.5}$$

where P_{avg} is the average power of the laser, τ_r is the laser repetition rate, τ_p is the laser pulse width, and A_{eff} is the effective area. Substituting Eq. (B.5) into Eq. (B.4), and replacing the expression of U_o in Eq. (B.1) then we get for the self-phase of modulation of the pulse.

$$\phi_{spm}(t) = \frac{n_2 \omega_o L}{c} \frac{16\pi\sqrt{\ln 2} P_{avg} \tau_r}{\sqrt{\pi} nc \tau_p} \times 10^7 \exp\left(-4 \ln 2 \left(\frac{t}{\tau_p} \right)^2 \right) \qquad \text{(B.6)}$$

and the expression used in the text for n_2 in terms of the self-phase modulation strength is

$$n_2 = \frac{nc\lambda\tau_p A_{eff}}{L\tau_r} \left(32\pi^2 \sqrt{\frac{\pi}{\ln 2}} \times 10^7 \right)^{-1} \left(\frac{\omega_o \tau_p Q}{P_{avg}} \right) \qquad \text{(B.7).}$$

APENDIX C

COMPUTER PROGRAM USED TO CURVE-FIT THE EXPERIMENTAL DATA

The curve-fit the normalized experimental data, the following set of programs were developed in C-language, and run in a Sparc-10 Sun work station. Remarkable the same program can be run in a personal computer using any of the available C-compilers for PC. We program uses nonlinear curve fitting routines from the standard Numerical Recipes [1]. The subroutine call in the program is called MRQMIN, it is base on the Levenberg-Marquardt method. This method is powerful when the model does not depend linearly on the set of N unknown parameters like the case of Eq. (5.2?). Even though there is only one parameter to be fit, the model does no depend linearly on that parameter. The user must provide the model and the first derivative of the model. The first derivative is easy to calculate because is taken with respect to the fitting parameter, and can always be performed inside the integral sign.

The program calls a subroutine called FUNC1. This function evaluates the fitting function and its derivative with respect to the fitting parameter. The program stops converging when the best chi-square estimate is found such that the quantity defined as

$$\chi^2 \equiv \sum_{i=1}^{N} \left(\frac{y_i - y(x_i; a_1 \cdots a_N)}{\sigma_i} \right)^2 \qquad \text{(C.1)}$$

is a minimum. In Eq. (C.1) the y_i are the experimental data points, and the y are the calculated by the model. The σ_i are the standard deviation of each experimental data point. The convergence time for the program is found to be in between 5 to 10 sec for 256 to 512 data points. Remember that when the electromagnetic field is express in term

of complex numbers, at the end of the calculation the real part is the one that must be retained.

```
#include <stdio.h>
#include <math.h>
void funcs1();
float WAMP[2000];
float WTIME[2000];
int LISTA[5];
float SIG[2000];
int MFIT;
float *CHSQ,*CHSQ1;
float PARM[5];
float F;
main(argc, argv)
int argc;
char *argv[];
{
float **covar,**alpha;
float *alamda;
float n;
float n1,n2;
int nparm;
FILE *fp,*fl;
int ndat;
double part;
int i;
void mrqmin();
float **matrix(),*vector();
if(argc!=2)
 {
  printf("used SPM Strength Q\n");
  exit();
 }
/* set the initial value for the fitting parameters*/
sscanf(argv[1],"%f\n",&PARM[1]);
nparm=1;
MFIT=nparm;
LISTA[1]=1;
covar=matrix(1,nparm,1,1);
alpha=matrix(1,nparm,1,1);
CHSQ=vector(1,nparm);
fp=fopen("expdata","r");
fl=fopen("PARM2","w");
i=1;
```

```
/*read the input data*/
while(fscanf(fp,"%f %f\n",&WTIME[i],&WAMP[i])!=EOF)
 {
  SIG[i]=1.0;
  i++;
 }
ndat=i-1;
fclose(fp);
n=-1.0;
/*call the fitting routine whith alamada set to -1*/
alamda = &(n);
mrqmin(WTIME,WAMP,SIG,ndat,PARM,nparm,LISTA,MFIT,covar,alpha,CHS
Q,FUNCS1,alamda);
n2=0.0;
n1=*(CHSQ);
printf("%f %f\n",n1,n2);
while(abs(n1-n2) > 0.0001)
 {
  n2=*CHSQ;

mrqmin(WTIME,WAMP,SIG,ndat,PARM,nparm,LISTA,MFIT,covar,alpha,CHS
Q,FUNCS1,alamda);
  n1=*CHSQ;
  printf("%f  %f %f\n",n1,n2,PARM[1]);
 }
n=0.0;
alamda = &(n);
mrqmin(WTIME,WAMP,SIG,ndat,PARM,nparm,LISTA,MFIT,covar,alpha,CHS
Q,FUNCS1,alamda);
fprintf(fl,"%f\n",PARM[1]);
}
```

MFIT subroutine called by the main program; this program calculated the value of the model for each data point, and its first derivative with respect to the fitting parameter.

```
#include <stdio.h>
#include <math.h>
float x;
float a2,a3;
void FUNCS1(x1,a,afunc,dyda,ma)
float x1;
float a[];
float *afunc, *dyda;
```

```
int ma;
{
float R,R1;
int n;
float midpnt();
float volt(),volt1();
float upper,lower;
x=x1;
upper=0.6959098;
lower=-0.6959098;
a2=a[1];
a3=a[2];
for(n=1;n<8;n++)
 R=midpnt(volt,lower,upper,n);
*afunc= 0.9183411086214*R*R;
for(n=1;n<6;n++)
 R1=midpnt(volt1,lower,upper,n);
dyda[1]=0.9183411086214*R1*R1;
return;
}
float volt(b)
float b;
{
 float F;
 F = exp(-1.39*(b*b + pow(b+x,2.0)))*cos(a2*(exp(-2.77*pow(b+x,2.0)) - exp(-
2.77*b*b)));
 return (float) F;
}
float volt1(b1)
float b1;
{
 float F;
 float F1;
 float F2;
 F1 = exp(-1.39*(b1*b1 + pow(b1+x,2.0)))*sin(a2*(exp(-2.77*pow(b1+x,2.0)) - exp(-
2.77*b1*b1)));
 F2 = exp(-2.77*pow(b1+x,2.0)) - exp(-2.77*b1*b1);
 F = F1*F2 + a3;
 return (float) F;
}
```

APPENDIX D

THE NONLINEAR SUSCEPTIBILITY FOR A QUASI-THREE LEVEL SYSTEM IN THE PRECENSE OF A PUMP LASER

D.1 Semiclassical Theory for $\chi^{(3)}$ in a Quasi-Three Level System

In this appendix we derive in detail the nonlinear susceptibility for a quasi-three level system in the presence of a pump laser. Using the Hamiltonian given in Eq. (2.26) and Eq. (2.24) the equation of motion for the density matrix operator is given by

$$\begin{aligned}
\frac{\partial \rho_{11}}{\partial t} &= A_{21}\rho_{22} - R_{13}(\rho_{11} - \rho_{33}) - R_{14}(\rho_{11} - \rho_{44}) - i\Omega_s(\rho_{12} - \rho_{21}) \\
&\quad - i\Omega_p(\rho_{13} - \rho_{31}) - i\Omega_{pr}(\rho_{14} - \rho_{41}) \\
\frac{\partial \rho_{22}}{\partial t} &= A_{32}\rho_{33} - A_{21}\rho_{22} + i\Omega_s(\rho_{21} - \rho_{12}) \\
\frac{\partial \rho_{33}}{\partial t} &= R_{13}(\rho_{11} - \rho_{33}) - A_{32}\rho_{33} + i\Omega_p(\rho_{13} - \rho_{31}) \\
\frac{\partial \rho_{44}}{\partial t} &= R_{14}(\rho_{11} - \rho_{44}) + i\Omega_{pr}(\rho_{14} - \rho_{41}) \\
\\
\frac{\partial \rho_{12}}{\partial t} &= -(\gamma_{12} + i\Delta_{12})\rho_{12} - i\Omega_s(\rho_{22} - \rho_{11}) \\
\frac{\partial \rho_{13}}{\partial t} &= -(\gamma_{13} + i\Delta_{13})\rho_{13} - i\Omega_p(\rho_{33} - \rho_{11}) \\
\frac{\partial \rho_{14}}{\partial t} &= -(\gamma_{14} + i\Delta_{14})\rho_{14} - i\Omega_{pr}(\rho_{44} - \rho_{11})
\end{aligned} \tag{D.1}$$

In Eq. (D.1) γ_{nm} represent the dipole diphase relaxation time, Ω_n are the Rabi frequencies for each of the fields and are equal to $\mu_n E_n/\hbar$, and the $\Delta_{nm}=\omega_j - \omega_{nm}$ are the detuning factor from the resonance transition frequencies. In addition, the R_{nm} are the pumping rates for the pump and the probe fields. We have to assume that the probe fields can promote

considerable amount of carriers to state |4⟩. The A's are the corresponding relaxation rate for each transition.

The rate equation for the system is the time evolution of the populations of the different levels. They are express in terms of : The pumping rates R_{mn}, the transition probabilities W_{mn}, and the relaxation rates A_{mn}. Where m,n=1,2,3,4 corresponding to the different energy levels. Particles leaving n-level per unit time will contribute negatively to the time evolution of that level (depopulation).

$$\begin{aligned}
\frac{dN_1}{dt} &= R_{13}N_1 + R_{31}N_3 - W_{12}N_1 + W_{21}N_2 + A_{21}N_2 - R_{14}N_1 + R_{41}N_4 \\
\frac{dN_2}{dt} &= W_{12}N_1 - W_{21}N_2 + A_{32}N_3 - A_{21}N_2 \\
\frac{dN_3}{dt} &= R_{13}N_1 - R_{31}N_3 - A_{32}N_3 \\
\frac{dN_4}{dt} &= R_{14}N_1 - R_{41}N_4 \\
N &= N_1 + N_2 + N_3 + N_4
\end{aligned} \tag{D.2}$$

Solving the above set of equations for the steady state case. Assuming that the relaxation rate is $A_{32}>>A_{21}$, the non-radioactive decay rate A_{32} is dominant over the pumping rate $R=R_{13}=R_{31}$, and that $R'=R_{14}=R_{41}$, we can obtain from Eq. (D.2)

$$\begin{aligned}
N_1 &= \frac{(\tau W_{21}+1)}{(\tau W_{21}+1)(k+1)+R\tau+W_{12}\tau} \\
N_2 &= \frac{R\tau+W_{12}\tau}{(\tau W_{21}+1)(k+1)+R\tau+W_{12}\tau} \\
N_3 &= 0 \\
N_4 &= \frac{k(\tau W_{21}+1)}{(\tau W_{21}+1)(k+1)+R\tau+W_{12}\tau}
\end{aligned} \tag{D.3}$$

in Eq. (D.3) we used $A_{21}=\tau^{-1}$ which is the fluorescence life time, and $k=R'\tau_1$. The population in level $|3\rangle$ is zero because of the predominant non-radioactive decay to level $|2\rangle$. Using the following definitions for the transitions and pumping rates

$$W_{12}\tau = \frac{1}{1+\eta}\frac{I_s}{I_s^{sat}},\quad W_{21}\tau = \frac{\eta}{1+\eta}\frac{I_s}{I_s^{sat}},\quad R\tau = \frac{I_p}{I_p^{th}},\quad R'\tau_1 = \frac{I_{pr}}{I_{pr}^{th}},\quad I_i^{sat,th} = \frac{\hbar\omega_i}{\left[\frac{\sigma_i^{peak}}{1+\delta_i}\right]\tau_i}$$

$$\delta_i = \frac{2(\omega_i-\omega_{i1})}{\Delta\omega_{i1}},\quad \sigma_i^{peack} = \frac{\lambda_i^2}{2\pi n^2\tau_i\Delta\omega_{i1}}\ for\ i=2,3,4\quad \rho_{ij}=\sigma_{ij}\exp(-i\omega_j t)\ for\ j=p,pr,s$$

in the above relations the $I_{s,p,pr}$ correspond to the signal, pump, and probe intensities, $\Delta\omega_{ij}$ to the FWHM of the homogenously transition such that $\gamma_{12}=\Delta\omega_{12}/2$ is the inverse of the dipole relaxation time. There is thresholds pump power where the system is fully inverted, and a probe and signal saturation power where the system is totally bleached denote by *th*, and *sat.* the ω_{ij} denotes the frequency difference between level I and j, and we allow for some detuning factor in the transitions.

Solving Eq. (D.1) for the steady state case we get after some algebra for the non-diagonal elements of the density matrix

$$\begin{aligned}\sigma_{12} &= \Omega_s\frac{(\sigma_{11}-\sigma_{22})}{\gamma_{12}-i\Delta_{12}}\\ \sigma_{13} &= \Omega_p\frac{(\sigma_{11}-\sigma_{33})}{\gamma_{13}-i\Delta_{13}}\\ \sigma_{14} &= \Omega_{pr}\frac{(\sigma_{11}-\sigma_{44})}{\gamma_{14}-i\Delta_{14}}\end{aligned}\qquad (D.4)$$

As we pointed in chapter 3 in the rotating wave approximation the term with the negative exponent in the electric field is a better driving field, then the total polarization of the system can be expressed as

$$P = \varepsilon_o \{\chi_p \exp(-i\omega_p t) + \chi_s \exp(-i\omega_s t) + \chi_{pr} \exp(-i\omega_{pr} t)\} = Ntr(\mu_{12}\rho_{12} + \mu_{13}\rho_{13} + \mu_{14}\rho_{14})$$

using the above expression we get for the susceptibility for each of the fields

$$\begin{aligned} \chi_s &= \frac{N\mu_{12}^2}{\hbar} \frac{(\rho_{22} - \rho_{11})}{(\Delta_{12} - i\gamma_{12})} \\ \chi_p &= \frac{N\mu_{13}^2}{\hbar} \frac{(\rho_{33} - \rho_{11})}{(\Delta_{13} - i\gamma_{13})} \\ \chi_{pr} &= \frac{N\mu_{14}^2}{\hbar} \frac{(\rho_{44} - \rho_{11})}{(\Delta_{14} - i\gamma_{14})} \end{aligned} \tag{D.5}$$

Where N is the density of the rare earth atoms in the system. Using the rate equations to calculated the population difference, we get for the total susceptibility at the signal field

$$\chi_s(\omega_s) = \frac{nNc\sigma_s^{peak}}{\omega_s} \frac{(\delta_s + i)}{1 + \delta_s^2} \frac{\left(\frac{I_p}{I_p^{th}} - 1\right)}{\left(\frac{I_s}{I_s^{sat}} + 1\right)\left(\frac{I_p}{I_p^{th}} + \frac{I_{pr}}{I_{pr}^{th}} + 1\right)} \tag{D.6}$$

In the Eq. (D.6) n is the index of refraction, and we have defined the dipole relaxation time to be equal to twice the FWHM of the homogeneously broadened transition, or $\gamma_{12}=\Delta\omega_{12}/2$. The detuning normalized factor is defined as

$$\delta_j = \frac{2 \cdot (\omega_j - \omega_{mn})}{\Delta\omega_{mn}} \tag{D.7}$$

If the intensity of the probe beam in Eq. (D.6) is neglected, we recover the same result of Desurvire [30]. In that case, there is a resonance enhancement of the refractive index due to the presence of the pump field. On the other hand, if there is no pump field and no probe field, then the susceptibility is the same as the case of a two level system, which is described in [31]. Eq. (D.7) is the total signal susceptibility. To get the nonlinear

susceptibility, we expand Eq. (D.7) in powers of I_s and retain the linear terms in I_s, that gives us

$$\chi_s(\omega_s) = \frac{nNc\sigma_s^{peak}}{\omega_s}\frac{(\delta_s + i)}{(\delta_s^2+1)}\frac{\left(\frac{I_p}{I_p^{th}} - 1\right)}{\left(\frac{I_p}{I_p^{th}} + \frac{I_{pr}}{I_{pr}^{th}} + 1\right)}\left(1 - \frac{I_s}{I_s^{sat}} + ...\right) \tag{D.8}$$

Using the expression $\chi = \chi^{(1)} + 3\chi^{(3)}\left|\mathcal{E}^2\right| + ...$, we get for the real part of the third order nonlinear susceptibility

$$\chi_s^{(3)}(\omega_s) = \frac{n^2\varepsilon_o Nc^2\sigma_s^{peak}}{\omega_s \bar{I}_s^{sat}}\frac{\delta_s}{(\delta_s^2+1)}\frac{\left(1 - \frac{I_p}{I_p^{th}}\right)}{\left(\frac{I_p}{I_p^{th}} + 1\right)^2} \tag{D.9}$$

The linear susceptibility at the probe field is given by

$$\chi_{pr}(\omega_{pr}) = \frac{nNc\sigma_{pr}^{peak}}{\omega_s}\frac{(\delta_{pr} + i)}{1+\delta_{pr}^2}\frac{\left(\frac{I_p}{I_p^{th}} - 1\right)}{\left(\frac{I_p}{I_p^{th}} + \frac{I_{pr}}{I_{pr}^{th}} + 1\right)} \tag{D.10}$$

Finally expanding Eq. (D.10) in term of powers of I_{pr}, and retaining only the linear terms in I_{pr}, we obtain for the nonlinear susceptibility at the probe field frequency as a function of pump power I_p

$$\chi_{pr}^{(3)} = \frac{n^2\varepsilon_o Nc^2\sigma_{pr}^{peak}}{\omega_s \bar{I}_{pr}^{sat}}\frac{\delta_{pr}}{\delta_{pr}^2+1}\frac{\left(\frac{I_p}{I_p^{th}} + 2\right)}{\left(\frac{I_p}{I_p^{th}} + 1\right)^2} \tag{D.11}$$

REFERENCES

1. R. F. Haglund Jr. "Ion Implantation as a tool in the synthesis of practical thrid-order nonlinear optical materials," *Mater. Sci. and Eng*, **A**253, 275-283, 1998.

2. K. J. Boller, A. Imamoglu, and S. E. Harris, "Observation of Electromagnetic Induce Transparency," *Phys. Rev. Lett.* **66**, 2593-2596, 1991.

3. H. Schmidt, and A. Imamoglu, "Giant Kerr nonlinearities obtained by electromagnetically induced transparency," *Opt. Lett.* **21**, 1936-1938, 1996.

4. N. G. R. Broderick, T. M. Monro, P. J. Bennett, and D. J. Richardson, "Nonlinearity in holey optical fibers and future opportunities," *Optc. Lett.* **24**, 1395-1397, 1999.

5. B. R. Suydam., in *The Supercontinuum Laser Source,* R. R. Alfano Ed. (Springer-Verlag, New York, 1989.

6. R. A. Chraplyvy, "Limitations on Lightwave Communication Imposed by Optical-Fiber Nonlinearities," *J. Lightwave Technol.*, Vol. 8, No. 10, p. 1548, 1984.

7. P. J. Gordom and L. F. Mollenauer, "Effects of Fiber Nonlinearities and Amplifiers Spacing on Ultra-Long Distance Transmission," *J. Lightwave Technol*, Vol. 9, No. 2, p. 170, 1991.

8. M. J. O`Mahony, "Physical Limitations in Optical Cross-connect Networks," Tu.B.T.3, *ECOC'95,* p. 63, 1995.

9. W. E. Williams, M. J. Soileau, and W. Van Stryland, "Optical switching and n_2 measurements in CS_2." *Opt. Commun.*, Vol. **50,** 256-260, 1984.

10. M. Sheik-Bahae, A. A. Said, Tai-huei Wei, D. J. Hagan, E. W. Stryland, "Sensitive measurement of optical nonlinearities using a single bean," *IEEE J. Quantum Electron., Vol* **QE-26,** 760-769, 1990.

11. M. J. Moran, C. Y. She, and R. L. Carman, "Interferometric measurements of nonlinear refractive-index coefficient relative to CS_2 in laser-system-related materials," *IEEE J. Quantum Electron.,* Vol **QE-11,** 259-263, 1975.

12. S. R. Friberg, and P. W. Smith, "Nonlinear optical glasses for ultra-fast optical switches," *IEEE J. Quantum Electron.,* Vol **QE-23,** 2089-2094, 1987.

13. R. Adair, L. L. Chase, and S. A. Payne, "Nonlinear refractive index measurement of glasses using three-wave frequency mixing," *J. Opt. Soc. Am.* **B4,** 875-881.

14. Owyoung, "Ellipse rotation studies in laser host materials," *IEEE J. Quantum Electron.,* Vol **QE-9,** 1064-1069, 1973.

15. R. H. Stolen and C. Lin, "SPM in silica optical fibers," *Phys. Rev.* **A17**, 1978.

16. A. M. Levine, E. Özizmir, R. Trebino, C. C. Hayden, A. M. Johnson, and K. L. Tokuda, "Induce-Grating autocorrelation of ultrashort pulses in a slowly responding medium," *J. Optc. Soc. Am. B.* **11**, 1609-1618, 1994.

17. X. Steve Yao, Vince Dominic, Jack Feinberg, "Theory of beam coupling and pulse shaping of mode-locked laser pulses in photorefractive crystal," *J. Opt. Soc. Am. B* **7**, 2347-2355 (1990).

18. R. Trebino, E. K. Gustafson, A. E. Siegman, "Fourth-order partial-coherence effects in the formation of integrated-intensity gratings with pulsed light sources," *J. Opt. Soc. Am. B* **10**, 1295-1304 (1986).

19. P. A. Franken, A. E. Hill, C. W. Peters, G. Weinrich, *Phys. Rev. Lett.* **7**, 118 (1961).

20. T. H. Maiman, *Nature* 187, 493 (1960).

21. D. F. Eaton, "Nonlinear Optical Materials," *Science*, Vol. 44, 281, (1991).

22. R. W. Boyd, "The Nature of the Nonlinear Optical Susceptibility," in *Laser Sources and Applications* (SUSSP, Scotland, 1997), p. 1.

23. S. S. Jha, and N. Bloembergen, "Nonlinear Optical Susceptibilities in Group-IV and III-V Semiconductors," *Phys. Rev.* Vol. 171, 891 (1968).

24. N. L. Boling, A. J. Glass, and A. Owyoung, "Empirical Relationships for Predicting Nonlinear Refractive Index Changes in Optical Solids," *IEEE J. Quantum Electron.*, vol. **QE-14**, pp. 601-608, 1978.

25. M. Sheik-Bahae, D. C. Hutchings D. J. Hagan, and E. W. Van Stryland, "Dispersion of Bound Electronic Nonlinear Refraction in Solids," *IEEE J. Quantum Electron.*, vol. **QE-27**, pp. 1296-1309, 1991.

26. D. A. Miller, C. T. Seaton, M. E. Price, and S. D. Smith, "Band gap reso-nant nonlinear refraction in III-V semiconductors," *Phys. Rev. Lett.*, vol. 47, pp. 197-200, 1981.

27. B. S. Wherrett, D. Hutchings, and D. Russell, "Optically bistable interfe-rence filters: Optimization considerations," *J. Opt. Soc. Amer. B,* vol. 3, pp. 351-362, 1986.

28. V. Mizrahi, K. W. DeLong, G. I. Stegemen, M. A. Saifi, and M. J. Andrejco, "Two-photon absorption as a limitation to all-optical switching," *Opt. Lett.*, vol. 14, pp. 1140-1142, 1989.

29. Yariv, Quantum Elelctronics (John Wiley & Sons, New York, ed. **2**, (1975).

30. E. Desurvire, "Study of the complex susceptibility of Erbium-Doped fiber amplifiers," *J. Lightwave Technol.*, vol. 8, no. 10, p.1517, 1990.

31. R. W. Boyd, Nonlinear Optics (Academic Press, San Diego, Ca, 1992).

32. Y. L. Xue, P. L. Chu, and W Zhang, "Resonance-enhanced refractive index and its dynamics in rare-earth-doped fibers," *J. Opt. Soc. Am. B.*, vol. 10, no. 10, p. 1840, 1993.

33. M. H. Dunn, "Electromagnetically Induce Transparency," in *Laser Sources and Applications* (SUSSP, Scotland, 1997), p. 411.

34. F. Shimizu, "Frequency broadening in liquids by a short light pulse," *Phys. Rev. Lett.* **19**, 1097 (1967).

35. R. R. Alfano and S. L. Shapiro, "Observation of self-phase modulation in crystals and glasses," *Phys. Rev. Lett.* **24**, 592 (1970); **24**, 1217 (1970).

36. E. P. Ippen, C. V. Shank, T. K. Gustafson, *Appl. Phys. Lett.* **24**, 190 (1974).

37. R. H. Stolen and C. Lin, "Self-phase modulation in silica optical fibers," *Phys. Rev.* **A17,** (1978).R. H. Stolen and C. Lin, *Phys. Rev.* A **17**, 1448 (1978).

38. G. P. Agrawal, "Nonlinear Fiber Optics," Academic Press, INC, San Diego, Ca, 1989.

39. Q. Z. Wang, P. P. Ho, and R. R. Alfano., in *The supercontinuum Laser Source,* R. R. Alfano Ed. (Springer-Verlag, New York, 1989).

40. E. P. Gross, *Nuovo Cimento* **20**, p. 454 (1961); L. P. Pitaevskii, *Sov. Phys. JETP* **13,** p. 451, (1961).

41. K. Huang "Quantum Field Theory," (John Wiley & Sons, New York, 1998).

42. C. N. Yang, *Rev. Mod. Phys.* **34**, 4 (1964).

43. K. Burnett, M. Edward, and C. W. Clark, "The theory of Bose-Einstein Condensation of Dilute Gases," *Phys. Today.* vol. 5, 37, 1999.

44. B. S. Wherrett, A. L. Smirl, T. F. Boggess, "Theory of Degenerate Four-Wave Mixing in Picosecond Exitation-Probe Experiments," *IEEE J. Quantum Electron.*, vol. **QE-19**, 680-689 (1983).

45. A. M. Johnson, Hernando Garcia, private communication.

46. A. L. Smirl, G. C. Valley, K. F. Bogges, Jr., "Picosecond photorefractive and Free-carrier transient energy transfer in GaAs at 1 μm," *IEEE J. Quantum Electron.*, vol. **QE-24**, 289-303 (1988).

47. S. L. Palfrey, T. F. Heinz, "Coherent interaction in Pump-Probe absorption measurements: the effect of phase gratings," *J. Opt. Soc. Am. B* **2**, 674-679 (1985).

48. N. Kukhtarev, V. B. Markov, S. G. Odulov, *Opt. Commun.* **23**, 338 (1977).

49. K. L. Sala, G. A. Keney, and G. E. Hall, "CW Autocorrelation Measurements of picosecond Laser Pulses," *IEEE J. Quantum Electron.*, vol. **QE-16**, 990-996 (1980).

50. A. M. Levine, E. Özizmir, R. Trebino, C. C. Hayden, A. M. Johnson, and K. L. Tokuda, "Induce-grating autocorrelation of ultrashort pulses in a slowly responding medium," *J. Opt. Soc. Am. B* **11**, 1609-1618 (1994).

51. R. Trebino, C. C. Hayden, A. M. Johnson, W. M. Simpson, and A. M. Levine, "Chirp and self-phase modulation in induce-grating autocorrelation measurements of ultrashort pulses," *Optc. Lett.* **15**, 1079, (1990).

52. S. L. Palfrey, T. F. Heinz, "Coherent interaction in Pump-Probe absorption measurements: the effect of phase gratings," *J. Opt. Soc. Am. B* **2**, 674-679 (1985).

53. N. Kukhtarev, V. B. Markov, S. G. Odulov, *Opt. Commun.* **23**, 338 (1977).

54. X. Steve Yao, Vince Dominic, Jack Feinberg, "Theory of beam coupling and pulse shaping of mode-locked laser pulses in photorefractive crystal," *J. Opt. Soc. Am. B* **7**, 2347-2355 (1990).

55. R. Trebino, E. K. Gustafson, A. E. Siegman, "Fourth-order partial-coherence effects in the formation of integrated-intensity gratings with pulsed light sources," *J. Opt. Soc. Am. B* **10**, 1295-1304 (1986).

56. R. W. Boyd, *Nonlinear Optics*, Academic Press, INC, San Diego, Ca, 1992.

57. S. Ducharme, and J. Feinberg, "Altering the photorefractive properties of $BaTiO_3$ by reduction and oxidation at 650° C," *J. Opt. Soc. Am. B* **3**, 283-292 (1986).

58. F. P. Strohkendl, J. M. C. Jonathan, and R. W. Hellwarth, "Hole-electron competition in photorefractive gratings," *Optc. Lett.* **11**, 312, (1986).

59. P. Gunter, Phys. Rep. **92**,199 (1982).

60. A. M. Glass, A. M. Johnson, D. H. Olson, W. Simpson, A. A. Ballman, "Four-wave Mixing in semi-insulating InP and GaAs using the photorefractive effect," *Appl. Physic. Lett.*, vol **44**, 948-950, May 1984.

61. J. Strait, A. M. Glass, "Time-resolved photorefractive four-wave mixing in semiconductor materials," *J. Optc. Soc. Amer. B* **3,** 342-344 (1986).

62. Partovi, J. Millerd, E. M. Garnire, M. Ziari, W. H. Steier, S. B. Trivedi, M. B. Klein, "Photorefractivity at 1.5 μm in CdTe:V," *Appl. Phys. Lett.*, vol **57**, 846-848 (1990).

63. M. B. Klein, and R. N. Schwartz, "Photorefractive effect in $BaTiO_3$: microscopic origins," *J. Optc. Soc. Amer. B* **3,** 293-305 (1986).

64. A. L. Smirl, K. Bohnert, G. C. Valley, R. A. Mullen, and T. F. Boggess, "Formation, decay, and erasure of photorefractive gratings written in barium titanate by picosecond pulses," *J. Optc. Soc. Amer. B* **6,** 606-615 (1989).

65. G. Brost, K. Magde, and S. B. Trivedi, "Progress in II-VI photorefractives," *SPIE* **2481**, 227-231, 1997.

66. R. N. Schwartz, C. C. Wang, S. Trivedi, G. V. Jagannathan, F. Davidson, P. R. Boyd, and U. Lee, "Spectroscopy and photorefractive characterization of cadmium telluride crystals codoped with vanadium and manganese," *Phys. Rev. B* **55**, 378-381, (1997).

67. G. C. Valley, J. Dubard, A. L. Smirl, and A. M. Glass, "Picosecond photorefractive responses of GaAs:EL2, InP:Fe, and CdTe:V," *Optc. Lett.* **14**, 961, (1989).

68. Quantronix Model 416 Laser, Technical Manual, Quantronix Corporation, New York.

69. R. A. Chraplyvy, "Limitations on Lightwave Communication Imposed by Optical Fiber Nonlinearities," *J. Lightwave Technol.*, vol. **8**. No. 10, 1548-1557, 1984.

70. J. J. Refi, "Optical Fibers for Optical Networking," *Bell. Labs. Tech. J.*, 246-261, January-March, 1999.

71. P. V. Mamyshev, "Fibre Nonlinearities," in *Laser Source and Applications*, A Miller, and D. M. Finlayson, SUSSP P ublications, St Andrews, June, 1995.

72. M. J. O'. Mahony, D. Simeonidou, A. Yu, and J. Zhou, "The Design of a European Optical Network," *J. Lightwave Technol.*, vol. **13**. No. 5, 817-828, 1995.

73. G. P. Agrawal, *Nonlinear Fiber Optics*, Academic Press, New York, 1989.

74. Y. Namihira, "Relationship between nonlinear effective area and modefield diameter for dispersion shifted fibres," *Electron. Lett.*, **30**, 262-264, 1994.

75. Y. Namihira, A. Miyata, and N. Tanahashi, "Nonlinear coefficient measurements for dispersion shifted fibres using self-phase modulation method at 1.55 μm," *Electron. Lett.*, 1994.

76. E. Desurvire, *Erbium Doped Fiber Amplifier,* John Wiley & Sons, Inc, New York, 1994.

77. W. H. Press, B. P. Flannery, S. A. Teukolsky, W. T. Vetterling, *Numerical Recipes*, Cambridge University Press, New York, 1986.

78. R. H. Stolen, and C. Lin, "Self-phase modulation in silica optical fibers," *Phys. Rev. B.*, **17**, 1448-1453, 1978.

79. H. E. Lee. Jr, "Erbium Doped Fiber Amplifiers," www.jps.net/hansel/erbium.html, 1996.

80. A. Bjarklev, *Optical Fiber Amplifiers: Design to System Applications,* Artec House, Boston, London, 1993.

81. Y. L. Xue, R. A. Betts, P. L. Chu, and T. Tjugiarto, "Nonlinear refractive index in Er^{3+} doped optical fibre," in *Proc.*, ACOFT, IREE Sydney, 117-120, 1990.

82. R. A. Betts, T. Tjugiarto, Y. L. Xue, and P. L. Chu, "Nonlinear Refractive Index in Erbium doped optical fiber: Theory and experiment," *IEEE J. Quantum. Electron.*, **27**, 908-913, 1991.

83. Y. L. Xue, R. A. Betts, P. L. Chu, and T. Tjugiarto, "Nonlinear refractive index in Er^{3+}-doped optical fibers," *Proc. Fifteenth Australian Conference on Fibre Technology,* 299-302, 1990.

84. P. L. Chu, and B. Wu, "Optical switching in twin-core erbium-doped fibers," *Opt. Lett.* **17**, 225-257, 1992.

85. P. A. Wysocki private communication.

86. H. W. Etzel, H. W. Gandy, and R. J. Ginther, "Stimulated emission of infrared radiation from ytterbium activated silica glass," *Apll. Opt.*, 1962, **1**, 534-526, 1962.

87. D. Inniss, D. J. DiGiovanni, T. A. Strasser, A. Hale, C. Headley, A. J. Stentz, R. Pedrazzani, D. Tipton, S. G. Kosinski, D. L. Brownlow, K. W. Quoi, K. S. Kranz, R. G. Huff, R. Espindola, J. D. LeGrange, and G. Jacobovitz-Veselka, "Ultrahigh-power single-mode fiber laser from 1.065 to 1.472 μm using Yb-doped cladding-pumped and cascaded Raman Laser," in *Conference on Lasers and Electro-Optics*, **11**, 1997 OSA Technical Digest Series (Optical Society of America, Washington, D.C., 1997), 651-652.

88. P. C. Becker, N. A. Olsson, J. R. Simpson, *Erbium-Doped Fiber Amplifiers Fundamentals and Technology*, Academic Press, New York, 1999.

89. D. H. Hanna, R. M. Percival, I. R. Perry, R. G. Smart, P. J. Suni, J. E. Townsend, A.C. Tropper, "Continuous-Wave Oscillation of monomode Ytterbium-doped fibre laser," *Electron. Lett*, **24**, 1111-1113, 1988.

90. K. V. Yumashev, N. N. Posnov, P. V. Prokoshin, V. P. Kozich, and V. P. Mikhailov, "Nonlinear refraction measurements in Yb^{3+}:$KY(WO_4)_2$ based on Z-scan technique," *Optc. Lett*, 1998.

91. S. F. Fleming, T. J. Whitley, "Measure of pump induced refractive index change in Erbium Doped fibre amplifier," *Electron. Lett*, **27**, 1959-1961, 1991.

92. Y. L. Xue, P. L. Chu, "Nonlinearity of erbium-doped fibre at the signal wavelength," in *Proceedings of the Sixteenth Australian Conference on Fibre Technology*, 44-47, 1991.

93. Y. L. Xue, P. L. Chu, and W. Zhang, "Resonance-enhanced refractive index and its dynamics in rare-earth-doped fibers," *J. Optc. Soc. Am. B*, **10**, 1840-1847, 1993.

94. E. Desurvire, "Analysis of Gain Difference Between Forward-and Backward-Pumped Erbium-Doped Fiber Amplifiers in the Saturation Regime," *IEEE Photon. Technol. Lett.* **4**, 711-714, 1992.

95. M. Sheik-bahae, A. A. Said, and E. W. Van Stryland, "High-sensitivity, single beam n_2 measurements," *Opt. Lett.*, vol. 14, No. 17, pp. 955-957, 1989.

96. H. Garcia, A. M. Johnson, and Sudhir Trivedi, "Photorefractive Beam Coupling- a new approach to the measurement of the nonlinear refractive index of short (<25-m) lengths of Silica and Erbium-doped fibers," in Conference on Lasers and Electro-Optics, OSA Technical Digest (Optical Society of America, Baltimore MD, 1999), pp. 209-210.

97. H. Garcia and A. M. Johnson, "Photorefractive Autocorrelation Measurement of the Nonlinear Refractive Index in Silica Fiber," Ibero-America Meeting (III RIAO)/6^{th} Latin-America Meeting on Optics, Lasers, and Applications (OPTILAS '98), Sept. 28-Oct. 3, 1998, Cartagena, Colombia, South America.

98. M. Sheik-bahae, D. C. Hutchings, D. J. Hagan, and E. W. Van Stryland, "Dispersion of Bound Electronic Nonlinear Refraction in Solids," *IEEE J. Quantum Electron.*, Vol. 27, No. 6, pp. 1296-1309, 1991.